REPUBLIQUE ALGERIENNE DEMOCRATIQUE ET POPULAIRE
MINISTERE DE L'ENSEIGNEMENT SUPERIEUR ET DE LA RECHERECHE SCIENTIFIQUE

UNIVERSITE BLIDA 1
Faculté de Technologie
Département d'Automatique et électrotechnique

THESE DE DOCTORAT

Spécialité : Automatique

MODELLING, IDENTIFICATION AND CONTROL OF PV SYSTEMS UNDER UNIFORM AND NON-UNIFORM CLIMATE CONDITIONS

Par

BELMADANI Hamza

Devant le jury composé de

Kamel KARA	Professeur, U. de Blida	Président
Elghalia BOUDISSA	MCA, U.de Blida	Examinatrice
Abdelkarim AMMAR	MCA, U.de Boumerdes	Examinateur
Rafik BRADAI	MCA, U.de Blida	Directeur de thèse
Aissa KHELDOUN	Professeur, U. de Boumerdes	Co-Directeur de thèse

Keywords

Photovoltaic Systems, Single Diode Model, Double Diode Model, Triple Diode Model, Maximum Power Point Tracking, Partial Shading, Metaheuristic Algorithms

ملخص

يؤكد الصعود السريع للأنظمة الكهروضوئية باعتبارها لاعبًا رئيسيًا في السعي العالمي لحلول الطاقة المستدامة على الحاجة الملحة لتحسين أدائها. في ظل هذه الخلفية، يتكشف بحثنا في ثلاثة أبعاد رئيسية: تطوير خوارزمية متقدمة لاستخراج النموذج الكهروضوئي، وتصميم خوارزمية جديدة لتتبع نقطة الطاقة القصوى (MPPT) للأنظمة الكهروضوئية المستقلة، واستكشاف خوارزميات تحسين لتحديد النظام والتحكم فيه. يتأثر أداء الأنظمة الكهروضوئية بعوامل مختلفة، مثل الإشعاع الشمسي ودرجة الحرارة والتظليل. ومن أجل تعظيم ناتج الطاقة للأنظمة الكهروضوئية، من المهم تطوير نماذج دقيقة وخوارزميات تحكم فعالة. في هذا العمل، تم تطوير خوارزمية جديدة لاستخراج نماذج الأجهزة الكهروضوئية وأثبتت أن أداء الخوارزمية أفضل من معظم التقنيات الموجودة في الأدبيات. في جانب التحكم، تم تصميم خوارزمية سريعة وفعالة لتتبع نقطة الطاقة القصوى (MPPT) والتحقق من صحتها تجريبيًا. وقد صُممت خوارزمية MPPT المقترحة بطريقة تتعامل مع ظروف التظليل الجزئي المعقدة بفعالية مع قدرات بحث عالية وسرعة اتخاذ القرار. وعلاوة على ذلك، أظهرت الخوارزمية المصممة أداءً أفضل من التقنيات الأخرى المعتبرة في جميع الجوانب. بشكل عام، يساهم هذا العمل في تقدم التكنولوجيا الكهروضوئية، حيث يقدم حلولاً مبتكرة لتحسين دقة النمذجة وكفاءة التحكم في الأنظمة الكهروضوئية.

Abstract

The rapid rise of PV systems as a key player in the global pursuit of sustainable energy solutions underscores the urgency of optimizing their performance. Against this backdrop, our research unfolds in three key dimensions: the development of an advanced algorithm for extracting PV model parameters, the design of a novel Maximum Power Point Tracking (MPPT) algorithm for standalone PV systems, and the exploration of Metaheuristic algorithms for system identification and control. The performance of PV systems is affected by various factors, such as solar irradiance, temperature, and shading. In order to maximize the power output of PV systems, it is important to develop accurate models and effective control algorithms. In this work, a new metaheuristic algorithm for extracting the parameters of PV devices has been developed. The algorithm proved to have superior performance than most the existing techniques in the literature. In the aspect of control, a fast and efficient Maximum Power Point Tracking (MPPT) algorithm has been designed and experimentally validated. The proposed MPPT algorithm was designed in such a way that it handles complex Partial Shading Conditions effectively with its high global search capabilities and faster decision making. Moreover, the designed algorithm has shown greater performance than other well-regarded techniques in all aspects. In overall, this work contributes to the advancement of PV technology, offering innovative solutions for improving the modelling accuracy and control efficiency of Photovoltaic systems.

Résumé

La montée rapide des systèmes photovoltaïques en tant qu'acteur clé dans la quête mondiale de solutions énergétiques durables souligne l'urgence d'optimiser leur performance. Dans ce contexte, notre recherche se déploie selon trois dimensions clés : le développement d'un algorithme avancé pour l'extraction des paramètres du modèle photovoltaïque, la conception d'un nouvel algorithme de suivi du point de puissance maximale (MPPT) pour les systèmes photovoltaïques autonomes, et l'exploration des algorithmes métaheuristiques pour l'identification et le contrôle du système. La performance des systèmes photovoltaïques est affectée par divers facteurs, tels que l'irradiance solaire, la température et l'ombrage. Afin de maximiser la production d'énergie des systèmes photovoltaïques, il est important de développer des modèles précis et des algorithmes de contrôle efficaces. Dans ce travail, un nouvel algorithme métaheuristique pour l'extraction des paramètres des dispositifs photovoltaïques a été développé. L'algorithme s'est avéré avoir une performance supérieure à la plupart des techniques existantes dans la littérature. En ce qui concerne le contrôle, un algorithme de suivi du point de puissance maximale (MPPT) rapide et efficace a été conçu et validé expérimentalement. L'algorithme MPPT proposé a été conçu de manière à gérer efficacement les conditions de l'ombrage partiel complexe grâce à ses capacités de recherche globale élevées et à sa prise de décision plus rapide. De plus, l'algorithme conçu a montré une meilleure performance que d'autres techniques bien considérées dans tous les aspects. Dans l'ensemble, ce travail contribue à l'avancement de la technologie photovoltaïque, offrant des solutions innovantes pour améliorer la précision de la modélisation et l'efficacité du contrôle des systèmes photovoltaïques.

Table of Contents

List of Figures

List of Tables

List of Abbreviations

ABC	Artificial Bee Colony
ACO	Ant Colony Optimization
AE	Absolute Error
AVOA	African Vultures Optimization Algorithm
BHCS	Biogeography-based Heterogeneous Cuckoo Search
BMA	Barnacles Mating Optimizer
CCNMHHO	Horizontal and vertical crossover of Harris hawk optimizer Nelder-Mead simplex
CLJAYA	Comprehensive Learning JAYA Algorithm
COA	Coyote Optimization Algorithm
CS	Cuckoo Search
CPMPSO	Classified Perturbation Mutation Particle Swarm Optimization
DE	Differential Evolution
DDM	Double Diode Model
EABOA	Enhanced Adaptive Butterfly Optimization Algorithm
EO	Equilibrium Optimizer
EJADE	Enhanced Adaptive Differential Evolution Algorithm
EPSO	Enhanced Leader Particle Swarm Optimization
FE	Function evaluation
FFA	Farmland Fermlity Optimizer
FPA	Flower Pollination Algorithm
GBAS	Grouped Beetle Antennae Search
GBO	Gradient-based optimizer
GCPSO	Guaranteed Convergence Particle Swarm Optimization
GNDO	Generalized Normal Distribution Optimization
GOTLBO	Generalized Oppositional Teaching Learning based Optimization
GWO	Grey Wolf Optimizer
HHO	Harris Hawks Optimizer
HROA	Hybrid ROA Optimization Algorithm
HSMA	Hyperbolic Slime Mould Algorithm
IAVOA	Improved AVOA
IGWO	Improved Grey Wolf Optimizer
IJAYA	Improved JAYA Algorithm
IMPA	Improved Marine Predators Algorithm
InC	Incremental Conductance Algorithm
LETLBO	Teaching Learning based Optimizer with Learning Experience

LFBSA	Backtracking Search Algorithm with Lévy flight
L-SHADE	Improved Success History based Adaptive Differential Evolution
MPP	Maximum Power Point
MPPT	Maximum Power Point Tracking
NFEs	Number of functions evaluations
NLBMA	Conscious Neighbourhood Scheme-based Laplacian Barnacles Mating
NLMSOLMFO	Orthogonal Nelder-Mead Moth Flame Optimizer
NM	Nelder-Mead Technique
NWS	Neighbourhood-based Wandering Search
PGJAYA	Performance Guided JAYA Algorithm
pSFS	Perturbed Stochastic Fractal Search
Rcr-IJADE	Repaired Adaptive Differential Evolution
RGNDO	Improved Generalized Normal Distribution Algorithm
SDM	Single Diode Model
SO	Snake Optimizer
SSA	Salp Swarm Algorithm
SMA	Slime Mould Algorithm
P&O	Perturb and Observe Algorithm
PS	Partial Shading
PSO	Particle Swarm Optimization
PV	Photovoltaic
TDM	Triple Diode Model
TLBO	Teaching Learning Based Optimization
UIC	Uniform Irradiance Conditions
LFBSA	Backtracking Search Algorithm with Lévy flight
L-SHADE	Improved Success History based Adaptive Differential Evolution
NFEs	Number of functions evaluations
NLMSOLMFO	Orthogonal Nelder-Mead Moth Flame Optimizer
MPA	Marine Predators Algorithm
NM	Nelder-Mead Technique
NLBMA	Conscious Neighbourhood Scheme-based Laplacian Barnacles Mating
NWS	Neighbourhood-based Wandering Search
PGJAYA	Performance Guided JAYA Algorithm
pSFS	Perturbed Stochastic Fractal Search
Rcr-IJADE	Repaired Adaptive Differential Evolution
RGNDO	Improved Generalized Normal Distribution Algorithm
RMSE	Root Mean Square Error
SAE	Sum of Absolute Errors
SDM	Single Diode Model

SDO	Supply-demand-based Optimization
SEDE	Self-adaptive Ensemble-based Differential Evolution
SFO	Sun Flower Optimization
SO	Snake Optimizer
SSA	Salp Swarm Algorithm
SMA	Slime Mould Algorithm
STD	Standard Deviation
TDM	Triple Diode Model
TLABC	Teaching Learning Based Artificial Bee Colony
TLBO	Teaching Learning based Optimizer
TVACPSO	Time Varying Acceleration Coefficients Particle Swarm Optimization
WDO	Wind Driven Optimization
WHHO	Whippy Harris Hawks Optimization
WOA	Whale Optimization Algorithm
I	Current
I_{ph}	Photo current
I_o	Reverse saturation current
I_{o1}	First reverse saturation current
I_{o2}	Second reverse saturation current
I_{o3}	Third reverse saturation current
a	Diode ideality Factor
a_1	First Diode ideality Factor
a_2	Second Diode ideality Factor
a_3	Third Diode ideality Factor
R_s	Series resistance
R_{sh}	Shunt resistance
V	Voltage
$\mathrm{V_{PV}}$	Photovoltaic voltage
$\mathrm{I_{PV}}$	Photovoltaic current
P	Power
q	Electron charge
K	Boltzmans' Constant

Acknowledgements

I extend my deepest gratitude to my supervisors, Dr. Bradai Rafik and Prof. Kheldoun Aissa, whose unwavering support, insightful guidance, and scholarly mentorship have been instrumental in shaping the trajectory of this research. Their collective expertise and commitment to excellence have been a constant source of inspiration throughout this doctoral journey. I am fortunate to have had the privilege of working under their guidance, and I am sincerely appreciative of the invaluable contributions they have made to the fruition of this thesis.

A special debt of gratitude goes to my parents, whose boundless love, encouragement, and sacrifices have been the bedrock of my academic pursuits. Their unwavering belief in my abilities and their enduring support have been the driving forces that propelled me forward. I am deeply thankful for their sacrifices and the endless encouragement that has been the cornerstone of my academic journey.

I would like to express my heartfelt appreciation to my dear friend Siad Rihab, whose unwavering support and encouragement provided solace during the challenging phases of this research. Rihab's friendship has been a source of strength, and I am profoundly grateful for the encouragement and understanding that she extended throughout this journey. Her belief in my capabilities has been a constant motivator, and I am thankful for the shared moments of joy and resilience.

To all those who have contributed in myriad ways, whether through intellectual discussions, moral support, or understanding during demanding times, I extend my sincere appreciation. The completion of this dissertation stands as a collective achievement, and I am indebted to the supportive network of individuals who have played a part, no matter how small, in this academic endeavor.

Introduction

1.1 BACKGROUND AND MOTIVATIONS

The compelling necessity to thin out climate changes and carbon emissions laid the groundwork for a transition in the energy sectors towards renewables in many countries around the globe. Fostered by the substantial decline in solar modules prices, the growing demand for electricity generation and government engagements, photovoltaic systems uptake is expected to reach a cumulative capacity of 2840 GW globally by 2030 and 8519 GW by 2050 [1]. To ensure optimal performance, inverters and Maximum Power Point Trackers are embedded alongside PV generators to handle the fluctuating nature of the operating conditions and keep their efficiency as high as possible [2]. The development of such systems involves extensive theoretical studies and performance assessment through simulation tools prior to hardware implementations and experimental testing [3-5]. For these reasons, accurate modelling of PV devices is vital for the development of reliable simulators, to get insights on their behaviour under diverse operating conditions. Till date, there have been many efforts to design effective circuit configurations that imitate solar cells, among which the Single diode model (SDM) and the Double diode model (DDM) attracted the most significant amount of attention. However, these models are governed by a set of parameters usually not provided by the manufacturers of solar modules in their datasheets [6]. On that account, one has to find means to identify these unknown factors that accurately imitate the behaviour of the corresponding PV panel and hence conduct simulations and performance analyses effectively.

Once the PV model has been estimated, the Besided the low efficiency of PV devices, their generated power is strongly dependent on the incoming solar irradiance and temperature. This influence can be visualized using power-voltage curves and current-voltage curves. At a certain uniform illuminance level, the generated P-V curve is hill-shaped, characterized by a unique top associated with the PV generator's Maximum Power Point (MPP) as shown in Figure 2.1.

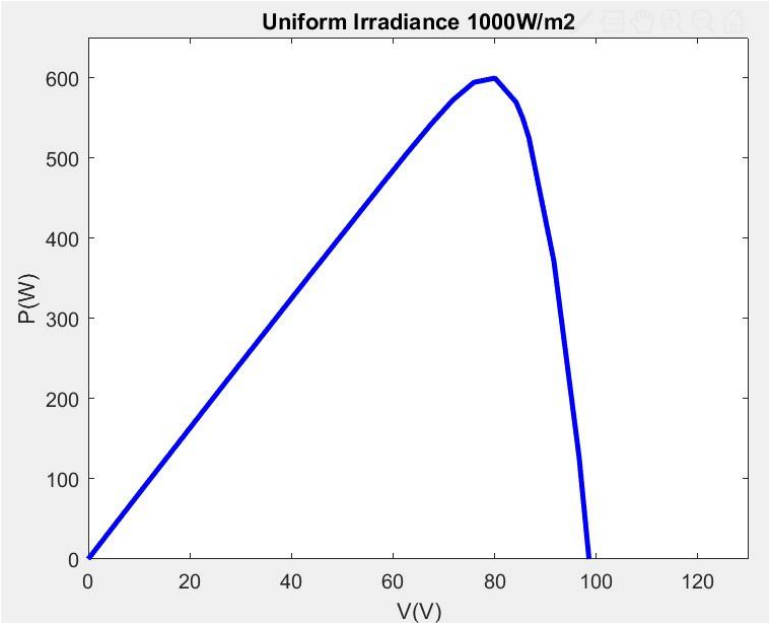

Figure 2.1 PV curve of a PV device under Uniform Irradiance

In effect, the PV system needs to operate at this point to maximize its efficiency and reduce power losses. However, when a load is directly coupled to the PV generator, the operating point is dictated by the intersection of the load line and the I-V characteristic curve [7]. In practice, the resultant operating point is hardly the MPP level, leading to a substantial reduction in the system overall efficiency [8]. To resolve this issue, DC-DC converters are employed as an interface between the PV generator and the system's load side, allowing the impedance seen by the PV device to be changeable. In turn, by properly adjusting the duty cycle of the DC-DC converter, the operating point can be varied accordingly so that it coincides with the MPP level of the PV array. For these reasons, Maximum Power Point Tracking (MPPT) algorithms are incorporated into PV systems to monitor the operating point and keep the power as high as possible under any conditions as shown in the block diagram of Figure 2.2.

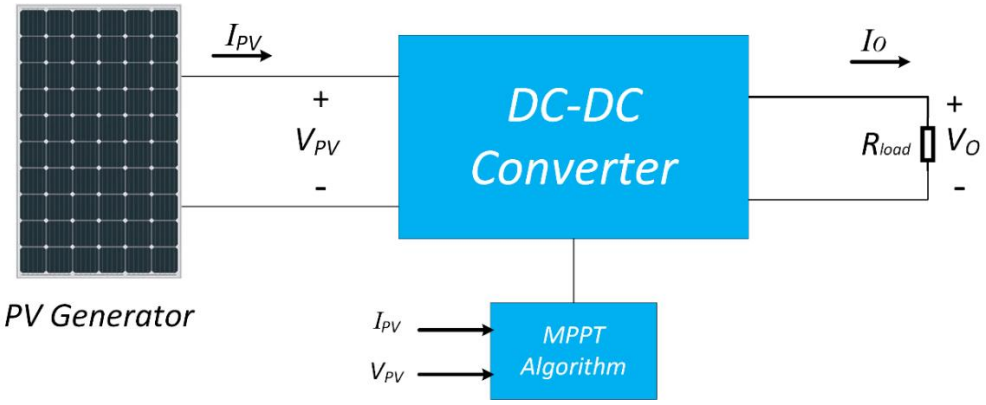

Figure 2.2 PV system based on MPPT

Undeniably, conventional MPPT techniques like the Perturb and Observe (P&O) [9] and the Incremental Conductance (InC) [10-11] are the most widely investigated and employed [6]. Broadly speaking, these classical approaches are generally grounded on the hill-climbing concept, which is based on perturbing the system along the direction of increasing power. However, one of the major defects of these algorithms is the appearance of oscillations around the MPP level, and their inability to handle partial shading conditions. During such circumstances, the shaded cells are impelled to operate in the reverse bias mode leading to the hot spot phenomenon, which causes severe damage to the PV device. At that time, bypass diodes are inserted in parallel with PV modules to provide an alternative path to the current, eliminating the hot spot problem. In effect, although equipping PV modules with bypass diodes affords protection to them, their presence leads to the distortion of the PV and IV characteristics under non-uniform irradiance conditions [12]. The distortion is in the format of multiple peaks occurring in the characteristic curves due to the mismatch conditions. The peak with the largest power level corresponds the global MPP, while the remaining peaks are Local MPPs with lower power levels as shown in Figure 2.3.

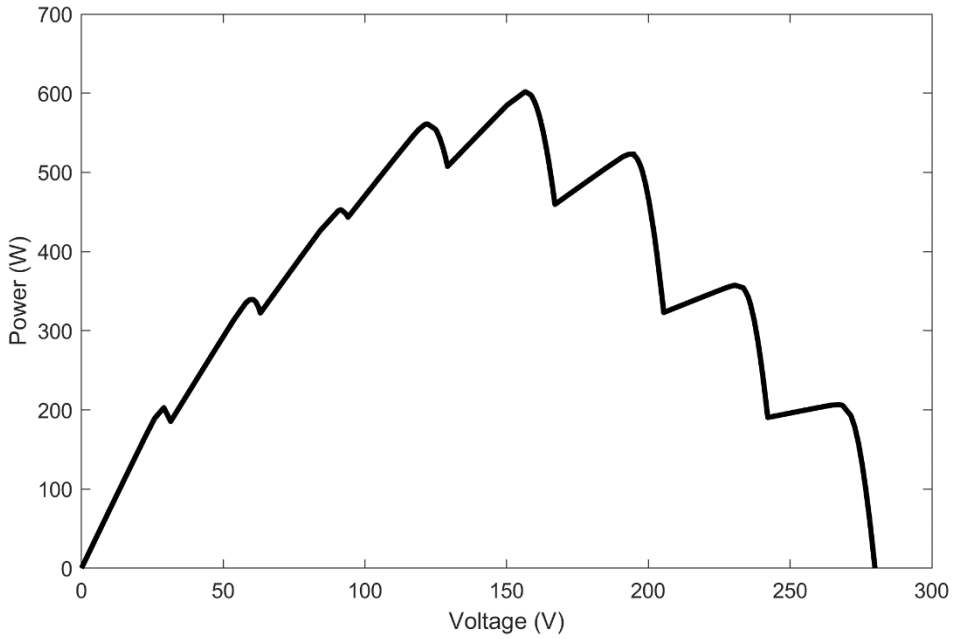

Figure 2.3 Effect of Partial Shading on the PV Characteristics Curves

Because the PV characteristics turn into multimodal curves under PSCs, the task of Maximum Power Point Tracking becomes even more challenging and classical MPPT techniques often fail to handle such cases. With their basic structure, they cannot traverse the different regions of the PV characteristics and often get stagnated at one of the local peaks.

1.2 AIMS AND OBJECTIVES

The key objectives of this thesis can be outlined as follows:

- Investigation of Metaheuristic algorithms and their applications in PV systems.
- Development of highly accurate optimization techniques for the extraction of the different PV models' parameters.
- Design of fast, efficient and reliable Maximum Power Point Tracking Algorithms under Partial Shading Conditions.

1.3 THESIS OUTLINE

The remainder of this thesis is organized as follows:

Chapter 1 provides a brief overview of Metaheuristic algorithms, and existing work on the identification of PV parameters as well as Maximum Power Point Tracking. Chapter 2 dives in the Modelling and identification of PV parameters and the developed algorithm for this aspect. Chapter 3 delves into the designed Maximum Power Point Tracking algorithm, its foundations, simulation and implementation outcomes. The last chapter culminates the thesis with the main conclusions drawn from the conducted work and recommendations for future work.

Chapter 2: Literature Review

2.1 INTRODUCTION TO METAHEURISTIC ALGORITHMS

A wide variety of engineering problems entail the extraction of parameters and variables that results in the best potential performance. In past times, deterministic algorithms were frequently utilized to address a broad spectrum of problems. The intensive computations of gradients and derivatives required by this class of approaches, however, renders them incompatible for a sizable class of problems. As a result of their gradient-based framework, deterministic algorithms often experience local-optimum stagnation, which typically happens when the starting point is outside of the global optimum zone. In effect, the current trend in applied optimization is dominated by Metaheuristic Algorithms, which have stochastic behavior. Unlike deterministic methods, a Metaheuristic algorithm often does not produce the exact same results every time is executed due to the incorporated randomness in its search procedure. Metaheuristic algorithms are often Nature-inspired, in other words, their framework equations and search operations were derived from certain behaviors or phenomenon from nature such as animals, physical laws. Based on the source of inspiration, Metaheuristic algorithms are classified into four broad families :

- **Evolutionary Algorithms (EA):** The Darwinian paradigm of evolution's survival of the fittest theory serves as the inspiration for evolutionary algorithms. The Genetic Algorithm (GA) and the Differential Evolution algorithm (DE) are the most popular algorithms in this family of Metaheuristics.
- **Swarm Intelligence based algorithms (SI):** On the other hand, Metaheursitics based on Swarm Intelligence imitate the social behavior of living things in nature such animals and insects. These behaviors typically involve the food-search and hunting operations of animals. Particle Swarm Optimization (PSO), Grey Wolf Optimization (GWO), Whale Optimization Algorithm (WOA), are a few popular examples of SI based algorithms.

- **Physics-based algorithms (PH):** As the name indicates, this class of Metaheuristics are based on laws, theories or hypotheses in physics, astronomy or chemistry. The most well-known algorithms with this class of inspiration include Simulated Annealing (SA), Gravitational Search Algorithm (GSA)[13], and the Multi-verse Optimizer (MVO).
- **Human based Algorithms (HA):** The final category of metaheuristic algorithms is based on how people behave and interact.

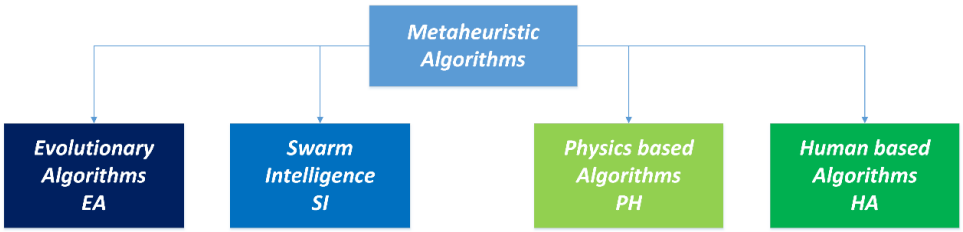

Figure 2.4 Classifications of Metaheuristic Algorithms

Besides the inspiration classifications, Metaheuristic algorithms can also be categorized according to the number of generated solutions. In this regard, there are two main types of algorithms: Trajectoy-based algorithms and Population-based algorithms. The first category employs a single solution to be improved in each iteration until convergence conditions are met. Conversely, in the second category, a specific number of solutions are generated and get updated iteratively based on the algorithm equations. Due to the higher number of generated solutions in Population-based metaheuristics, they often achieve better performance than single-based solutions especially with problems having multimodal characteristics. The latter fact led to population-based metaheuristics dominating optimization approaches.

The key benefit of employing Metaheuristic algorithms lies in their gradient-free framework. In other words, no derivatives nor analytical expressions are required to handle the given problem at hand. Because of this, nature-inspired algorithms are suitable for practically all engineering optimization problems. Plainly, a fitness function that quantifies how good the generated solutions are, have to be constructed to execute the algorithm. The general flow of metaheuristic algorithms is illustrated in Figure 2.5. The process is decomposed into three main successive stages:

- **The Initialization Phase:** In here, the major parameters that governs the optimization process have to be set. This includes the maximum number

of iterations, the number of solutions to be generated each iteration, the lower and upper bounds of the solutions and the parameters related to the algorithm itself. Once the parameters have been fixed, the initial population of solutions have to be randomly generated and evaluated by the specified fitness function.

- **Iterative Process:** When the initial solutions have been evaluated by the fitness function, the algorithm enters the iterative loop. In here, the algorithm performs its operations, generates the required number of solutions to be evaluated by the fitness function and save the best solutions. This process gets repeated each iteration in an attempt to improve the candidate solutions.
- **Convergence:** When the generated solutions become close to each other or the maximum number of iterations has been attained, the algorithm stops the iterative process.

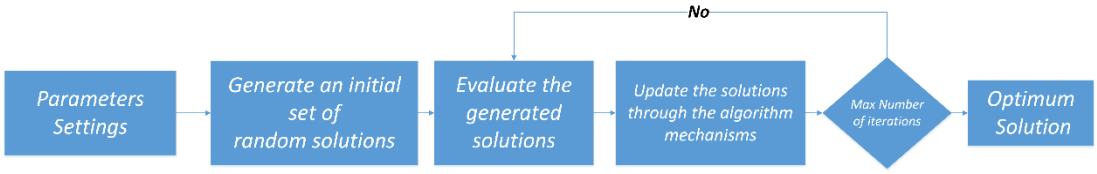

Figure 2.5 Metaheuristic Algorithms Process Flow

Despite the different equations possessed by each metaheuristic algorithm, their overall iterative process is usually driven by two main operations. The first operation, referred to as the exploration phase, aims to produce scattered candidate solutions in order to scan as much regions in the search space as possible. The second operation, referred to as the exploitation phase aims to dive in the best spotted regions in an attempt to improve the solutions quality. In essence, the two operations work in tandem and are intertwined throughout the iterative process.

2.2 EXISITING WORK IN THE IDENTIFICATION OF PV PARAMETERS

Till date, a wide collection of techniques have been applied to extract the unknown parameters of PV cells and modules, and can be classified into three main categories; Analytical techniques, Numerical methods, and Metaheuristic Algorithms. Analytical techniques that are derived from the model equations through a set of

assumptions and approximations[14 - 20] and numerical methods that are gradient-based techniques [21-24] might produce deficient results due to the highly nonlinear and multimodal nature that characterize PV systems. Metaheuristic algorithms on the other hand appear to be typical to handle the PV parameters estimation problem, due to their simplicity, robustness and effectiveness, regardless of the system mathematical model. A general diagram of the identification process is provided in Figure 2.6.

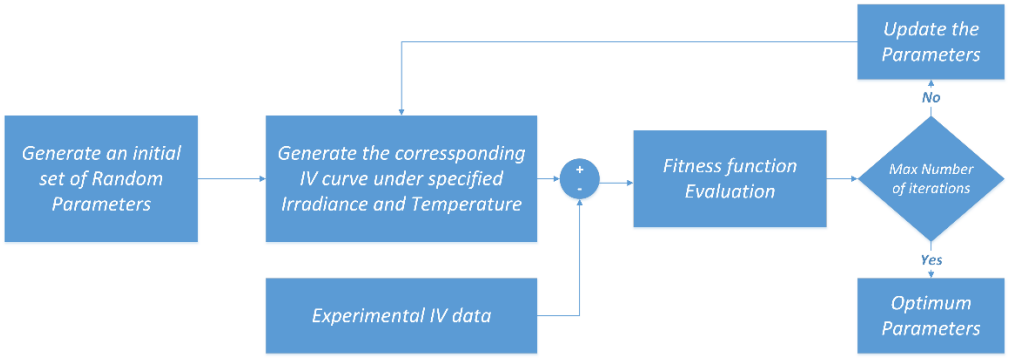

Figure 2.6 Identification Process with Metaheuristic Algorithms

Nowadays, Metaheuristics constitute a large percentage of the applied approaches for PV modelling [25]. A great deal of metaheuristic-based approaches are based on modifications incorporated to the canonical versions of some well-regarded algorithms such as Differential Evolution (DE) [26], Particle Swarm Optimization (PSO) [27], JAYA Algorithm [28], Whale optimization Algorithm (WOA) [29], Artificial Bee Colony (ABC) [30], and Teaching Learning Based Optimization (TLBO) [31]. For instance, in [32], a recent Differential Evolution variant (EJADE) that incorporates a new crossover sorting mechanism was introduced. The resulting algorithm has also adopted a dynamic population reduction strategy to speed up the convergence process, which was of valuable reinforcement as outlined in the reported results. In light of the wide deployment of Differential Evolution variants in the electrical characterization of PV devices, the authors in [33] conducted a comparative study covering 11 state-of-the-art DE derivatives. The findings demonstrated the superiority of Rcr-IJADE and L-SHADE over their remaining counterparts. PSO variants have also been widely applied for PV modelling [34]. In [35], a Time-Varying Acceleration Coefficients PSO (TVACPSO) was introduced and applied for three benchmark cases, wherein its outperformance was testified against well-known

algorithms. The Enhanced Leader PSO (ELPSO) is another efficient version recently published by [36], equipped with five successive mutation mechanisms for the global best particle, leading to an improved exploration capability as testified by the conducted trials. In [37], Liang, J. et al. developed a Classified Perturbation Mutation PSO (CPMPSO), incorporating a strategy through which, a trial solution is generated based on the goodness of the particle, however, the obtained results seem not to be superior to the ones obtained by the aforementioned PSO variants. The JAYA algorithm has also been extensively adopted in the electrical characterization of PV devices due to its simplicity and its parameter-free attribute. Kunjie.Y, et al. [38] developed an improved version (IJAYA) by incorporating a logistic map and a learning strategy based on random solutions from the population to enhance its diversity. Moreover, in [39], the authors introduced a self-adaptive chaotic perturbation to the IJAYA, while maintaining nearly the same framework. The reported results on three benchmark cases indicate that the PGJAYA performs slightly better than the IJAYA and other techniques. The popular TLBO algorithm, on the other hand, accounts for a remarkable proportion of metaheuristic algorithms applied for PV modeling. In [40], a recently improved TLBO that modifies the framework equations of the standard version was developed and proved to outperform previously applied TLBO variants [41 - 44]. Besides those above popular optimizers, numerous works have employed novel metaheuristic algorithms proposed recently. For instance, in [45], Shan. J, et al. designed an enhanced version of the recent Harris Hawks Optimizer [46] by incorporating Orthogonal learning to speed up the algorithm and improve its accuracy, in conjunction with Opposition learning to enhance the population diversity .In [47], the authors were the first to apply the standard Farmland Fermlity Optimizer [48] for PV modelling, which is inspired by the way farmers examine the soil quality at each section of their farmland. The Sunflower optimization algorithm (SFO), which was published in 2018 [49], was examined by [50] for triple diode modelling of three commercial PV modules that are not notably used in literature, yet, the obtained IV curves were in good agreement with the experimental data. In [51] the authors examined the Coyote Optimization Algorithm introduced in 2018 [52], where the comparative study revealed an excellent competence in the single diode and double diode models of the RTC cell as well as the Photowatt-PWP20 module. In [53], the authors modified the novel Barnacles Mating Optimizer (BMA) [54] by adding a Laplacian-based Crossover Search (LCS) and a Neighbourhood-based Wandering

Search (NWS). The resultant optimizer (NLBMA) was assessed on one cell and two PV benchmark modules and outperformed the considered contenders. Raja.K, et al. [55] designed a hybrid scheme that takes advantage of the Chimp Optimization Algorithm [56] and the popular Sine and Cosine algorithm [57] to estimate the single and double diode models of PV devices based on the manufacturer datasheets.

2.3 EXISITING WORK IN MAXIMUM POWER POINT TRACKING

Due to the fact that Conventional techniques such the P&O algorithm and the InC technique cannot handle partial shading conditions and possess steady state oscillations , Metaheuristic algorithms have become a typical substitute due to their stochastic gradient-free foundation and population-based nature. Because they treat problems as black boxes, neither input data nor training is required to lay out the system [58]. Accordingly, with metaheuristic algorithms, Maximum Power Point Tracking is treated as an optimization problem, with the power being the objective function controlled through the duty cycle as the decision variable. During the tracking stage, metaheuristic algorithms usually divide the search mechanisms into two main phases : exploration and exploitation. The exploration process is devoted to generate distant solutions to scout as many optimum regions in the search space as possible. The exploitation process in the other hand intends to inspect the best-discovered region until eventually converging to the global optimum solution. Despite the well performing global search abilities of metaheuristic algorithms, their behavior and outcomes are largely dictated by their tuned parameters [59]. More often, applying the algorithm as it was designed in its original version might lead to large perturbations during the tracking stage, slow convergence and eventually poor accuracy. To enhance their tracking performance, modifications are usually necessary to incorporate into their canonical versions. There have been a myriad number of proposed metaheuristic algorithms applied for MPPT among which, Particle Swarm Optimization (PSO) [60][62], Grey Wolf Optimizer (GWO) [63][64], Salp Swarm Algorithm (SSA) [65] [66], Artificial Bee Colony Algorithm (ABC) [67], Ant Colony Optimization (ACO) [68] and the Flower Pollination Algorithm [69] were widely employed. Due to its simple structure, the PSO algorithm has been extensively applied in literature along with incorporated amendments. Despite its successful global optimal tracking under partial shading conditions, it exhibits several issues during optimization. The search behavior generates large perturbations of duty cycles due to the velocity term, which

is influenced by the inertia ω and the cognitive and social constants. Although reducing these factors might reduce the velocity levels, the algorithm's exploration stage might be negatively affected, leading to local optima stagnation. For instance, in [70], an accelerated PSO version was developed by removing the personal best term form the velocity equation to boost its convergence trend. In other relevant works as in [71], the modifications involve adjusting the PSO parameters making them either increasing or decreasing over the lapse of iterations. In [72], an Enhanced Autonomous Group PSO algorithm was designed by updating the cognitive constants using a combination of cubic and root functions, leading to a better balance between exploration and exploitation. Moreover, the inverse tangent function was inserted into the velocity term to reduce the highly random nature of the algorithm. Accordingly, the results of the algorithm were superior to those of other PSO variants. In [73], the authors introduced a mechanism by which the duty cycles are effectively distributed within the search space to roughly recognize the global optimum region. Once the particles were scattered, the PSO algorithm takes the lead to carry on the tracking process. Even though improvements were observed with the different PSO variants, the conducted experiments in most of the reported works were missing complicated partial shading patterns in which the number of peaks is high and the Global MPP is close to the nearest local peak [74]. In such cases, the probability of local optima stagnation is very high and poses a challenging process to the performance of the given algorithm. In other works, the combination of two or more metaheuristic algorithms turned out to be beneficial. These hybrid schemes intend to take advantage of the merits of each algorithm in the exploration and exploitation phases. Some works divide the tracking process by assigning the first iterations to a certain optimizer due to its performant global search, and designating the other one to carry on the tracking process along the remaining iterations due to its good local search operation. For instance, the authors in [75] designed a two-stage MPPT controller that combines an improved version of the Artificial Bee Colony algorithm and the Simultaneous Heat Transfer Search Algorithm. The first algorithm was appointed to roughly find the global MPP region in the early stages, while the second algorithm took the lead of digging around that region in the remaining stages. Several other techniques split the duty ratios between two algorithms so that the framework equations of one algorithm update a portion of the solutions and the other portion is updated by the mechanisms of the second algorithm. The latter idea was effectively examined in [76] by combining Differential

Evolution and the Whale Optimization Algorithm resulting in a remarkable faster convergence. In [77], the authors merged the Grey Wolf Optimizer for its good exploration capabilities with the Nelder-Mead (NM) technique for its performant local search operation. The resulting hybrid scheme is constructed in such a way a portion of the candidate solutions are updated by the GWO algorithm and then passed to the NM technique undergoing its four fundamental operations. This passage between the GWO algorithm and the NM technique avoided repeated exploration of the search space, leading to a faster convergence trend as reported in the outcomes. Another interesting scheme was designed in [78] by integrating a detection method to distinguish between Partial Shading Conditions and Uniform Irradiance Conditions (UICs) to avoid unnecessary exploration. Moreover, by checking some inequalities on the PV voltage and the PV current, a skipping method was incorporated to eliminate some regions of the search space and perform the tracking process only on a reduced interval. Once the conditions are checked, the Snake Optimizer (SO) performs the search process on the specified search space with a rapid convergence trend.

2.4 SUMMARY AND IMPLICATIONS

In overall, a broad variety of strategies have been designed for the parameter estimation of PV devices, however, we address the following comments about these techniques:

- Majority of the designed algorithms suffer from local minima stagnation. This is noticeable in the reported results associated with the Single diode and Double diode estimated models of the benchmark RTC France cell.

- A large portion of these techniques were the result of considerable assortments of modifications and complicated hybrid schemes. However, no remarkable improvements in the accuracy can be observed when compared to relevant works.

- Little attention has been paid to Triple Diode Modelling.

Because the perfect set of model parameters are unresolved, any improvements in the estimated models accuracies would be substantially beneficial. Considering the former remarks, this work seeks to tackle the aforementioned issues and inspect for further prospects of improvements.

Despite the observed satisfactory performance, most of the designed MPPT algorithms were benchmarked on Partial Shading Conditions that involve few peaks, which are not quite difficult to handle. Moreover, one can observe from their framework equations that they entail multiple parameters to be tuned due to the incorporated amendments.

Chapter 3: Modelling and Identification of PV Devices' Parameters

The development of reliable simulators that finely imitate the behaviour of PV devices is vitally important for the design and optimization of efficient and stable photovoltaic systems. In this work, an improved variant of the African Vultures Optimization Algorithm named IAVOA is designed to serve as a powerful tool for extracting the unknown parameters of photovoltaic models. The introduced scheme incorporates a two-fold strategy in such a way that allows a portion of the search agents to conduct a global search while the remaining portion performs a local search. The embedded mechanism is based on two equations added to the standard version, and by which the exploration and exploitation capabilities of the algorithm have significantly been fostered. To testify the performance of the IAVOA, a comparative study based on the Root Mean Square Error (RMSE), was conducted on six distinct benchmark PV models, and the obtained results were, in most cases, remarkably superior to the ones achieved by its competitors. The algorithm was able to produce values for the ideality factors that have not been previously found by any existing work to the best of our knowledge. In turn, the Double Diode and Triple Diode models' accuracies were notably improved with RMSE scores of 6.9096E-4 and 7.40109E-4 respectively for the RTC France cell, and 1.42511E-2 for the STP6-120/36 module, outperforming the existing techniques. In light of that, it can be reliably presumed that the IAVOA is indeed a promising algorithm for the electrical characterization of PV devices.

3.1 PROBLEM FORMULATION

With distinct degrees of accuracy and complexity, there exist several electronic circuits that model PV devices, among which the Single Diode Model, the Double Diode Model, and the Triple Diode Model are the most widely employed in the literature due to their effective I-V characterization. This section elaborates on these three configurations.

3.1.1 The Single Diode Model

In its simplest form, the solar cell behaves as a photo-generated current source connected in parallel with a diode. However, this ideal configuration is rarely employed by PV simulators due to its deficient accuracy [79]. A more practical model incorporates a series resistance R_s that acts as the combination of contact resistance between silicon and electrodes surfaces, and the resistance of electrodes [80], as well as a shunt resistance R_{sh} related to the leakage current in the PN junction. The most popular configuration of the SDM circuit that embodies the stated components is depicted in Figure 3.1.

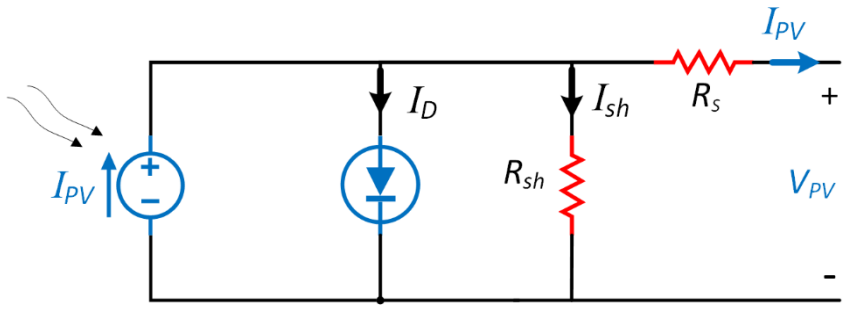

Figure 3.1 The Single Diode Model

The output current produced by the solar cell can then be obtained:

$$I_{PV} = I_{ph} - I_D - I_{sh} \tag{3.1}$$

Where I_{ph} is the photovoltaic current and it is proportional to the impinging solar radiation, I_{sh} denotes the shunt resistance current, and I_D is the diode current defined by the famous Shockley equation:

$$I_{sh} = \frac{V_{pv}+R_s I_{pv}}{R_{sh}} \tag{3.2}$$

$$I_D = I_s \left[\exp\left(\frac{q(V_{PV}+R_s I_{PV})}{aKT}\right) - 1\right] \tag{3.3}$$

Where I_s is the reverse saturation current of the diode. I_{pv}, V_{pv} are the output current and voltage of the PV cell, respectively. q is the electron charge (1.60217662 × 10-19 C). a is the diode ideality factor and it depends on the PV cell technology. K is the Boltzmann constant (1.38064852 × 10-23 J/K°) ,T is the temperature of the p-n junction in-unit kelvin.

Substituting equations 3.2 and 3.3 into equation 3.1, the output current of the solar cell based on the Single Diode Model can be computed using equation 3.4:

$$I_{pv} = I_{ph} - I_s \left[e^{\left(\frac{q(V_{pv}+R_s I_{pv})}{aKT} \right)} - 1 \right] - \frac{V_{pv} + R_s I_{pv}}{R_{sh}} \quad (3.4)$$

It is straightforward to recognize from the latter equation that the SDM configuration is characterized by five major parameters (I_{ph}, I_s , R_s, R_{sh}, a). For this reason, the Single Diode Model is occasionally referred to as the Five-parameter model. Accurate estimation of these factors is indispensable to fully depict the IV and PV characteristics of the PV cell.

3.1.2 Double Diode Model

The double diode model was designed to tackle the anomalies of the SDM at low irradiance levels, caused by neglecting the effect of current recombination loss in the depletion region [81]. Accordingly, a second parallel diode is embedded in the Single Diode Model, as depicted in the circuit of Figure 3.2.

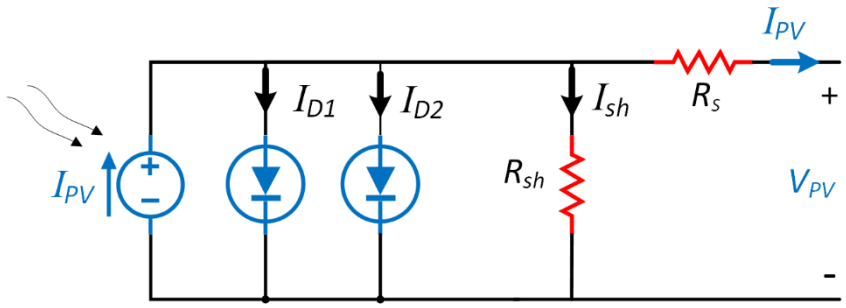

Figure 3.2 The Double Diode Model

The output current-voltage characteristic of the double diode model is then obtained by:

$$I_{pv} = I_{ph} - I_{s1} \left[e^{\left(\frac{q(V_{pv}+R_s I_{pv})}{a_1 KT} \right)} - 1 \right] - I_{s2} \left[e^{\left(\frac{q(V_{pv}+R_s I_{pv})}{a_2 KT} \right)} - 1 \right] - \frac{V_{pv} + R_s I_{pv}}{R_{sh}} \quad (3.5)$$

Similarly, the DDM is also known as the Seven-parameter model, due to the additional two parameters (I_{s2}, a_2) of the second diode, which would make the identification process a heavier task compared to the SDM, yet with an enhanced IV characterization accuracy.

3.1.3 Triple Diode Model

In like manner, a third diode is inserted into the DDM circuit to account for the impact of grain boundaries and large leakage current [82] as depicted in Figure 3.3.

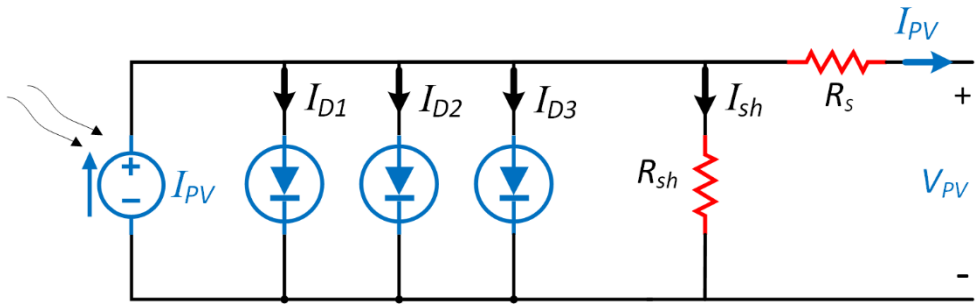

Figure 3.3 The Triple Diode Model

In the same way, the output current-voltage characteristic is described by the following equation:

$$I_{pv} = I_{ph} - I_{s1}\left[e^{\left(\frac{q(V_L+R_sI_L)}{a_1KT}\right)} - 1\right] - I_{s2}\left[e^{\left(\frac{q(V_L+R_sI_L)}{a_2KT}\right)} - 1\right] - I_{s3}\left[e^{\left(\frac{q(V_L+R_sI_L)}{a_3KT}\right)} - 1\right] - \frac{V_L + R_sI_L}{R_{sh}} \quad (3.6)$$

Which entails, an identification of nine unknown parameters.

3.1.4 SDM based PV Module Model

As illustrated in Figure 3.4, a PV module is a collection of individual solar cells that are linked together in series and/or in parallel.

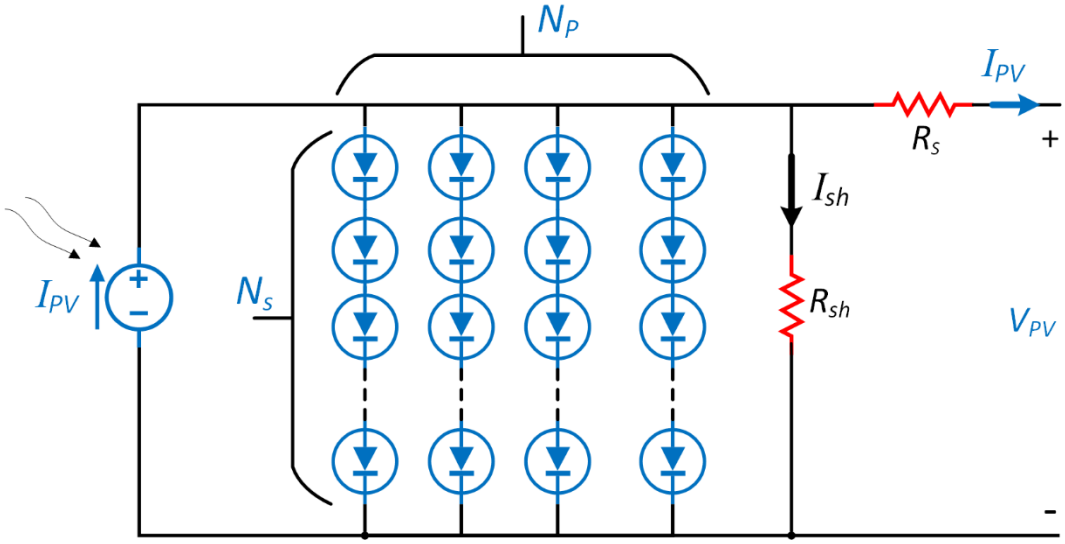

Figure 3.4 The Module Model

The output current-voltage relationship based on the SDM cells that form the module can then be inferred:

$$I_{pv} = N_P I_{ph} - N_P I_s \left[\exp\left(\frac{q\left(\frac{V_{pv}}{N_S} + \frac{R_S I_{pv}}{N_P}\right)}{AKT} \right) - 1 \right] - \frac{N_P}{R_{sh}} \left(\frac{V_{pv}}{N_S} + \frac{R_S I_{pv}}{N_P}\right) \quad (3.7)$$

Where N_S denotes the number of cells in series, and N_P denotes the number of cells that are in parallel.

3.2 EXTRACTION OF PV PARAMETERS

As mentioned earlier, in order to accurately simulate PV cells and modules, the unknown parameters of the applied model have to be finely estimated. Henceforth, it is required to set up an objective function that assesses the coherence between the experimental I-V data, and the calculated data that corresponds to the produced PV model. In other words, the error between the measured current values and the estimated ones needs to be minimized. In literature, the Root Mean Square Error (RMSE) has been the most widely used objective function in extracting the photovoltaic parameters, and it is defined as follows:

$$RMSE(x) = \sqrt{\frac{1}{N} \sum_{k=1}^{N} f_k(I_L, V_L, x)} \quad (3.8)$$

Where N denotes the number of sample data points, x is a solution vector that contains candidate PV parameters for the optimization problem, and f_k represents the error function between the measured current and the estimated one that corresponds to the solution vector x, at the kth data point.

For the SDM case, the error function is defined as follows:

$$f_k(I_L, V_L, x) = I_{ph} - I_s \left[e^{\left(\frac{q(V_L + R_S I_L)}{aKT}\right)} - 1 \right] - \frac{V_L + R_S I_L}{R_{sh}} - I_L \quad (3.9)$$

$$x = (I_{ph}, I_s, R_s, R_{sh}, a) \quad (3.10)$$

And for the DDM case:

$$f_k(I_L, V_L, x) = I_{ph} - I_{s1} \left[e^{\left(\frac{q(V_L + R_S I_L)}{aKT}\right)} - 1 \right] - I_{s2} \left[e^{\left(\frac{q(V_L + R_S I_L)}{aKT}\right)} - 1 \right] - \frac{V_L + R_S I_L}{R_{sh}} - I_L \quad (3.11)$$

$$x = (I_{ph}, I_{s1}, I_{s2}, R_s, R_{sh}, a_1, a_2) \quad (3.12)$$

Likewise, the TDM is estimated using:

$$f_k(I_L, V_L, x) = I_{ph} - I_{s1} \left[e^{\left(\frac{q(V_L + R_S I_L)}{aKT}\right)} - 1 \right] - I_{s2} \left[e^{\left(\frac{q(V_L + R_S I_L)}{aKT}\right)} - 1 \right] - I_{s3} \left[e^{\left(\frac{q(V_L + R_S I_L)}{aKT}\right)} - 1 \right] - \frac{V_L + R_S I_L}{R_{sh}} - I_L \quad (3.13)$$

$$x = (I_{ph}, I_{s1}, I_{s2}, I_{s3}, R_s, R_{sh}, a_1, a_2, a_3) \quad (3.14)$$

3.3 PROPOSED METHODOLOGY

3.3.1 The African Vultures Optimization Algorithm

The African Vultures Optimization Algorithm is a Swarm-intelligence algorithm developed by Benyamin Abdollahzadeh and Farhad Soleimanian Gharehchopogh in 2021 [83]. It is inspired by the hunting style of vultures which constitutes of four major mechanisms:

A. Mechanism 1

This mechanism involves selecting either the first or the second best so-far solution to direct the search process of each agent. This is operated by the Roulette Wheel selection:

$$R_i(t) = \begin{cases} \text{BestVulture1 if } p_i = L1 \\ \text{BestVulture2 if } p_i = L2 \end{cases} \quad (3.15)$$

BestVulture1 and BestVulture2 are respectively the best and the second best found solutions. $R_i(t)$ is the selected best solution for the ith search agent. $L1$ and $L2$ are constants to be set. p_i is the selection probability calculated as follows:

$$p_i = \frac{F_i}{\sum_{i=1}^{n} F_i} \quad (3.16)$$

B. Mechanism 2: The Rate of Starvation of Vultures:

When vultures are energetic and lusty, they fly long distances to scout their food. However, they cannot travel to distant locations when they are starving and drained. At that time, they try to roam close to the strongest vultures. The two situations are modelled using two factors :

$$t = h \times (sin^w \left(\frac{\pi}{2} \times \frac{Ite}{MaxIte}\right) + cos \left(\frac{\pi}{2} \times \frac{Ite}{MaxIte}\right) - 1) \quad (3.17)$$

$$F = (2 \times rand + 1) \times z \times \left(1 - \frac{Ite}{MaxIte}\right) + t \quad (3.18)$$

Ite and $MaxIte$ denote respectively the current iteration and the fixed maximum number of iterations. h and z are two numbers randomly produced within the intervals $[-2,2]$ and $[-1,1]$ respectively. The vulture's degree of satiation or starvation is indicated by the value of F, which is employed to determine whether the search agent will take part in the exploration operation or the exploitation operation. The agent will conduct a global search if the absolute value of F exceeds 1, and a local search process otherwise.

C. Mechanism 3: Diversification

This phase involves producing distant and scattered solutions in order to scan the different regions of the search space. The vultures' positions are updated by the following two equations:

$$P_i(t+1) = R_i(t) - |X \times R_i(t) - P_i(t)| \times F \quad (3.19)$$

$$P_i(t+1) = R_i(t) - F + rand \times ((UB - LB) \times rand + LB) \quad (3.20)$$

In equation 3.19, the vulture is being moved from the position of the selected powerful vulture $R_i(t)$ into another random position. F and the weighting factor X, influence how far the agent travels. The factor X is randomly produced as follows:

$$X = 2 \times rand \quad (3.21)$$

In equation 3.20, a random solution is produced within the search boundaries, where UB and LB denote the upper bound, and lower bound respectively.

D. Mechanism 4: Intensification

The intensification process involves diving into the best-located regions of search space in order to look for better candidate solutions. The AVOA optimizer divides this operation into two major stages:

- **Stage 1:** The first stage of the exploitation models the state when the vultures here are not fully exhausted which happens when $|F| > 0.5$. Two strategies are employed:
  - **The Siege-fight strategy:** A swarm of vultures may experience internal strife when they congregate around a single food source. As a result, the strongest vultures prefer to eat separately, while the weaker vultures will try to follow them in an effort to start a fight over food. The following equations model this situation:

$$P_i(t+1) = |X \times R_i(t) - P_i(t)| \times (F + rand) - d(t) \quad (3.22)$$

Where

$$d(t) = R_i(t) - P_i(t) \quad (3.23)$$

  - **The Rotating-flight strategy:** To emulate the hovering attitude of vultures, a spiral movement around the chosen powerful agent is generated as follows:

$$S1 = R_i(t) \times \left(\frac{rand \times P_i(t)}{2\pi}\right) \times \cos\left(P_i(t)\right) \quad (3.24)$$

$$S2 = R_i(t) \times (\frac{rand \times P_i(t)}{2\pi}) \times \sin(P_i(t)) \quad (3.25)$$

$$P_i(t+1) = R_i(t) - (S1 + S2) \quad (3.26)$$

The completion of Stage 1 in the intensification process is then achieved by employing one of its strategies for each vulture. The activation of either strategy is governed by a defined probability of selection, as outlined below:

$$P_i(t+1) = \begin{cases} Equation\ 3.22\ if\ rand_{P2} \geq P_2 \\ Equation\ 3.26\ if\ rand_{P2} < P_2 \end{cases} \quad (3.27)$$

Where $rand_{P2}$ is a random value in the interval [0,1], and P_2 is a constant that needs to be set.

- **Stage 2:** The intensification process attains the second stage when the vultures have been drained. This happens with the condition $|F| \leq 0.5$. Again, two operations characterize this stage:
  - **Foregathering of vultures around the food source:** When exhausted, the vultures crowd and scramble towards the food location. This behaviour is modelled ad follows:

$$P_i(t+1) = \frac{A_1 + A_2}{2} \quad (3.28)$$

Where A_1 and A_2 are calculated as follows:

$$A_1 = BestVulture_1 - \frac{BestVulture_1 \times P_i(t)}{BestVulture_1 - P_i(t)^2} \times F \quad (3.29)$$

$$A_2 = BestVulture_2 - \frac{BestVulture_2 \times P_i(t)}{BestVulture_2 - P_i(t)^2} \times F \quad (3.30)$$

  - **Aggressive Behaviour :** To simulate the aggressive food-foregathering, levy flight movement is employed with the following equation:

$$P_i(t+1) = R_i(t) - |d| \times F \times Levy(D) \quad (3.31)$$

With $|d|$ being the distance between the vulture and the chosen powerful agent R and D denotes the number of entailed variables. The Levy flight is generated as follows:

$$Levy(\lambda) = 0.01 \times \frac{U}{|V|^{1/\lambda}} \quad (3.32)$$

Where U and V follow the normal distribution of zero mean and deviations σ_v and σ_u

$$U \sim N(0, \sigma_u^2) \quad (3.33)$$

$$V \sim N(0, \sigma_v^2) \quad (3.34)$$

σ_v and σ_u are set to:

$$\sigma_v = 1 \quad (3.35)$$

$$\sigma_v^2 = \left[\frac{\Gamma(1+\lambda)}{\lambda\Gamma((1+\lambda)/2)} \cdot \frac{\sin(\frac{\pi\lambda}{2})}{2^{(\lambda-1)/2}}\right]^{1/\lambda} \tag{3.36}$$

Where Γ represents the gamma function.

Similarly, the completion of Stage 2 is performed by choosing either one of the two mentioned behaviours. Again, a probability of selection P_3 is employed to activate either action:

$$P_i(t+1) = \begin{cases} Equation\ 3.28\ if\ rand_{P3} \geq P_3 \\ Equation\ 3.31\ if\ rand_{P3} < P_3 \end{cases} \tag{3.37}$$

The general layout of the African Vulture Optimizer is given in the flowchart of Figure 3.5.

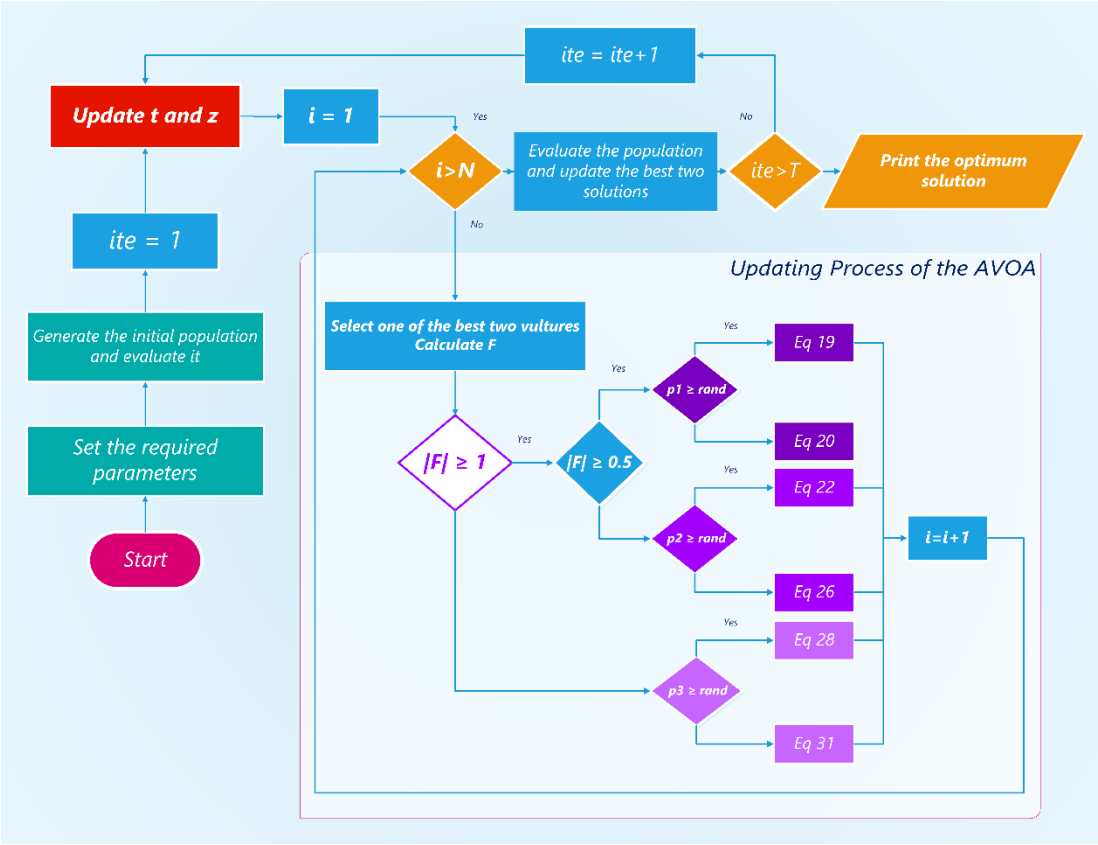

Figure 3.5 The AVOA Flowchart

3.3.2 Improved African Vultures Algorithm

While the standard AVOA optimizer demonstrated good performance in solving benchmark functions and various engineering problems, we have incorporated a few amendments that will help the algorithm achieve a better exploration-exploitation

balance and, consequently, higher performance. The motives are explained below, along with the associated suggested enhancements.

A. Refined Exploration Process:

When testing the standard AVOA optimizer, it was discovered that when equation 3.20 is invoked, the vultures regularly move either close or beyond the limits of the search space, reducing the algorithm's global search capabilities. To address this problem, equation 3.20 has been replaced with a simpler, yet more performant, one:

$$P_i(t+1) = V_{r1}(t) + F \times (V_{r2}(t) - V_{r3}(t)) \tag{3.38}$$

V_{r1}, V_{r2}, V_{r3} are three different solutions randomly selected from the population.

B. Two-fold Strategy:

The search operations of the conventional African Vultures Optimizer are in most cases directed by the best two found solutions. As a result, the diversification phase is constrained to the vicinity of those best two vultures. This might orient the population to stray away from other potential optimum regions and therefore increasing the likelihood of premature convergence. To prevent local optimum entrapment, equation 3.38 is incorporated in a second search phase when the standard operations of the African Vultures Optimizer are completed. This way provides the algorithm a chance to scan more regions of the search space that would otherwise be missed by the AVOA's equations.

To ensure that the exploration phase is not over-promoted, we incorporate alongside with equation 3.38, a new mechanism having local search tendencies to enhance the intensification process:

$$P_i(t+1) = R_i(t) + rand \times e^{-abs(R_i(t)-P_i(t))^2} \times (R_i(t) - P_i(t)) \tag{3.39}$$

The two equations form together a Two-fold search mechanism that incorporates both exploration and exploitation movements. The position update of an individual vulture is conducted as follows:

$$P_i(t+1) = \begin{cases} V_{r1}(t) + F \times \left(V_{r2}(t) - V_{r2}(t)\right) \ \ if\ rand \geq 0.5 \\ R_i(t) + rand \times e^{-abs(R_i(t)-P_i(t))^2} \times (R_i(t) - P_i(t)) \ \ if\ rand < 0.5 \end{cases} \tag{3.40}$$

C. Memory Saving:

To enhance the quality of solutions as the iterative process progresses, the new position of the individual vulture replaces its previous position if it produces a better fitness value.

The flowchart of the Improved African Vultures Optimizer is illustrated in Figure 3.6. As can be seen, the integrated approach offers a second search operation for the population and an effective scan of the search space.

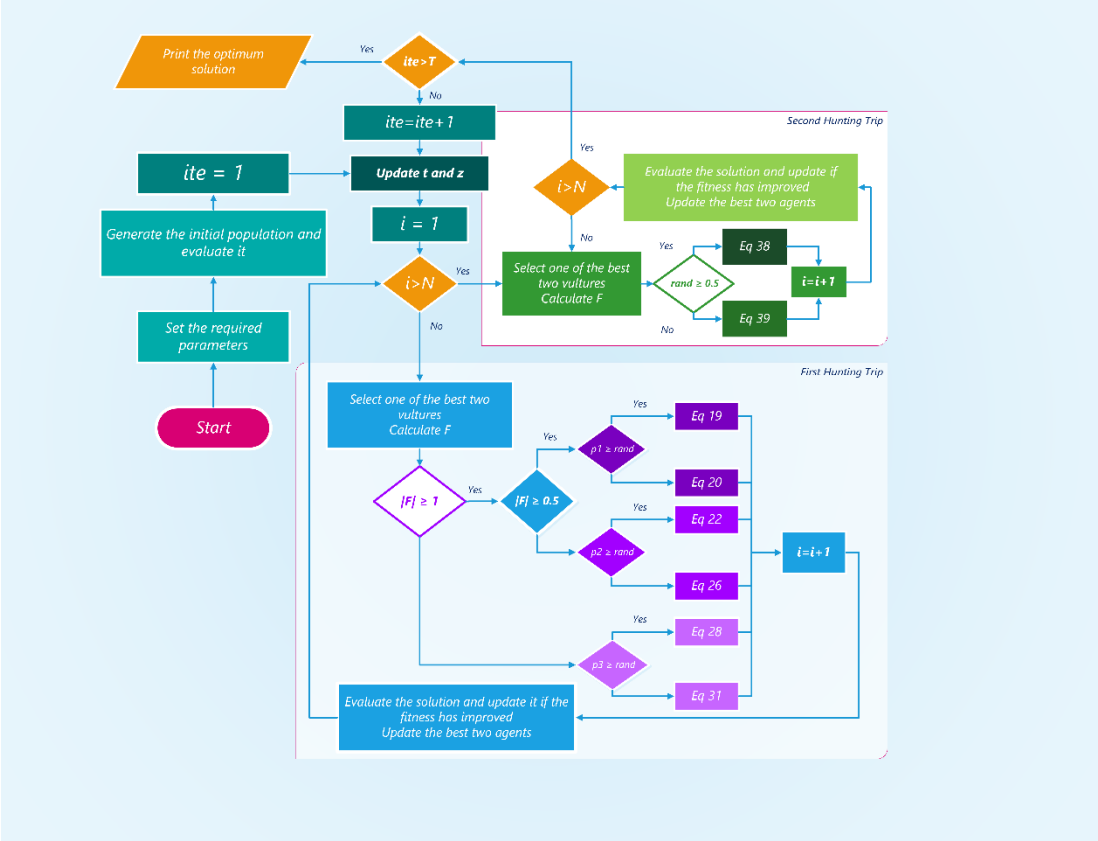

Figure 3.6 The IAVOA Flowchart

3.4 EXPERIMENTAL VALIDATION

This section is devoted to the evaluation of the proposed algorithm in extracting the unknown parameters of photovoltaic devices. All the assessments on the proposed IAVOA were carried out in MATLAB R2017b and all simulations are executed on a PC with Intel Core™ I3-4005U CPU @ 1.70GHz, 4GB RAM, under Windows 10 64-bit OS.

3.4.1 Dataset Description

The benchmark assessments conducted in this work involve the following case studies:

- The RTC France model, which is a 57mm diameter commercial silicon based solar cell. The experiments covered SDM, DDM and TDM cases, and the experimental

IV data is taken from [15], at which the measurements were under a temperature of 33°C and an irradiance intensity of 1000/m².

- For PV modules modelling, three commercial models extensively used in the literature have been investigated in this study, each of which comprises 36 serially connected solar cells. The poly-crystalline Photowatt-PWP201 under temperature 45°C, acquired from [15], the mono-crystalline STM6-40/36 under temperature 51°C, and the poly-crystalline STP6-120/36 under temperature 55°C which are both adopted from [84].

3.4.2 Parameters Settings

To assess the overall performance of the designed algorithm in extracting the PV parameters, it was executed on 30 distinct run in each PV device. The best Root Mean Squared Error (RMSE) result obtained in each run was recorded. Regarding the population size and the maximum number of iterations, they have been fixed respectively at 30 and 1000 for the RTC France cell with the SDM case. However, both settings were increased respectively to 50 and 1200 for the DDM and the TDM cases due to the higher complexity associated with both models. For PV modules, the population size was set at 30, and the maximum number of iterations was fixed at 800 across all the investigated devices. The algorithm parametrization was set as recommended by the developers of the AVOA optimizer as given in Table 3.1, and the constraints for each PV parameter are provided in Table 3.2.

Table 3.1 Algorithm's Parameters

Parameter	Selected Value
L_1	0.8
L_2	0.2
p_1	0.6
p_2	0.4
p_3	0.6
w	2.5

Table 3.2 Selected bounds for the used models

Parameters	RTC France		Photowatt-PWP201		STM6-40/ 36		STP6-120/36	
	LB	UB	LB	UB	LB	UB	LB	UB
$I_{ph}(A)$	0	2	0	2	0	10	0	10
$I_o, I_{o1}, I_{o2}, I_{o3}(\mu A)$	0	$1E-3$	0	$1E-4$	0	$1E-4$	0	$1E-4$
a, a_1, a_2, a_3	0	20	0	100	0	100	0	100
$R_s(\Omega)$	0	0.5	0	2	0	2	0	2
$R_{sh}(\Omega)$	1	1000	1	1000	1	1500	1	1500

3.4.3 Performance Indicators

As mentioned earlier, the Root Mean Square Error (RMSE) has been employed as the central objective function for the optimization process. To provide a comprehensive analysis on the accuracy of the designed algorithm, the Absolute errors (AE) between the produced and the measured current pairs have been calculated. This indicator gives a point-by-point deviation between the used experimental data and the produced PV model.

$$AE(i) = |I_{Measured}(i) - I_{Calculated}(i)| \quad i = 1,2 \dots\dots, N \tag{3.41}$$

$$SAE = \sum_{i=1}^{N} AE(i) \tag{3.42}$$

3.4.4 Case study 1: RTC France

Given its widespread usage in the literature, the conducted experiments on the R.T.C France cell covered the SDM, the DDM, and the TDM cases. For each model, the best, the worst, and the mean of the recorded RMSE values are reported in the results.

A. Single Diode Model (SDM):

The produced parameters associated with the best conducted run for the SDM based RTC France cell are provided in Table 3.3. It is perceivable from the table that the best and the worst RMSE values are nearly equal, which reflected in the small obtained Standard deviation. Regarding the convergence speed, the designed IAVOA optimizer consumed on average 27500 functions evaluations across 30 distinct executions. For visual confirmation, Figure 3.7 exposes the convergence plot corresponding to a certain trial form the conducted 30 runs. The pronounced downward trend in the plot at the early iterations underscores the optimizer's rapid convergence behaviour.

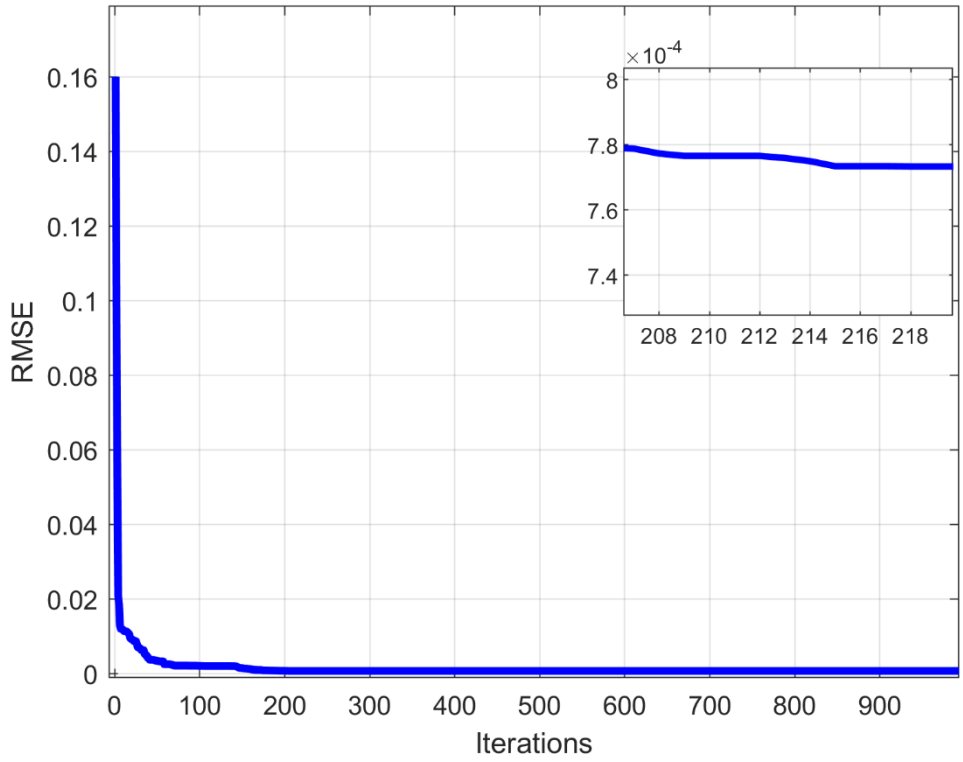

Figure 3.7 Convergence Curve of the SDM based RTC Cell

In order to evaluate the algorithm's accuracy even further, Table 3.4 records the Absolute Errors (AE) between the estimated currents of the produced PV model and the experimental currents for every data point. By screening the table, the largest error value was 0.001585 obtained at the 13th point, which is negligibly small. To provide a clearer picture of the accuracy, the produced PV parameters have been used to create the IV and PV plots along with the experimental data points as shown in Figure 3.8. The figure demonstrates the great fitting accuracy of the produced model in passing along all the experimental data points, reflecting the high performance of the developed algorithm.

Table 3.3 Results of the IAVOA Optimizer in the SDM based RTC France Cell

Extracted parameters		RMSE Values		NFEs	
$I_{ph}(A)$	0.7608	Min	0.000773006268994119	Min	15420
$I_o(\mu A)$	0.31068	Max	0.000773006385642382	Max	36270
a	1.4773	Mean	0.000773006277758790	Mean	27500
$R_s(\Omega)$	0.0365	STD	$2.7641587930413E-11$		
$R_{sh}(\Omega)$	52.8898				

Table 3.4 Calculated Current of the estimated RTC France Single Diode Model

Data point	$V_{measured}(V)$	$I_{measured}(A)$	$I_{Calculated}(A)$	Absolute Error(A)
1	-0.2057	0.764	0.764149	0.000149
2	-0.1291	0.762	0.762702	0.000702
3	-0.0588	0.7605	0.761374	0.000874
4	0.0057	0.7605	0.760155	0.000345
5	0.0646	0.76	0.759039	0.000961
6	0.1185	0.759	0.758011	0.000989
7	0.1678	0.757	0.757046	4.57E-05
8	0.2132	0.757	0.756085	0.000915
9	0.2545	0.7555	0.755022	0.000478
10	0.2924	0.754	0.753597	0.000403
11	0.3269	0.7505	0.751327	0.000827
12	0.3585	0.7465	0.747305	0.000805
13	0.3873	0.7385	0.740085	0.001585
14	0.4137	0.728	0.727426	0.000574
15	0.4373	0.7065	0.707026	0.000526
16	0.459	0.6755	0.6754	9.97E-05
17	0.4784	0.632	0.630998	0.001002
18	0.496	0.573	0.572175	0.000825
19	0.5119	0.499	0.499539	0.000539
20	0.5265	0.413	0.413485	0.000485
21	0.5398	0.3165	0.317162	0.000662
22	0.5521	0.212	0.212017	1.67E-05
23	0.5633	0.1035	0.102637	0.000863
24	0.5736	-0.01	-0.0093	0.000702
25	0.5833	-0.123	-0.12436	0.001361
26	0.59	-0.21	-0.2091	0.000898
SAE				0.0176321

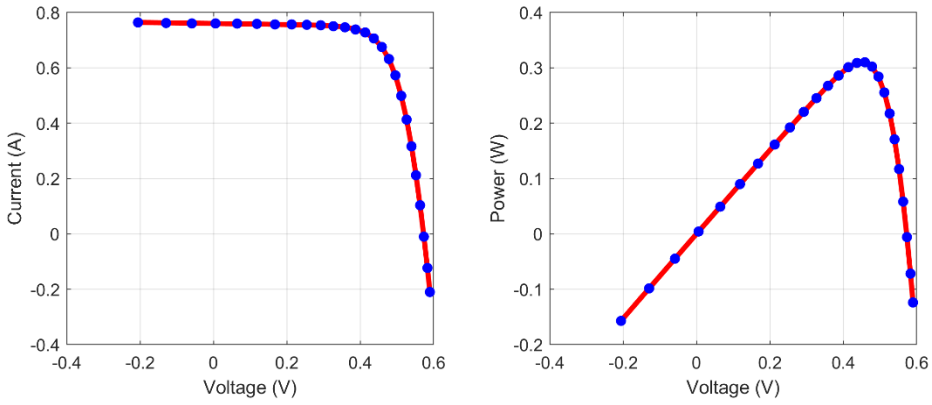

Figure 3.8 Estimated SDM Curves for the RTC Cell

To showcase the superior performance of the designed optimizer, the results of some of the well-regarded and recent algorithms for the Single Diode Model are provided in Table 3.5. The table clearly indicates that the Improved AVOA optimizer surpassed most of the techniques, except the NLBMA and the HROA algorithms, both of which provided fitness values of 7.73006E-4.

Table 3.5 Comparison among several existing works for the SDM based RTC France

Algorithm	$I_{ph}(A)$	$I_o(\mu A)$	a	$R_s(\Omega)$	$R_{sh}(\Omega)$	RMSE
IAVOA	0.7608	0.31068	1.4773	0.0365	52.8898	$7.73006E-4$
NLBMA[46]	0.7608	0.31068	1.5177	0.0365	52.8898	$7.73006E-4$
HROA[63]	NA	NA	NA	NA	NA	$7.73006E-4$
COA[44]	0.760788	0.31069	1.47727	0.03655	52.8898	$7.7301E-4$
TVACPSO[28]	0.760788	0.3106827	1.475258	0.036547	52.889644	$7.7301E-4$
ELPSO[29]	0.760787966	0.3106775	1.475256	0.036547	52.88979426	$7.7301E-4$
AEA[62]	0.76079	0.31067	1.4771	0.036547	52.8891	$7.7301E-4$
FFO[40]	0.7608	0.3223	1.5215	0.0364	53.8989	$7.75184E-4$
EJADE[25]	0.7608	0.3230	1.4812	0.0364	53.7185	$9.8602E-4$
GNDO[65]	0.76078	0.32302	1.48118	0.03638	53.71852	$9.8602E-4$
CCNMHHO[76]	0.760776	3.2302	1.4811827	0.036377	53.7181	$9.8602E-4$
EABOA[69]	0.760771077	0.322929	1.481153457	0.036379593	53.76600144	$9.8602E-4$
EHHO[38]	0.760775	0.323	1.481238	0.036375	53.74282	$9.8602E-4$
pSFS[59]	0.76078	0.32302	1.48118	0.03638	53.71852	$9.8602E-4$
SDO[71]	0.7608	0.3230	1.4812	0.0364	53.7185	$9.8602E-4$
WHHO[73]	0.76077551	0.32302031	1.48110808	0.03637710	53.71867407	$9.8602E-4$
ITLBO[33]	0.7608	0.3230	1.4812	0.0364	53.7185	$9.8602E-4$
IMPA[74]	0.760775530	0.323020816610	1.481183592125	0.0363770925809	53.71852392	$9.86021E-4$
EOTLBO[85]	0.76077553	0.32302083	1.48118359	0.03637709	53.71852514	$9.86022E-4$
IEO[72]	0.760775529	0.323	1.481183	0.036377	53.71852	$9.86023E-4$
CPMPSO[30]	0.760776	0.323021	1.481184	0.036377	53.71852	$9.86022E-4$
SEDE[70]	0.760776	0.323021	1.4811836	0.03637709	53.718524	$9.86022E-4$
NMSOLMFO[59]	0.760775529	0.323021	1.481183605	0.036377092	53.71853135	$9.86022E-4$
BHCS[61]	0.76078	0.32302	1.48118	0.03638	53.71852	$9.86022E-4$
IJAYA[31]	0.7608	0.3228	1.4811	0.0364	53.7595	$9.8603E-4$
GWOCS[75]	0.760773	0.32192	1.4808	0.03639	53.6320	$9.8607E-4$
GBAS[66]	0.7607	0.3247	1.4817	0.0363	53.7669	$9.861E-4$

B. Double Diode Model (DDM):

The identified PV parameters for the DDM based RTC France Cell, along with the major results of the 30 conducted runs are outlined in Table 3.6. Regarding the convergence speed, the average NFEs dissipated by the optimizer was higher than that of the SDM experiments, due to the higher number of parameters.

One can observe that the extracted value of the ideality factor a_1 exceeds the values commonly found in the literature. This is due to the extended search interval used for both a_1 and a_2, allowing an in-depth scan of the different optimum regions in the search space. As reported, the produced value of a_1 was 7.1823, which to the best of our knowledge was not previously found by any existing work. This value clearly was the key to reach an RMSE score of 6.9096E-4, beating all of the other optimizers as shown in Table 3.8.

Table 3.6 Results of the IAVOA Optimizer in the DDM based RTC France Cell

Extracted parameters		RMSE values		NFEs	
$I_{ph}(A)$	0.7610	Min	0.000690958517348360	Min	29509
$I_{o1}(\mu A)$	0.31068	Max	0.000691056936394593	Max	48750
$I_{o2}(\mu A)$	0.21763	Mean	0.000690962488814250	Mean	39429

a_1	7.1823	STD	$1.802294898129788E-11$
a_2	1.4432		
$R_s(\Omega)$	0.0365		
$R_{sh}(\Omega)$	52.8898		

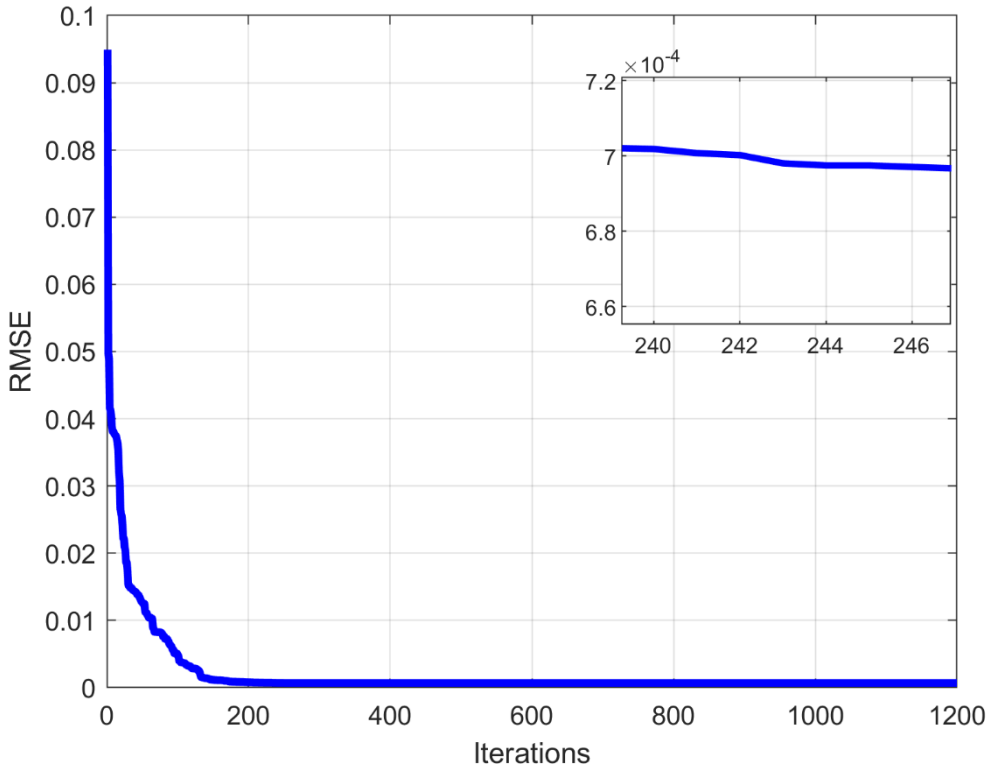

Figure 3.9 Convergence Curve of the IAVOA Optimizer in the DDM based RTC Cell

The deviations between the measured currents and the calculated currents associated with the produced model are provided in Table 3.7. By screening the chart, the largest AE value was 0.001337 obtained at the 25th point, and the Sum of the Absolute Errors was 0.0157, which are both smaller than the errors produced with the SDM experiments. This outstanding fitting performance is clearly visible in generated IV and PV plots of Figure 3.10.

Table 3.7 Calculated Current of the estimated RTC France Double Diode Model

Data point	$V_{measured}(V)$	$I_{measured}(A)$	$I_{Calculated}(A)$	Absolute Error$((A)$
1	-0.2057	0.764	0.763397	0.000603
2	-0.1291	0.762	0.762393	0.000393
3	-0.0588	0.7605	0.761409	0.000909
4	0.0057	0.7605	0.760464	3.55E-05
5	0.0646	0.76	0.759516	0.000484
6	0.1185	0.759	0.758559	0.000441
7	0.1678	0.757	0.75757	0.00057
8	0.2132	0.757	0.756495	0.000505
9	0.2545	0.7555	0.755246	0.000254
10	0.2924	0.754	0.753588	0.000412
11	0.3269	0.7505	0.751079	0.000579
12	0.3585	0.7465	0.746866	0.000366
13	0.3873	0.7385	0.739559	0.001059
14	0.4137	0.728	0.726955	0.001045
15	0.4373	0.7065	0.706741	0.000241
16	0.459	0.6755	0.675376	0.000124
17	0.4784	0.632	0.631203	0.000797
18	0.496	0.573	0.572493	0.000507
19	0.5119	0.499	0.499825	0.000825
20	0.5265	0.413	0.413624	0.000624
21	0.5398	0.3165	0.317111	0.000611
22	0.5521	0.212	0.211811	0.000189
23	0.5633	0.1035	0.102373	0.001127
24	0.5736	-0.01	-0.00949	0.000509
25	0.5833	-0.123	-0.12434	0.001337
26	0.59	-0.21	-0.20883	0.001175
SAE				0.0157215

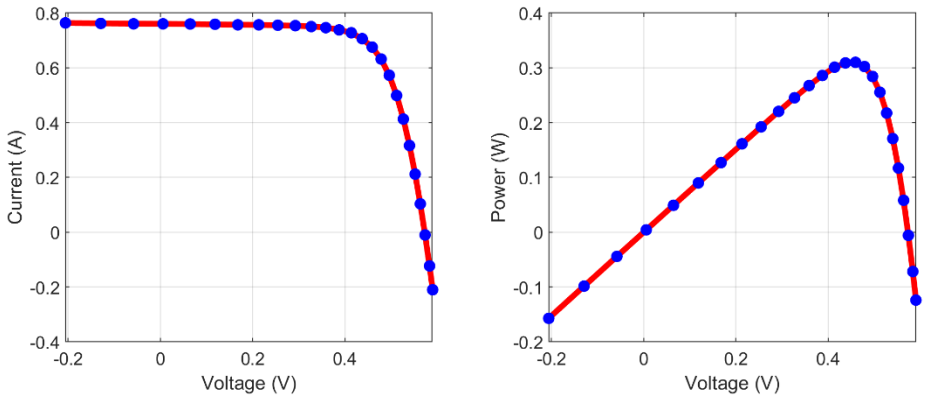

Figure 3. 10 Estimated DDM Curves for the RTC Cell

Table 3.8 Comparison among several existing works for the DDM based RTC France

	$I_{ph}(A)$	$I_{o1}(\mu A)$	$I_{o2}(\mu A)$	a_1	a_2	$R_s(\Omega)$	$R_{sh}(\Omega)$	RMSE
IAVOA	0.7610	0.31068	0.21763	7.1823	1.4432	0.0365	52.8898	$6.9096E-4$
COA[44]	0.76081	0.08656	0.21597	1.37278	2.00000	0.03803	58.3562	$7.3265E-4$
ELPSO[29]	0.760808	1	0.099168	1.835767	1.386091	0.037551	55.920471	$7.424E-4$
TVACPO[28]	0.760809	0.040467	0.927465	1.327160	1.735315	0.037973	56.549605	$7.4365E-4$
AEA[62]	0.76081	0.089974	0.13523	1.8662	1.4111	0.037239	55.5501	$7.4623E-4$
HROA[63]	NA	NA	NA	NA	NA	NA	NA	$7.4943E-4$

NLBMA[46]	0.7605	0.0823	1.8092	1.4078	2	0.0380	60.9892	$7.5242E-4$
FFO[40]	0.7605	0.0302	1.0891	1.3425	1.8042	0.0384	59.4346	$7.63569E-4$
EJADE[25]	0.7608	0.2260	0.7493	1.4510	2	0.0367	55.4854	$9.8248E-4$
ITLBO[33]	0.7608	0.2260	0.7493	1.4510	2	0.0367	55.4854	$9.8248E-4$
GNDO[65]	0.76078	0.74935	0.22597	2.00000	1.45102	0.03674	55.48544	$9.8248E-4$
IMPA[74]	0. 7607810	0. 225974	0.74934	1. 9999	1. 4510	0. 0367404	55.485443	$9.824848E-4$
EOTLBO[85]	0. 7607810	0. 225974	0.74934	1. 9999	1. 4510169	0. 0367404	55.485436	$9.824848E-4$
IEO[72]	0.760781	0.749	0.226	1.451016	1.999999	0.036740	55.48544	$9.824848E-4$
CPMPSO[30]	0.76078	0.74935	0.22597	2	1.45102	0.03674	55.48544	$9.824849E-4$
SEDE[70]	0.7608	0.7493	0.2260	2.0000	1.4510	0.0367	55.4854	$9.824849E-4$
NMSOLMFO[59]	0.76078107	0.749349	0.22597	1.45101665	2	0.03674043	55.4854380	$9.82485E-4$
WHHO[73]	0.76078094	0.228574	0.727182	1.451895	2	0.03672887	55.42643282	$9.82487E-4$
CCNMHHO[76]	0.76078	0.749	0.226	1.451895	2	0.03674	55.42643282	$9.8249E-4$
SDO[71]	0.7608	0.7879	0.2214	2.0000	1.4493	0.0368	55.5705	$9.8250E-4$
pSFS[58]	0.76078	0.84161	0.21545	2	0.03679	0.03679	55.72835	$9.8255E-4$
EHHO[38]	0.760769017	5.86184E-1	0.240965	1.456910409	1.9684514	0.036598831	55.63943956	$9.8360E-4$
EABOA[69]	0.76082865	0.25072	0.72069	1.45988481	1.99997318	0.03662660	55.3660129	$9.8607E-4$

C. Triple Diode Model (TDM):

The extracted parameters for the TDM based RTC France cell, along with the obtained RMSE and NFE scores are provided in Table 3.9. The convergence plot associated with an arbitrary experiment is depicted in Figure 3.11. Similar to the scenario encountered in the Double Diode Model (DDM) experiments, the application of the suggested extended range for the ideality factors resulted in values outside the commonly used interval [0, 2]. The obtained a_1 and a_2 reached 6.8367 and 6.8576 respectively yielding an RMSE value of 7.40109E-4 which surpasses existing works as reported in Table 3.11.

Table 3.9 Results of the IAVOA Optimizer in the TDM based RTC France Cell

Extracted parameters		RMSE Values		NFEs	
$I_{ph}(A)$	0.7610	Min	0.000741019433626185	Min	33872
$I_{o1}(\mu A)$	111.31	Max	0.000741234876708584	Max	49959
$I_{o2}(\mu A)$	440.72	Mean	0.00074104333430949	Mean	43152
$I_{o3}(\mu A)$	0.20418	STD	$4.190561506156936E-8$		
a_1	6.8367				
a_2	6.8576				
a_3	1.4372				

$R_s(\Omega)$	0.0377
$R_{sh}(\Omega)$	85.7248

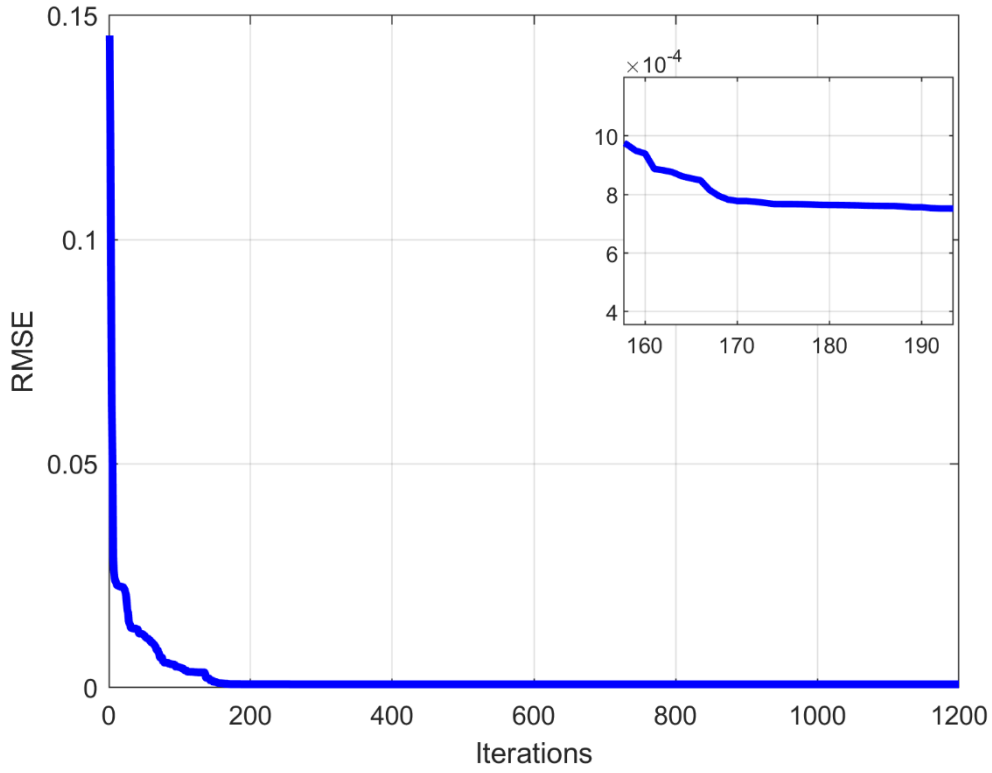

Figure 3. 11 Convergence Curve of the IAVOA Optimizer in the TDM based RTC Cell

Table 3.10 Calculated Current of the estimated RTC France Triple Diode Model

Data point	$V_{measured}(V)$	$I_{measured}(A)$	$I_{Calculated}(A)$	Absolute Error$((A)$
1	-0.2057	0.764	0.763383	0.000617
2	-0.1291	0.762	0.762381	0.000381
3	-0.0588	0.7605	0.761399	0.000899
4	0.0057	0.7605	0.760537	3.69E-05
5	0.0646	0.76	0.759513	0.000487
6	0.1185	0.759	0.758557	0.000443
7	0.1678	0.757	0.757566	0.000566
8	0.2132	0.757	0.756487	0.000513
9	0.2545	0.7555	0.75523	0.00027
10	0.2924	0.754	0.753564	0.000436
11	0.3269	0.7505	0.751053	0.000553
12	0.3585	0.7465	0.74685	0.00035
13	0.3873	0.7385	0.739569	0.001069
14	0.4137	0.728	0.727012	0.000988
15	0.4373	0.7065	0.706857	0.000357
16	0.459	0.6755	0.675548	4.78E-05
17	0.4784	0.632	0.630569	0.001431
18	0.496	0.573	0.572688	0.000312
19	0.5119	0.499	0.499976	0.000976
20	0.5265	0.413	0.413707	0.000707
21	0.5398	0.3165	0.317124	0.000624
22	0.5521	0.212	0.21177	0.00023
23	0.5633	0.1035	0.102308	0.001192

24	0.5736	-0.01	-0.00954	0.000456
25	0.5833	-0.123	-0.12434	0.001339
26	0.59	-0.21	-0.20877	0.001234
SAE				0.0165147

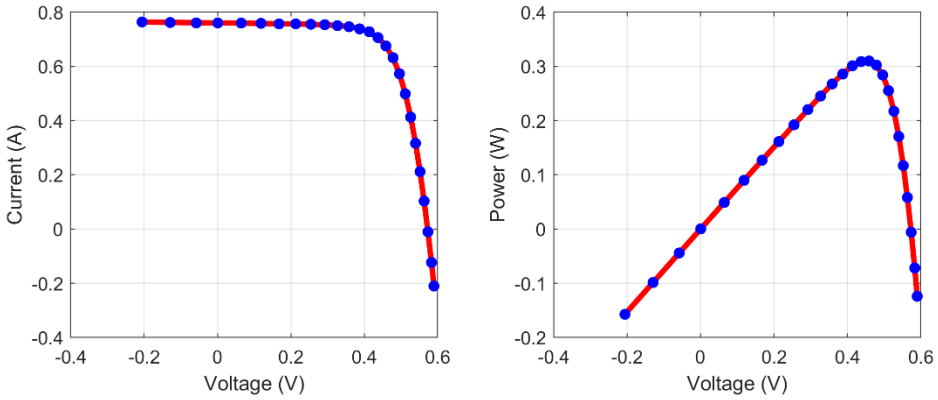

Figure 3.12 Estimated TDM Curves for the RTC Cell

Table 3.11 Comparison among different existing works

	IAVOA	GNDO[67]	WHHO[73]	GBO[60]	I-GWO[68]	GBAS[66]
$I_{ph}(A)$	0.7610	0.760500	0.76078248	0.7607769	0.7607	0.7607
$I_{o1}(\mu A)$	0.20363	9.08e-8	0.23910895	0.78129	0.227	0.0231
$I_{o2}(\mu A)$	$6.3016E-6$	1.96e-6	0.43972073	0.2215560	0.314	0.0363
$I_{o3}(\mu A)$	545.35	1.58e-7	0.8	0.00721	0.234	0.2746
a_1	1.4370	1.3766	1.45393749	1.9999	1.9256	1.9933
a_2	19.4996	2	2	1.449384849	1.96	1.7794
a_3	6.8188	2	2.40415974	1.9756526	1.45	1.4697
$R_s(\Omega)$	0.0377	0.0380	0.03672493	0.036758	0.0367	55.5354
$R_{sh}(\Omega)$	85.6027	61.3221	55.64995795	55.62330625	54.888	55.5354
RMSE	$7.40109E-4$	$7.50683E-4$	$9.80751E-4$	$9.82503E-4$	$9.83310E-4$	$9.88820E-4$

3.4.5 PV Modules Modelling:

A. Case Study 4: The Photowatt-PWP201 Module

The yielded PV parameters for the Photowatt-PWP201 module are documented in Table 3.12 along with the RMSE and the NFE detailed outcomes. For further accuracy examination, the produced PV model is employed to generate the IV and the PV plots alongside the data points as depicted in Figure 3.14. Once again, the PV model curves align perfectly with the experimental data, reflecting the high fitting accuracy of the designed optimizer.

Table 3.12 Results of the IAVOA Optimizer in the SDM based Photowatt-PWP201

Extracted parameters		RMSE Values		NFEs	
$I_{ph}(A)$	1.0324	Min	0.00203999227321625	Min	11486
$I_o(\mu A)$	2.4966	Max	0.00204294894604182	Max	25933
a	1.3166	Mean	0.00204107788803000	Mean	20142
$R_s(\Omega)$	1.2405	STD	$5.412072283699546E-7$		
$R_{sh}(\Omega)$	748.323				

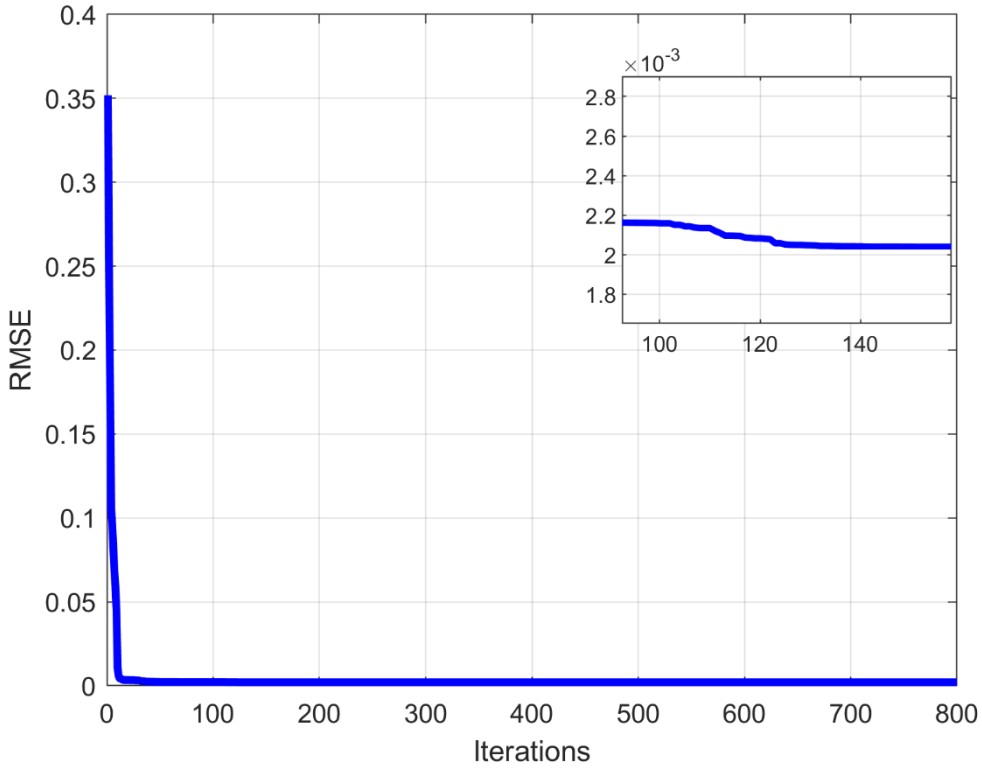

Figure 3. 13 Convergence Curve of the IAVOA Optimizer in the SDM based Photowatt-PWP201 Module

Table 3.13 Calculated Current of the estimated Photowatt-PWP201

Data point	$V_{measured}(V)$	$I_{measured}(A)$	$I_{Calculated}(A)$	Absolute Error(A)
1	-1.9426	1.0345	1.033242	0.001258
2	0.1248	1.0315	1.030478	0.001022
3	1.8093	1.03	1.028211	0.001789
4	3.3511	1.026	1.026093	9.33E-05
5	4.7622	1.022	1.02404	0.00204
6	6.0538	1.018	1.021878	0.003878
7	7.2364	1.0155	1.019269	0.003769
8	8.3189	1.014	1.015591	0.001591
9	9.3097	1.01	1.009786	0.000214
10	10.2163	1.0035	1.000208	0.003292
11	11.0449	0.988	0.984576	0.003424
12	11.8018	0.963	0.96009	0.00291
13	12.4929	0.9255	0.923857	0.001643
14	13.1231	0.8725	0.873621	0.001121
15	13.6983	0.8075	0.808297	0.000797
16	14.2221	0.7265	0.728648	0.002148
17	14.6995	0.6345	0.636704	0.002204
18	15.1346	0.5345	0.535455	0.000955
19	15.5311	0.4275	0.428182	0.000682

20	15.8929	0.3185	0.317799	0.000701
21	16.2229	0.2085	0.206939	0.001561
22	16.5241	0.101	0.097576	0.003424
23	16.7987	-0.008	-0.00864	0.000639
24	17.0499	-0.111	-0.11099	1.23E-05
25	17.2793	-0.209	-0.20858	0.000425
26	17.4885	-0.303	-0.30084	0.002163
SAE				0.0437556

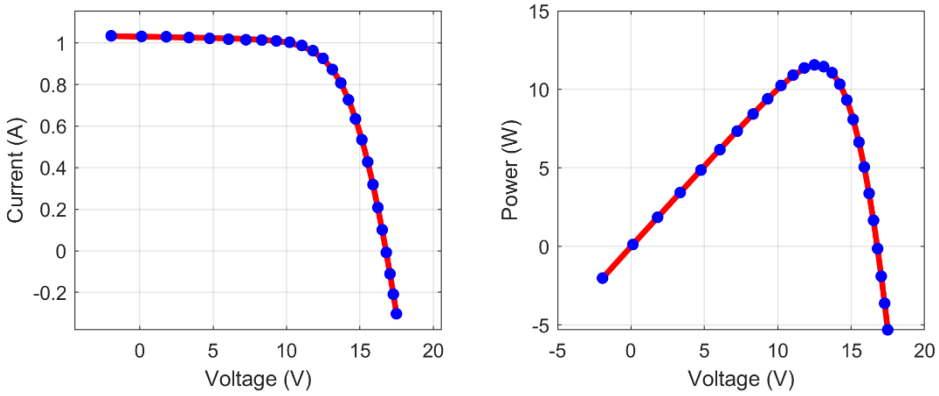

Figure 3.14 Estimated Model Curves for the Photowatt-PWP201 Module

Table 3.12 reports the outcomes obtained by other existing techniques from the literature. The table shows that the NLBMA secures the first position with a fitness value of 1.9827E-3, followed by the designed IAVOA optimizer with a fitness score of 2.04E-3 surpassing the other remaining contenders.

Table 3.14 Comparison among several existing works for the Photowatt-PWP201

Algorithm	$I_{ph}(A)$	$I_o(\mu A)$	a	$R_s(\Omega)$	$R_{sh}(\Omega)$	RMSE
NLBMA[46]	1.0326	2.5001	1.4059	0.0344	20.2805	$1.9827E-3$
IVAOA	1.0324	2.4966	1.3166	1.2405	748.323	$2.04E-3$
COA[44]	1.03143	2.63808	1.32217	0.03432	22.82338	2.05296E−3
HROA[63]	NA	NA	NA	NA	NA	2.05296E−3
TVACPSO[28]	1.031435	2.638610	47.556652	1.235611	821.59515	$2.053E-3$
SMA[64]	1.0321	2.7735	1.3274	1.2281	789.7152	$2.057E-3$
CCNMHHO[76]	1.0305144	3.480	48.6428	1.20127	981.9633	$2.4250E-3$
GNDO[65]	1.03051	3.482263	48.64283	1.20127	981.98230	$2.42507E-3$
pSFS[58]	1.03051	3.48226	48.64283	1.20127	981.98223	$2.42507E-3$
WHHO[73]	1.030514	3.482109	1.349987	1.201274	981.905230	$2.42507E-3$
IMPA[74]	1.0305142	3.482262	1.3511898	0.03336863	27. 277286	$2.42507E-3$
EOTLBO[85]	1.0305143	3.48226292	48.642834	1.201271	981.982201	$2.42507E-3$
IEO[72]	1.030514254	3.48	48.64292	1.201269	981.9956	$2.425074E-3$
SEDE[70]	1.03051	3.48226	48.642835	1.201271	981.98223	$2.425075E-3$
CPMPSO[30]	1.030514	3.4823	48.64284	1.201271	981.9823	$2.425075E-3$
EABOA[69]	1.03044416	3.5084	48.67132719	1.200630203	991.98307	$2.4250751E-3$

EJADE[25]	1.0305	3.4823	48.6428	1.2013	981.9824	$2.4250751E-3$
IJAYA[31]	1.0305	3.4703	48.6298	1.2016	977.3752	$2.4250751E-3$
ITLBO[33]	1.0305	3.4823	48.6298	1.2013	981.9823	$2.4251E-3$

B. Case Study 5: The STP6-120/36

Table 3.15 displays the obtained outcomes for the STP6-120/36 module. Examining Table 3.16 which documents the deviations between current pairs, and Figure 3.16, which plots the yielded IV and PV curves along with the measured data, it can be inferred that the identified parameters yielded a highly accurate model for the given PV module.

Table 3.15 Results of the IAVOA Optimizer in the SDM based STP6-120/36 Module

Extracted parameters		RMSE Values		NFEs	
$I_{ph}(A)$	7.4753	Min	0.0142510635576854	Min	12034
$I_o(\mu A)$	1.9309	Max	0.0142576674773600	Max	31893
a	12445	Mean	0.0142515255194510	Mean	19929
$R_s(\Omega)$	0.1689	STD	$1.419482301596843E-6$		
$R_{sh}(\Omega)$	570.975				

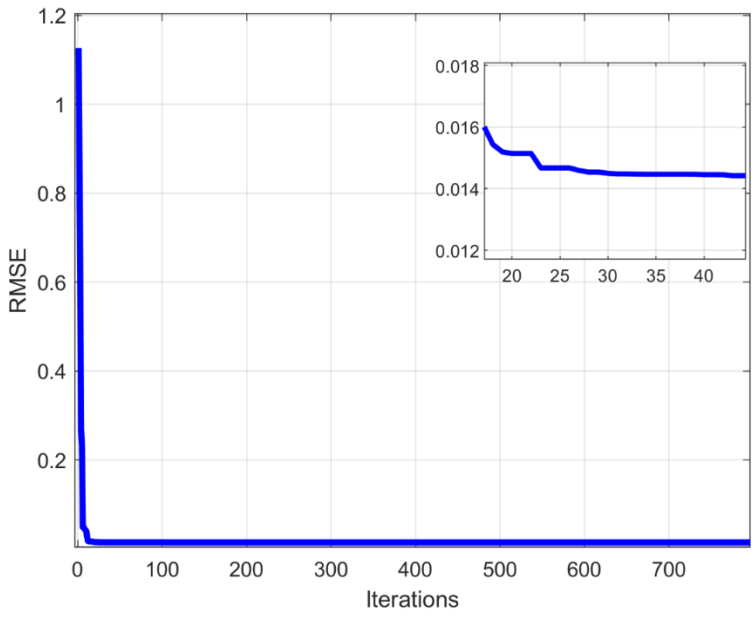

Figure 3.15 Convergence Curve of the IAVOA Optimizer in the SDM based STP6-120/36 Module

Table 3.16 Calculated Current of the estimated STP6-120/36 model

Data point	$V_{measured}(V)$	$I_{measured}(A)$	$I_{Calculated}(A)$	Absolute Error(A)
1	19.21	0	0.004162	0.004162
2	17.65	3.83	3.828384	0.001616
3	17.41	4.29	4.270786	0.019214
4	17.25	4.56	4.543763	0.016237
5	17.1	4.79	4.783935	0.006065
6	16.9	5.07	5.080907	0.010907
7	16.76	5.27	5.273346	0.003346
8	16.34	5.75	5.778048	0.028048
9	16.08	6	6.039533	0.039533
10	15.71	6.36	6.351545	0.008455
11	15.39	6.58	6.571061	0.008939
12	14.93	6.83	6.817934	0.012066
13	14.58	6.97	6.961175	0.008825
14	14.17	7.1	7.090251	0.009749
15	13.59	7.23	7.218851	0.011149
16	13.16	7.29	7.284475	0.005525
17	12.74	7.34	7.331176	0.008824
18	12.36	7.37	7.362455	0.007545
19	11.81	7.38	7.394498	0.014498
20	11.17	7.41	7.418459	0.008459
21	10.32	7.44	7.437027	0.002973
22	9.74	7.42	7.444627	0.024627
23	9.06	7.45	7.450536	0.000536
24	0	7.48	7.473067	0.006933
SAE				0.268231

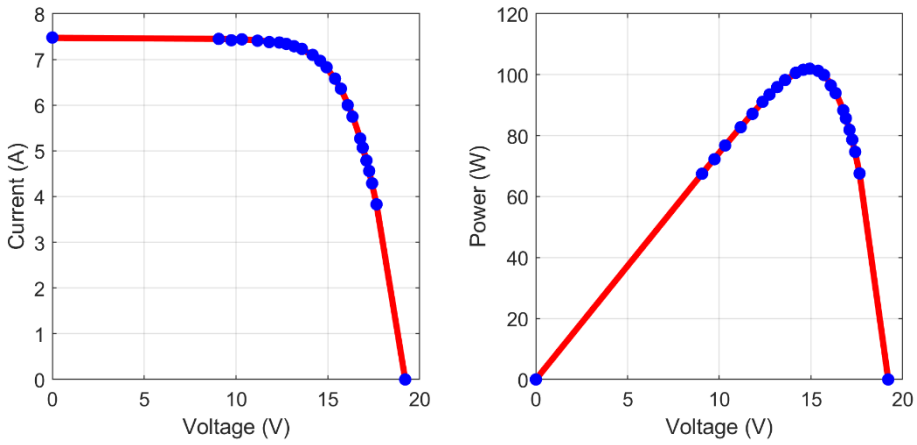

Figure 3.16 Estimated Model Curves for the STP6-120/36 Module

The outcomes obtained by other existing algorithms are summarized in Table 3.17. Once again, the designed algorithm outperformed all the techniques exept the HROA optimizer which obtained the same RMSE value of 1.42510635E-2.

Table 3.17 Comparison among different existing works for the STP6-120/36

Algorithm	$I_{ph}(A)$	$I_o(\mu A)$	a	$R_s(\Omega)$	$R_{sh}(\Omega)$	RMSE
IAVOA	7.4753	1.9309	1.2445	0.1689	570.975	$1.42511E-2$
HROA[63]	NA	NA	NA	NA	NA	$1.42511E-2$
IMPA[74]	7.4725299	2.334994942	1.26010347	0.004594634	22.2198987	$1.66006E-2$
CPMPSO[30]	7.47253	2.3350	1.26010	0.00459	22.21990	$1.66006E-2$
IEO[72]	7.472531264	2.33	1.260101	0.004595	22.21679	$1.66006E-2$
BHCS[75]	7.47253	2.33499	1.26010	0.00459	22.21990	$1.66006E-2$
EJADE[25]	7.4725	2.3350	1.2601	0.0046	22.2199	$1.6601E-2$
SDO[71]	7.4725	2.3350	1.2601	0.0046	22.2199	$1.6601E-2$
ITLBO[33]	7.4725	2.3350	1.2601	0.0046	22.2199	$1.6601E-2$

C. Case study 6: The STM6-40/36 Module

The estimated model parameters for the STM6-40/36 Module along with the main outcomes of the 30 conducted executions are outlined in Table 3.18. Using the estimated model parameters, the IV and the PV curves were generated as shown in Figure 3.17, which reveals a high degree of accordance with the experimental dataset. In comparison with other relevant works, the designed optimizer once again secures the top rank position with a minimum fitness value of 1.7219E-3 as documented in Table 3.20.

Table 3.18 Results of the IAVOA Optimizer in the SDM based STM6-40/36 Module

Extracted parameters		RMSE Values		NFEs	
$I_{ph}(A)$	1.6639	Min	0.00172192151204172	Min	11944
$I_o(\mu A)$	1.7412	Max	0.00172227866806160	Max	24664
a	1.5205	Mean	0.00172193391382820	Mean	18155
$R_s(\Omega)$	0.1536	STD	$6.513794607000694E-8$		
$R_{sh}(\Omega)$	573.5339				

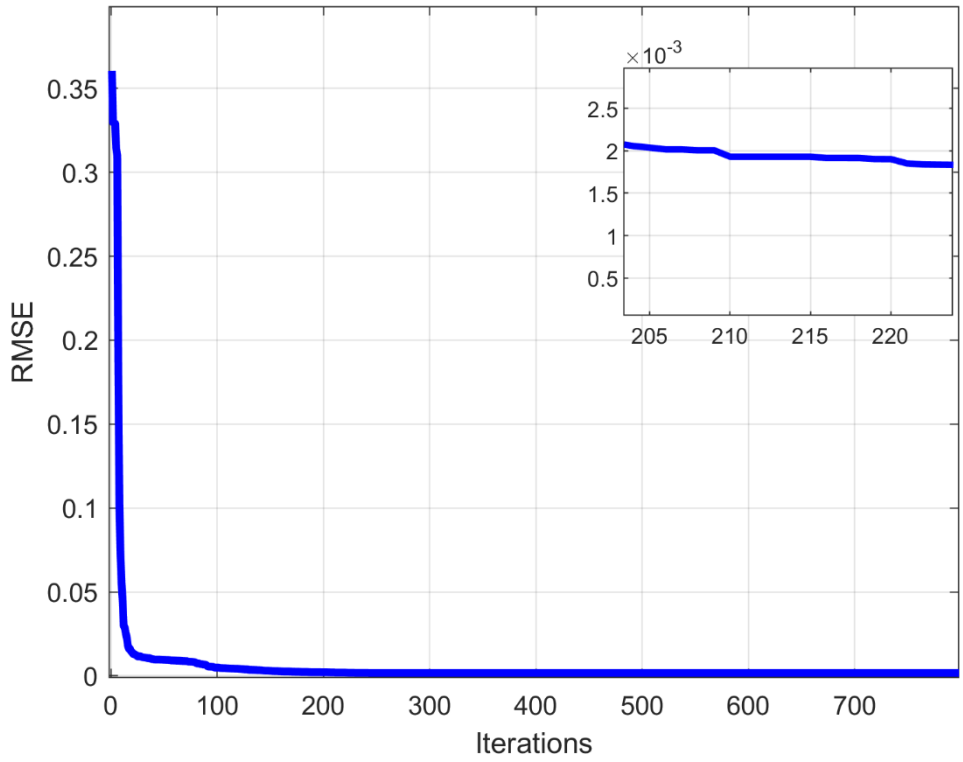

Figure 3.17 Convergence Curve of the IAVOA Optimizer in the SDM based STM6-40/36 Module

Table 3.19 Calculated Current of the estimated STM6-40/36 model

Data point	$V_{measured}(V)$	$I_{measured}(A)$	$I_{Calculated}(A)$	Absolute Error(A)
1	0	1.663	1.663458	0.000458
2	0.118	1.663	1.663252	0.000252
3	2.237	1.661	1.659551	0.001449
4	5.434	1.653	1.653916	0.000916
5	7.26	1.65	1.650568	0.000568
6	9.68	1.645	1.645433	0.000433
7	11.59	1.64	1.639236	0.000764
8	12.6	1.636	1.633716	0.002284
9	13.37	1.629	1.627289	0.001711
10	14.09	1.619	1.618314	0.000686
11	14.88	1.597	1.603065	0.006065
12	15.59	1.581	1.581582	0.000582
13	16.4	1.542	1.542323	0.000323
14	16.71	1.524	1.521221	0.002779
15	16.98	1.5	1.499202	0.000798
16	17.13	1.485	1.485268	0.000268
17	17.32	1.465	1.465641	0.000641
18	17.91	1.388	1.387601	0.000399
19	19.08	1.118	1.11839	0.00039
20	21.02	0	-2.6E-05	2.59E-05
SAE				0.0217919

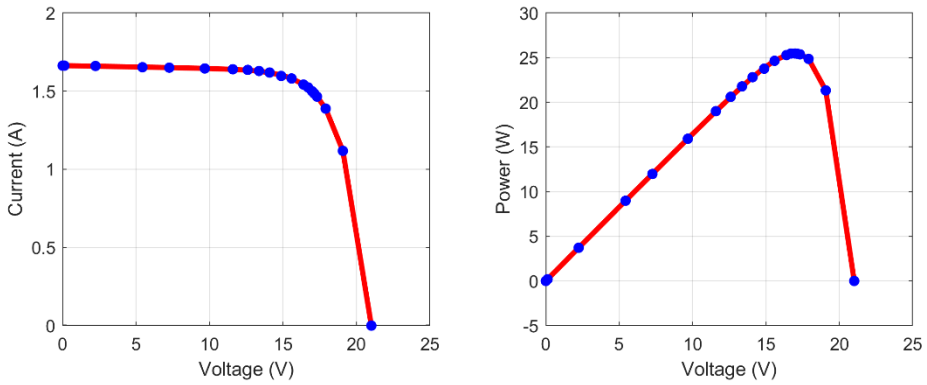

Figure 3.18 Estimated Model Curves for the STM6-46/36 Module

Table 3.20 Comparison among different existing works for the STM6-40/36

Algorithm	$I_{ph}(A)$	$I_o(\mu A)$	a	$R_s(\Omega)$	$R_{sh}(\Omega)$	RMSE
IAVOA	1.6639	1.4712	1.5202	0.1536	573.5339	$1.7219E-3$
EJADE[25]	1.6639	1.7387	1.5203	0.0043	15.9283	$1.7298E-3$
SDO[71]	1.6639	1.7387	1.5203	0.0043	15.9283	$1.7298E-3$
ITLBO[33]	1.6639	1.7387	1.5203	0.0043	15.9283	$1.7298E-3$
BHCS[75]	1.66390	1.73866	1.5203	0.00427	15.92829	$1.72981E-3$
IMPA[74]	1.663904777	1.738656929	1.520302923	0.0042737711	15.928294164	$1.7298137E-3$
CPMPSO[30]	1.663905	1.7387	1.520303	0.004274	15.92829	$1.729814E-3$
IEO[72]	1.663904802	1.74	1.520303	0.004274	15.92827	$1.729814E-3$
ELPSO[29]	1.666268	0.4596141	50.458643	0.5	497.747315	$2.1803E-3$

3.5 CONCLUSION

The current work aims to efficiently estimate the unknown parameters of photovoltaic models. A novel enhanced variant for the recent African Vultures Optimization Algorithm is designed for that purpose. A Two-fold strategy encapsulating both exploration and exploitation movements is incorporated into the standard AVOA, with no additional tuneable parameters. The new strategy guides a portion of the population to perform a global search to reduce the chances of local minima stagnation, and give the algorithm prospects to discover more promising regions within the search space. The remaining portion of the search agents will conduct a local search with a novel efficient equation to enhance the quality of solutions. The proposed scheme was examined through a wide range of experiments that cover the Single Diode, the Double diode, and the Triple diode models of the RTC

cell and SD modelling of three other benchmark PV modules. The obtained results demonstrated the effectiveness and reliability of the IAVOA in extracting accurate models that are highly consistent with the measurement datasets. The conducted comparative study with other state-of-the-art techniques testified the superiority and the high competitiveness of the proposed optimizer over its contenders. It should also be highlighted that the suggested expansion in the search bounds, were of valuable assistance in extracting values for the ideality factors that have led to an outstanding fitting accuracy. This was remarkable in the Double diode and Triple diode estimated models where the designed algorithm was able to yield RMSE scores as low as 6.9096E-4 and 7.40109E-4 for the two cases respectively, outperforming relevant works.

Although the introduced approach was powerful in handling the considered cases, future studies should cover more models and complicated conditions to further testify the robustness and accuracy of the IAVOA. Moreover, we intend to apply this identification scheme for the forecasting of electric power of PV power plants. Because most of the existing forecasting techniques are based on irradiance prediction in a given location, to estimate the associated power, one needs to use an accurate model of the PV power plants being installed in that location.

Chapter 4: Maximum Power Point Tracking of PV Systems

The design of new efficient Maximum Power Point Tracking techniques has become extremely important due to the rapid rise of PV systems mainstream. Because under shading conditions the characteristics of PV devices become multimodal having multiple power peaks, traditional MPPT techniques provide crappy performance. In turn, metaheuristic algorithms have become massively employed as a typical substitute in Maximum Power Point Tracking. In this work, a new optimizer which was named the Hyperbolic Slime Mould Algorithm (HSMA) is developed to be employed as an efficient MPPT algorithm. The Hyperbolic tangent function is incorporated into the optimizer framework equation to scale down large perturbations in the tracking stage and boost its convergence trend. Moreover, a new mechanism is made in such a way the search process is performed within the best two separate regions along the first iterations, to assure a performant exploration ability. The developed algorithm was examined through an assortment of complicated Partial Shading Conditions to challenge its global search and its exploitation processes. A comparative analysis was carried out against the well-regarded PSO, GWO and the standard Slime Mould Algorithm. In overall, the designed optimizer defeated its contenders in all aspects offering higher efficiency, superior robustness, faster convergence and fewer fluctuations to the operating point. An experimental setup that consists of the dSpace microcontroller and a PV emulator was employed to validate the algorithm performance. The recorded outcomes outline that the developed optimizer can achieve a tracking time of 0.6 seconds and 0.8 seconds on average, with 99.85% average efficiency under complex partial shading conditions.

4.1 MAXIMUM POWER POINT TRACKING

When the PV generator is connected directly to the load, the operating point is fixed by the intersection of load line and the IV characteristic curve. Because the intersection does not land usually on the maximum power point, an power interface has to be inserted between the PV array and the load side of the system. If a buck-boost converter is connected as shown in the arrangement of Figure 4.1, then the produced output voltage and current are dictated by equations 4.1 and 4.2 as follows:

$$V_o = \frac{V_{PV} D}{1 - D} \tag{4.1}$$

$$I_o = \frac{(1 - D)}{D} I_{PV} \tag{4.2}$$

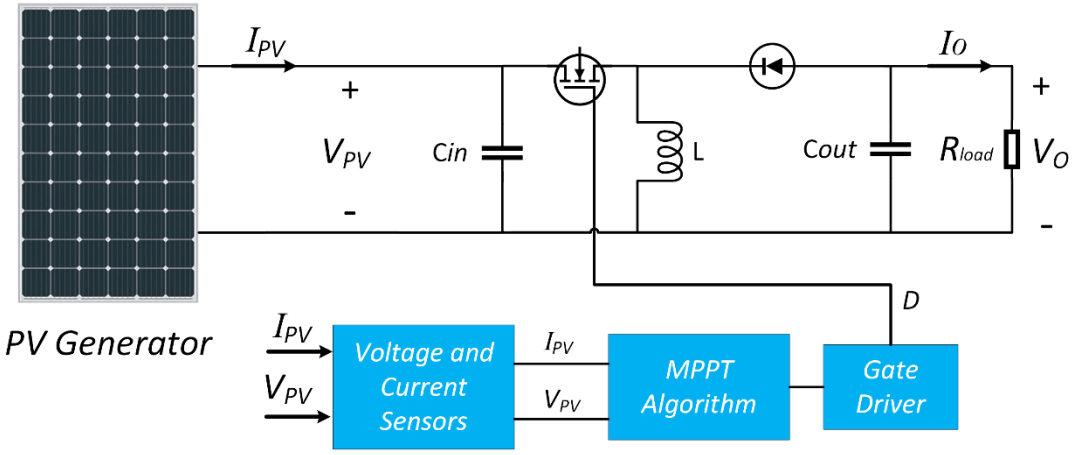

Figure 4.1 PV based on Buck-Boost Converter Driven by an MPPT Controller

With D being the duty cycle of the boost converter. The impedance seen by the PV generator which dictates the operating point can then be fixed by the duty ratio as demonstrated in the following equation:

$$R_{Eq} = \frac{V_{PV}}{I_{PV}} = \frac{\frac{(1 - D)}{D} V_o}{\frac{I_o D}{1 - D}} = \left(\frac{1 - D}{D}\right)^2 \frac{V_o}{I_o} = \left(\frac{1 - D}{D}\right)^2 R_{load} \tag{4.3}$$

The latter equation shows how the boost converter can be employed to set the impedance seen by the PV generator and hence the load line intersection. Using a proper algorithm that generates the required duty ratio, the operating point can be varied so that it coincides with the MPP level of the PV array. The employed algorithm is supposed to find the duty cycle value that leads to the Maximum Power Point in the

least possible time duration and detects any changes in irradiance levels to start the tracking process again.

4.2 THE PROPOSED METHODOLOGY

4.2.1 Slime Mould Algorithm

The Slime Mould Algorithm was developed based on the special foraging behavior of a single-celled organism known as slime Mould. The inspiration was educed from its main nutritional stage during which the organic matter in this organism look around food, ring it and then digest it. The search process of Slime mould involves generating a network of veins of distinct densities that extend to multiple food sources. The density is dictated by the goodness and the concentration of the food source. When the vein proceeds towards the food, the bio-oscillator of slime mould generates a propagating wave through which positive and negative feedbacks are established. An optimal path that connects various food regions would eventually be created. The mathematical model of the slime mould algorithm incorporates this behavior and involves two main mechanisms: Approaching food and Wrapping food.

A. Approach food:

Based on the odor in the air, slime mould approaches the food source with higher concentrations; the following equations are used to model the contraction mode near the food source:

$$\overrightarrow{X(t+1)} = \begin{cases} \overrightarrow{X_b(t)} + \overrightarrow{vb} \cdot \left(\overrightarrow{W} \cdot \overrightarrow{X_A(t)} - \overrightarrow{X_B(t)} \right), r < p \\ \overrightarrow{vc} \cdot \overrightarrow{X(t)}, r \geq p \end{cases} \quad (4.4)$$

(vb) $\vec{}$ takes on a value within a range of [-a, a] while (vc) $\vec{}$ is a parameter that decreases linearly from one to zero.(X) $\vec{}$ refers to the location of slime mould at iteration t, (X_b) $\vec{}$ denotes the food source with the highest odor concentration ever found , (X_A) $\vec{}$ and (X_B) $\vec{}$ are two solutions randomly selected from the solution vector, and W $\vec{}$ represents the weight of slime mould. p is given as follows:

$$p = tanh|S(i) - DF| \quad (4.5)$$

where $i \in 1, 2, \ldots, n$, $S(i)$ is the fitness value of the ith solution $\overrightarrow{X}$,and DF represents the best fitness obtained so far.

a and $\overrightarrow{W}$ are given as follows:

$$a = \text{arctanh}(-\left(\frac{t}{\text{T}}\right) + 1) \tag{4.6}$$

$$\overrightarrow{W(SmellIndex(\imath))} = \begin{cases} 1 + r \,.\, log\left(\frac{bF - S(i)}{bF - wF} + 1\right), i < \frac{N}{2} \\ 1 - r \,.\, log\left(\frac{bF - S(i)}{bF - wF} + 1\right), otherwise \end{cases} \tag{4.7}$$

With being the size of the solutions vector, r is a random value drawn from the interval [0, 1], bF represents the best fitness value obtained in the current iteration while wF denotes the worst fitness value obtained in the current iteration, SmellIndex denotes the sequence of fitness values sorted.

$$SmellIndex = sort(S) \tag{4.8}$$

B. Wrapping Food

Based on the previous mechanism, which simulates the positive and negative feedbacks between the vein thickness and the food concentration, variable weights are employed to quantify the food quantity in a particular region. When the explored region appears to have a low food concentration, the slime mould will decide to leave that area to explore other potential food zones. The complete updating mechanism is modeled as follows:

$$\overrightarrow{\text{X(t + 1)}} = \begin{cases} rand \,.\, (UB - LB) + LB, & rand < z \\ \overrightarrow{X_b(t)} + \overrightarrow{vb} \,.\, \left(W \,.\, \overrightarrow{X_A(t)} - \overrightarrow{X_B(t)}\right), & r < p \\ \overrightarrow{vc} \,.\, \overrightarrow{X\,(t)}, & r \geq p \end{cases} \tag{4.9}$$

LB and UB represent the lower and upper bounds of the search space, and z is constant parameter that is recommended to have the value $z = 0.03$

The process steps of the SMA can be summarized as follows:

Initialize the parameters: *population size* n, *Maximum number of iterations* T
Initialize the positions of slime mould $X_i(i = 1,2, \dots, n)$
While $(ite \leq T)$
    Calculate the fitness of all slime mould;
    Update bestFitness X_b;
    Calculate the weight W using equation 8;
    For each slime mould position:
        Update p, vb, vc;
        Update positions using equation 4.9;
    End For
    $ite = ite + 1$;
End While
Return X_b

4.2.2 Hyberbolic Slime Mould Algorithm HSMA

The Slime Mould Algorithm was successfully employed to tackle a wide range of engineering optimization problems and proved to exhibit good performance. However, in Maximum Power Point Tracking, the final output of the optimization process is not the only concern, the applied algorithm needs to be fast, accurate and exhibit the least possible amount of perturbations. The first and the last aspects arise from the fact that weather conditions might be highly unstable which causes the operating point of the system to fluctuate throughout the day. In turn, the algorithm needs to re-initialize every time the operating point changes, starting the optimization process all over again. For this reason, tracking time is an important factor to make sure that the system settles down at optimum steady conditions as fast possible. Moreover, the search stage of the algorithm needs to be skillful that it does not perturb the operating point drastically, causing considerable power losses during the process. Considering the previous facts, the original Slime Mould Algorithm was modified accordingly so that it fits better with MPPT.

Because the first and the third mechanisms of the SMA algorithm in equation 4.9 incorporate high randomness and distant movements, they have been removed in the developed SMA optimizer to reduce perturbations along the search stage. The new version maintains only a refined format of the second equation from the original SMA optimizer. The refinement employs the Hyperbolic Tangent function as a tool to minify large displacements that might result from the original equation. The Hyperbolic Tangent function maps values in the interval [0,1] nonlinearly to values in the interval [0,0.76] as shown in Figure 4.2.

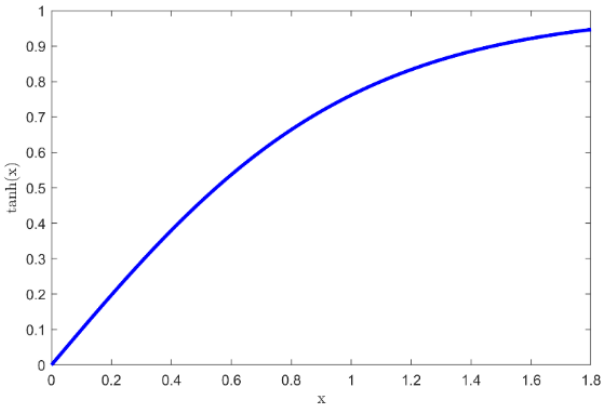

Figure 4.2 The Hyperbolic Tangent Function

The new framework equation is as follows:

$$D_i^{t+1} = Db + S(i) \times a \times \frac{|tan\,h(w(i) \times Db) - \tanh(G \times D_i^t)|}{d} \times e^{-|Db - D_i^t| \times t} \quad (4.10)$$

D_i^t denotes the ith duty cycle at iteration t and $w(i)$ is the corresponding weight value. Db is either the global best solution or the second global best solution. Half the duty cycles will be updated with respect to the global best solution while the second half will be updated with respect to the second global best solution. This is to ensure a performant exploration phase and avoid local peak entrapment. In many circumstances, the first and the second global best solutions might lie within the same region, at that time the algorithm might fall into a local peak area and get stagnated. To avoid such situations and ensure a successful exploration stage, an isolating mechanism is employed in such a way $Dbest_1$ and $Dbest_2$ are of distinct regions.

If $Dbest_1$ is the global best solution, then $Dbest_2$ is the second optimum solution that does not fall within the interval $[Dbest_1 - 0.08, Dbest_1 + 0.08]$. In other words, if any value of the duty cycle produces the second highest power but it falls within the region $[Dbest_1 - 0.08, Dbest_1 + 0.08]$, then it won't be considered as $Dbest_2$. This dynamic region clustering avoids the oversight of one optimum region and reduces early stagnation issues. Once the algorithm has perceived the global peak region, it will be of no use to employ $Dbest_2$ in the remaining search stages. For this reason, Db will take on $Dbest_1$ starting from the $3th$ iteration. The above mechanism can be summarized as follows:

if i*teration* = 1 or i*teration* = 2
  if i = 1 *or* $i = 2$
    $Db = Dbest_1$
  else
    $Db = Dbest_2$
  end if
else
  $Db = Dbest_1$
end if

Where

i is the index of the duty cycle candidate solution ($i = 1,2,3,4$)

$Dbest_1$: *Optimum dutycycle value*

$Dbest_2$: *Dutycyle value having the highest Power outside the region* $[Dbest_1 - 0.08, Dbest_1 + 0.08]$

$S(i)$ is a flag vector used to decide the direction of the movement. Two solutions are driven to land above Db and the two remaining solutions are driven to be below Db. This is to ensure an effective search operation within $Dbest_1$ and $Dbest_2$ and avoid overlooking a direction over another. For that matter the vector S is set as follow:

$$S = [1, -1, 1, -1] \tag{4.11}$$

The constant G takes one two values depending on how close D_i^t to Db according to the following arrangement:

$$G = \begin{cases} 0.8 & |Db - D_i^t| < 0.01 \text{ and ite} = 2 \\ 0.95, & |Db - D_i^t| < 0.01 \text{ and ite} = 3 \\ 1, & else \end{cases} \tag{4.12}$$

The employment of this mechanism is to avoid duplication of duty cycle values especially at the exploration phase. The latter phenomenon might cause loss of diversity and early stagnation issues.

d is a damping factor that takes on the value 2 in the second iteration and fixed at 1 in the remaining iterations.

$$d = \begin{cases} 2, & t = 2 \\ 1, & else \end{cases} \tag{4.13}$$

The exponential term in the equation is used to bring down the effect of the large distances between Db and D_i^t. The higher the distance between the two, the lower $e^{-|Db - D_i^t|t}$ it gets along the laps of iterations.

In the third iteration, Db takes on the value of $Dbest_1$ and t in its neighborhood. For the remaining iterations, the search will be narrowed down within the identified foremost region.

During the first iteration, the duty ratios are updated using a slightly different equation:

$$D_i^{t+1} = Db + S(i) \times a \times \text{rand} \times |\tanh(D_{r1}) - \tanh(D_{r2})| \tag{4.14}$$

Where D_{r1} and D_{r2} are two successive duty ratios randomly chosen from the solution vector. If $D_{r1} = 0.6$ then $D_{r2} = 0.8$. If D_{r1} happens to be $D_{r1} = 0.2$, then $D_{r2} = 0$. This equation assures an effective distribution of the duty ratios around the detected best two solutions. The convergence factor a in (4.6) of the original

version has been modified so that it decreases exponentially over the lapse of iterations to further boost the convergence rate of the HSMA optimizer:

$$a = e^{-\left(\frac{4t}{T}\right)^2} \tag{4.15}$$

The next section provides a profound explanation of the designed algorithm applied to Maximum Power Point Tracking.

4.2.3 HSMA based MPPT

The task in Maximum Power Point Tracking is to find the duty cycle value that would result in the highest possible power level the system can deliver. The employed algorithm would be implemented in a microcontroller to serve as the MPP tracker. Based on its mathematical framework, the algorithm in each iteration generates a set of duty cycle values to be transmitted to the DC-DC converter, and receives the corresponding Voltage and current for fitness evaluation. The duty cycle is then considered as the decision variable that directly affects the power of the system. Accordingly, Maximum Power Point Tracking can be regarded as an optimization Problem with the following objective function:

$$F(D_i) = P_i$$

Where D_i is the ith duty cycle generated by the algorithm and P_i is the corresponding PV power. The variable D is constrained within the range $0.1 \leq D_i \leq 0.9$. If at a certain iteration the distances between the generated duty cycles is very small or the associated power levels are so close, the iterative process will be terminated and the optimum duty cycle will transmitted to the power converter. This convergence criteria is set by the following condition:

$$\frac{|D_i - D_{i-1}|}{D_i} \leq 0.01 \ \ and \ \ \frac{|P_i - P_{i-1}|}{P_i} \leq 0.01 \tag{4.16}$$

Moreover, when the optimization stage is stopped, variations in irradiance levels have to be continuously checked by examining the associated Power level. If it happens that a change is detected, the optimization process shall be started all over again. The checking condition is as set as follows:

$$\frac{|P_{best}^t - P_{best}^{t+1}|}{P_{best}^t} \geq 0.02 \tag{4.17}$$

Where P_{best}^t is the power that corresponds to the optimum duty cycle found during the optimization process. The overall operating flowchart of the HSMA applied on MPPT is illustrated in Figure 4.3.

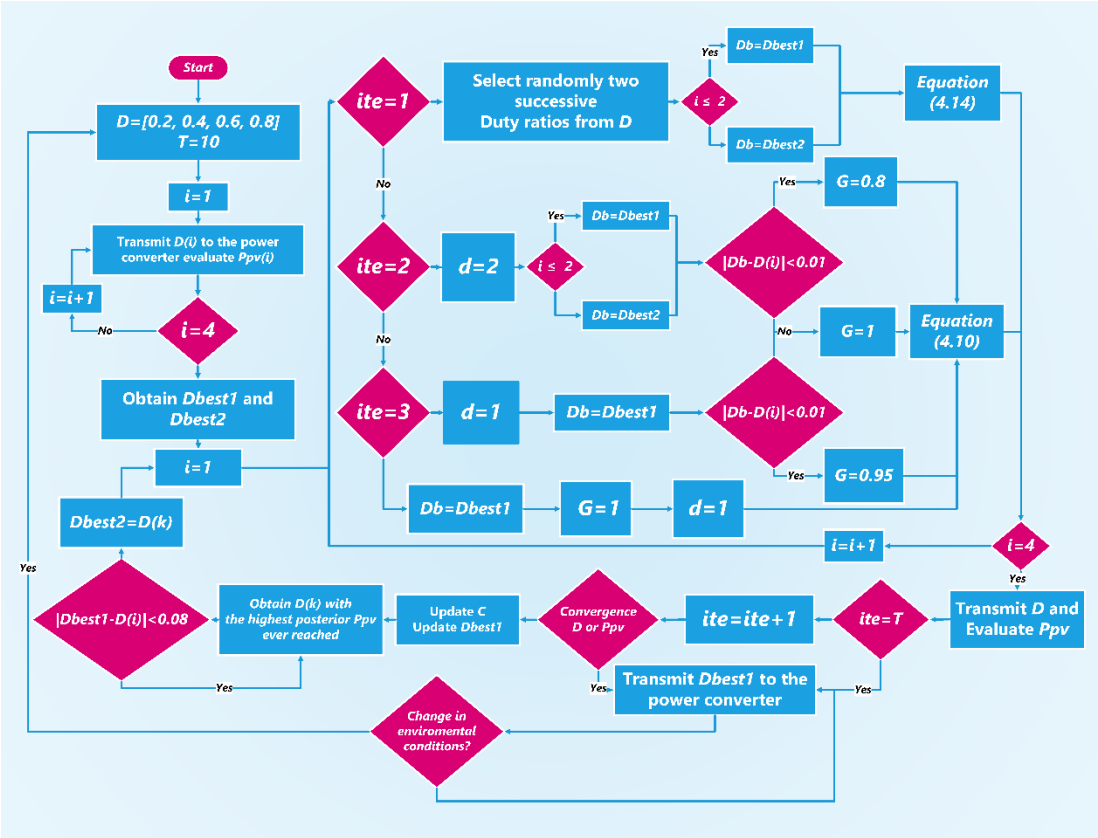

Figure 4.3 HSMA Operating Flowchart

- **Illustration of the working of HSMA**

In this section, the produced solutions trend of the designed algorithm will be visualized iteratively through a case example. A pictorial visualization of the duty ratio trend along the first three iterations is provided in the PV curves of Figure 4.4. As shown, the PV characteristics exhibit 4 peaks with the global MPP located at a power level of 703.1 W while the closest Local MPP is around 23 W away and located at 589.5 W in the extreme left. In the initial step, the algorithm sends the initial set of the duty cycles $D = [0.2,0.4,0.6,0.8]$ to the power converter to cover the entire PV curve. In this particular case, the duty cycle value $D_1 = 0.6$ produced the highest power level of 630.5W (Point A), and the algorithm stores it as $Dbest_1$. Likewise, $D_2 = 0.2$ produced the second highest power 559.5W(Point B), which makes it $Dbest_2$. In the first iteration, equation 4.14 will be used to convey half the solutions toward the neighborhood of $Dbest_1$ and the other half towards $Dbest_2$, with one driven above the respective Db and one below it. The resultant solution vector is $D = [0.652,0.514,0.301,0.129]$ and the associated power of each is recorded. As illustrated in the PV curve of Figure 4.4 (b), the solutions are equally deployed between

two distinct regions. After transmitting the updated set, $D_1 = 0.652$ produced 687.8W (Point C), which is the highest value ever found, making it the new $Dbest_1$. Without region clustering, the duty ratio $D = 0.6$ becomes the second-best solution as it delivers the second-largest power level. However, by applying the mechanism of region clustering incorporated in the HSMA optimizer, this value of the duty cycle won't be considered as $Dbest_2$ since it falls within the same region as $Dbest_1$. In other words, $|Dbest_1 - 0.6| < 0.08$. In the meanwhile, by neglecting the power associated with $D = 0.6$, $D_3 = 0.301$ produced a power level of 573.1W (Point D) which is the second largest level. Now since $D_3 = 0.301$ is not within $[Dbest_1 - 0.08, Dbest_1 + 0.08]$ it is now stored as the updated $Dbest_2$. In the next iteration, equation 4.10 with $d = 2$ will be used to dig around the newly discovered optimum regions. Again, half of the duty cycles set will be conveyed around $Dbest_1$, one from above and one from below; the same mechanism is applied for the remaining half, with $Dbest_2$. The new solution vector produced by this equation is now: [0.677, 0.633, 0.328, 0.274] which are allocated and split between the best-discovered regions as depicted in the PV curve of Figure 4.4 (c). After transmitting the new set of duty cycles, the value $D_1 = 0.677$ reached a new higher level of 703.1 W (Point E), making it the new optimal solution $Dbest_1$. In the meanwhile, although improvement has been achieved with $D_3 = 0.328$ in the $Dbest_2$ region producing a power level of 587.3 W (Point F), this is still inferior to the power level delivered by the opposite zone. In turn, the optimum region has now been fully perceived to the algorithm. Starting from the next iteration, which is the third one, Db is set to $Dbest_1$ and all solutions will be conveyed within the recognized optimum region using equation 4.11 with $d = 1$. Again half the solutions are landed above $Dbest_1$ and the other half is deployed below it. Accordingly, the generated solution vector is $D = [0.682, 0.6671, 0.6961, 0.6627]$ which are assembled in the global MPP level as shown in the last traced PV curve of Figure 4.4 (d).

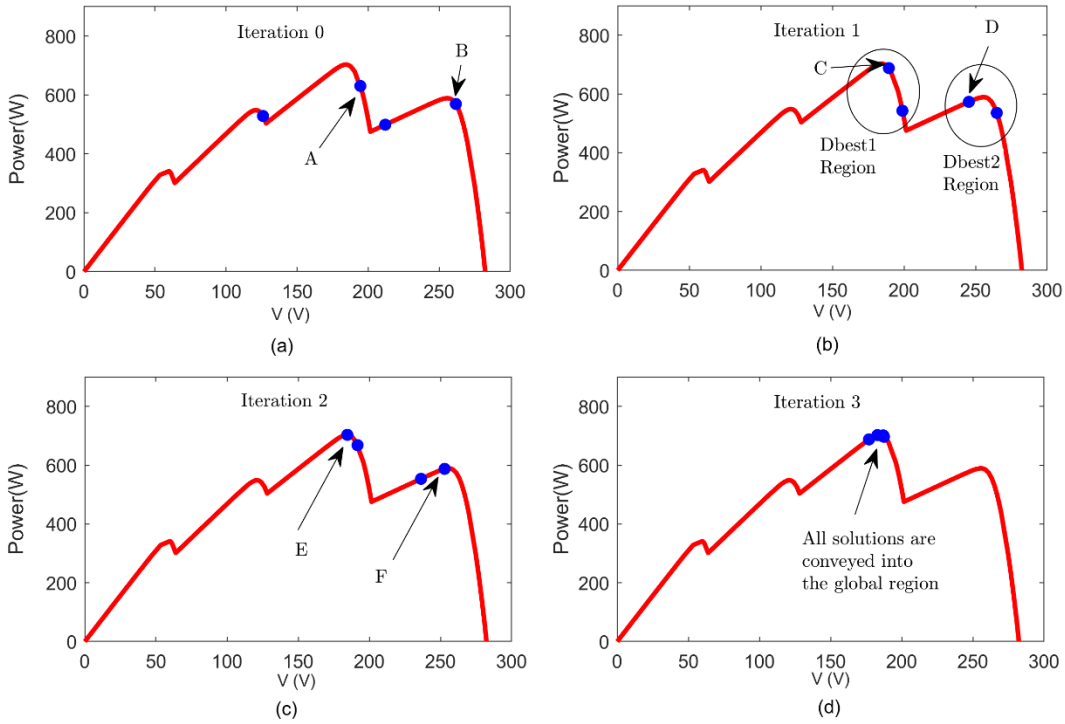

Figure 4.4 Operating Point Movement of the HSMA optimizer in the case example during (a) Iteration 0 (b) Iteration 1 (c) Iteration 2 (d) Iteration 3

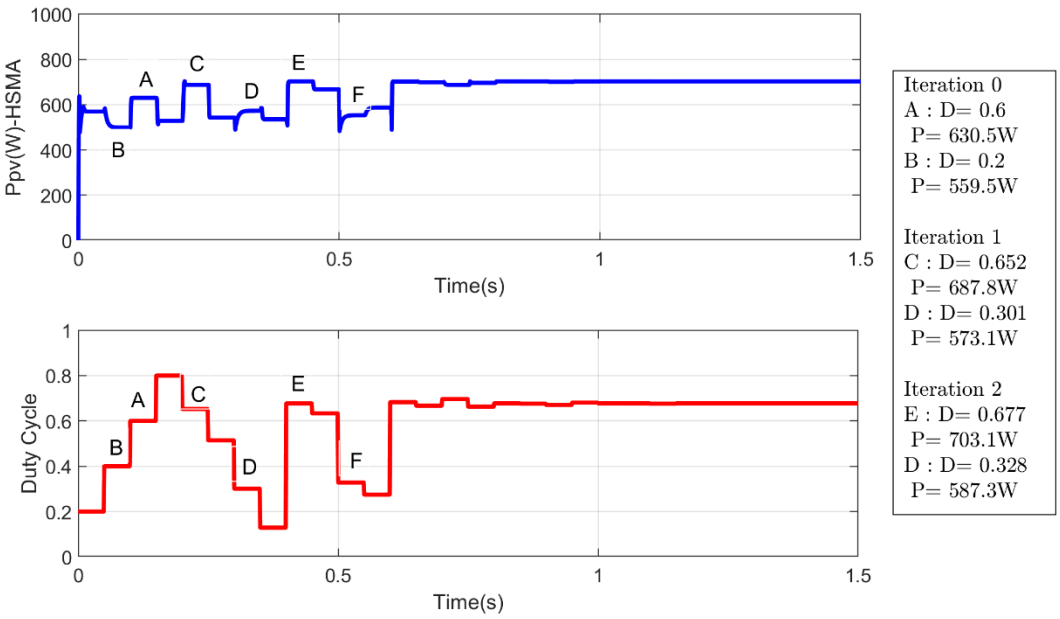

Figure 4.5 Power and Duty cycle curves of the HSMA optimizer in the case example

4.3 SIMULATION RESULTS

To examine the performance of the proposed HSMA optimizer, Matlab/Simulink is employed to simulate a standalone PV system undergoing distinct

complex partial shading conditions. The system consists of 8 serially connected PV modules of the same type, a boost converter operated by an MPPT algorithm, and a resistive load. The specifications of the employed PV module are provided in Table 4.1. The buck-boost converter consists of an input capacitor $C_{in} = 500\ \mu F$, an inductor $L = 150\ \mu H$ and an output capacitor $C_{out} = 0.9\ nF$. The considered cases involve patterns having 5 to 8 peaks with various scenarios of the global peak location, as depicted in the PV characteristics of Figure 4.6 and Table 4.2. Three other well-regarded algorithms were applied under the considered cases for the comparative study. The selected parameters for the PSO algorithm are as chosen in [39], while the parameters of the other algorithms were fixed as the default settings in their original articles. All the trials were carried out in MATLAB R2018b and executed on a PC with Intel Core™ I5-1145G7 CPU @ 2.60GHz, 16GB RAM, under Windows 11 64-bit OS. Moreover, for all the considered algorithms, the population size was set to 4 and the maximum number of iterations was fixed at 10. The sampling time was chosen to be 0.05s to match it with the experimental work later on.

Table 4. 1 Specifications of the Employed PV Module

Module	1Soltech 1STH-215-P	Open circuit Voltage (V_{OC})	36.3V
Maximum Power P_{MP}	213.5 W	Short circuit Current (I_{SC})	7.84
Voltage at P_{MP} (V_{MPP})	29 V	Cells per Module	60
Current at P_{MP} (I_{MPP})	7.35 A		

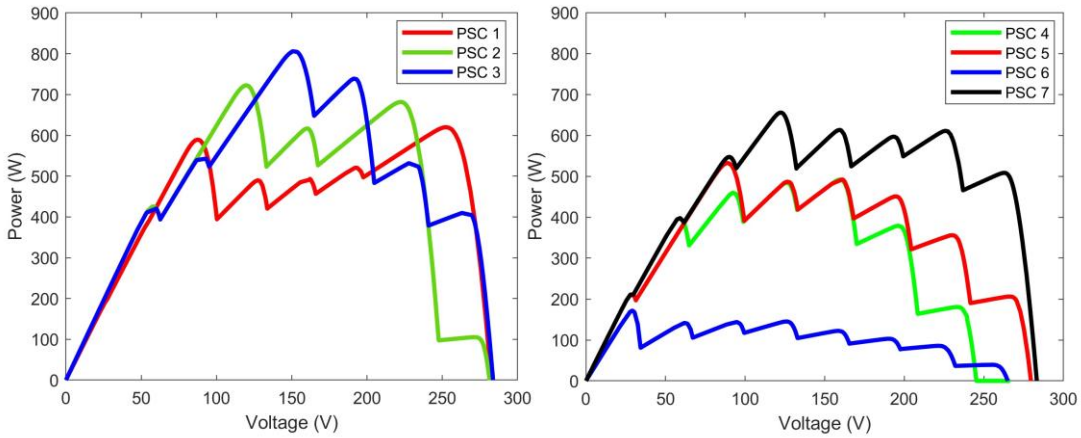

Figure 4.6 P-V curves of the investigated Partial Shading Conditions

Table 4.2 Details of the Investigated Partial Shading Conditions

PSC case	Pattern W/m^2	Number of Peaks	GMPP (W)	GMPP Location	LMPP 1 (W)
PSC1	950/920/900/500/400/350/320/320	5	619.8	Right	589.6
PSC 2	50/400/400/500/800/800/1000/1000	5	722.65	Middle	681.6
PSC 3	1000/1000/800/700/700/500/300/200	6	806.8	Middle	738.9
PSC 4	1000/900/600/0/500/400/250/200	7	492	Middle	484.7
PSC 5	1000/300/800/800/500/400/200/100	7	532.2	Middle	492.4
PSC 6	800/300/200/150/100/70/50/20	8	171.7	Left	145.1
PSC 7	1000/900/800/600/500/400/350/300	8	655.7	Middle	486

In the first scenario, the PV generator was subjected to irradiation levels of 950/920/900/500/400/350/320/320 W/m^2. The global MPP is located in the extreme right with a power level of 619.8 W, while the nearest local maximum is at 589.6 W. The resulting Power curves and duty ratio adaptation are traced in Figure 4.7. The HSMA, GWO, and PSO algorithms were all able to recognize the global region and successfully track the GMPP location with an efficiency level of 99.98%. The SMA algorithm attained a slightly lower level of 619.6 W, yielding an efficiency level of 99.967%. Despite the similar tracking accuracy, one can easily observe the rapid convergence trend of the HSMA optimizer compared to its contenders. The tracking time was 0.8 seconds which is way smaller than those of the GWO, PSO, and SMA optimizers which consumed 1.7, 1.9, and 2 seconds respectively. Moreover, it is notable from the power curves and the traced duty cycle that the HSMA generates fewer fluctuations to the operating point leading to lower power losses than those of the other algorithms. This is due to the masterful search strategy which is confined to the two foremost optimum regions, which assists the algorithm in rapidly deciding the global optimal area along the first two iterations.

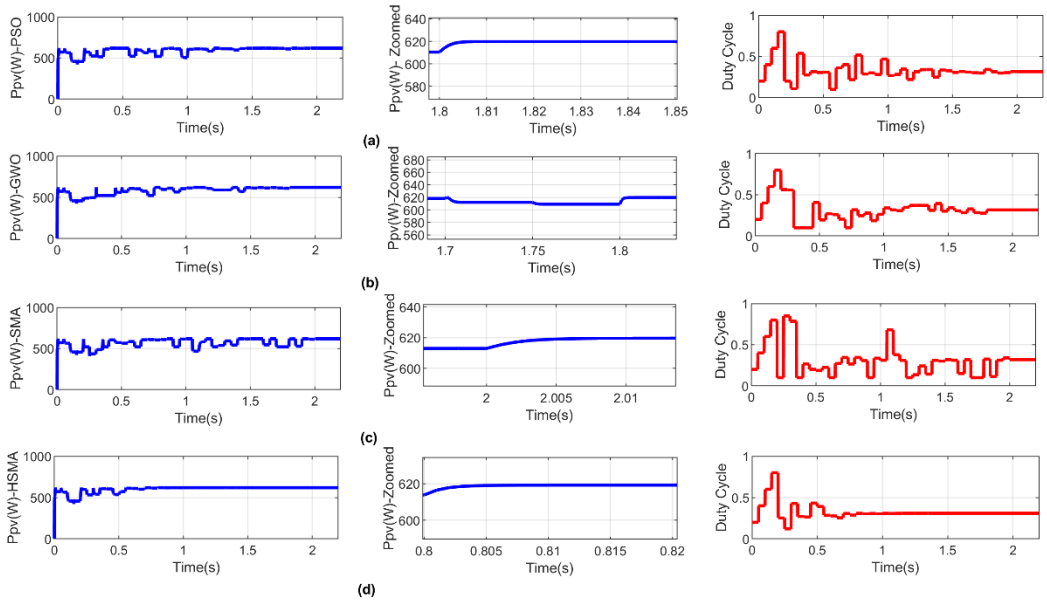

Figure 4.7 Power and Duty cycle Curves during PSC1 for (a) PSO (b) GWO (c) SMA (d) HSMA

In the second scenario, the PV generator receives irradiance levels of 50/400/400/500/800/800/1000/1000 W/m^2 resulting in a 5 peak PV curve. The corresponding global MPP is located at a power level of 722.65 W while the nearest local peak provides 681.2W. The resulting Power curves and duty ratio adaptation are provided in Figure 4.8. It is revealed from the graphs that except for the HSMA optimizer, the GWO, PSO, and the original SMA algorithms got entrapped at the local region. In this scenario, it happened that when transmitting the initial duty cycles, the one with the value D=0.2 produced a higher power than the ones with $D = 0.6$ and $D = 0.8$, which are supposed to belong to the global optimum zone. For that reason, the SMA, GWO and PSO algorithms got rapidly sucked into the 681 W region. Although the standard SMA optimizer attempted to escape from the local region at the seventh iteration, the attempt was insufficient. The HSMA on the other hand, could easily differentiate between the regions and eventually converge towards the global zone. This early recognition is due to the mechanism of exploring the neighborhood of the best two regions, giving both regions chances to reveal where the global optimum zone is located. In terms of convergence time, the HSMA is faster at 0.8s followed by the original SMA at 1.1 seconds, and the PSO and GWO algorithms at 1.4 and 1.6 seconds, respectively.

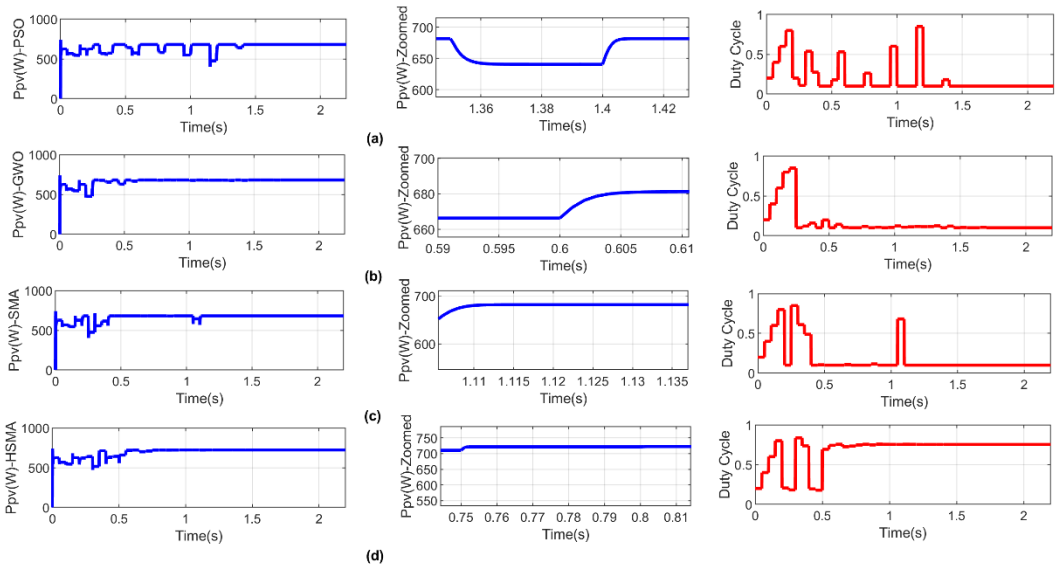

Figure 4.8 Power and Duty cycle Curves during PSC2 for (a) PSO (b) GWO (c) SMA (d) HSMA

In the third scenario, the system undergone a PSC pattern having irradiance levels of 1000/1000/800/700/700/500/300/200, resulting in a characteristic curve of 6 peaks. The associated global peak is located at 806.8 W in the middle, while the first local peak is around 70 W far from it. The resulting Power curves and duty ratio adaptation are provided in Figure 4.9. Although the HSMA, PSO and SMA algorithms scored the highest efficiency level of 806.5 W, the developed optimizer's tracking time, which was 0.8s, was way shorter than those of its contenders. In effect, both the PSO and the SMA optimizers consumed around 1.8s, while the GWO algorithm was the worst with a 2s tracking time. It can be observed from the power curves that the HSMA optimizer exhibits the least amount of fluctuations compared to those of the GWO, PSO, and SMA algorithms. This is due to the rapid decision-making attribute of the guided exploration stage, and by which the search process was not strayed away from the optimal peak regions.

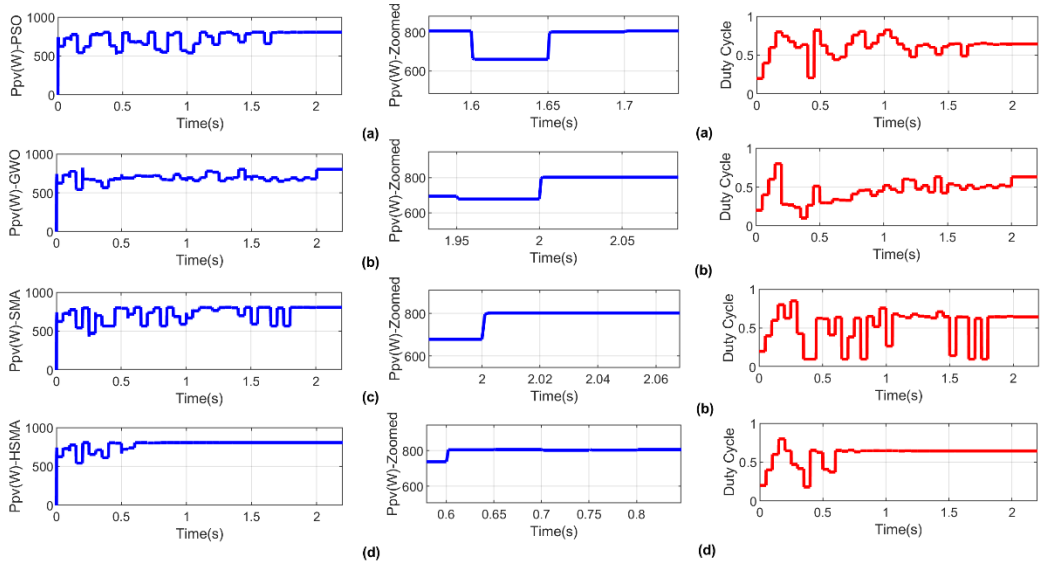

Figure 4.9 Power and Duty cycle Curves during PSC3 for (a) PSO (b) GWO (c) SMA (d) HSMA

The fourth trial involves a profile having levels of 1000/900/600/0/500/400/250/200 W/m^2 and the corresponding PV curve consists of 7 peaks. The global peak is at 492 W, and the associated duty cycle value is 0.356, while the closest local peak is only 7W away from it, making the case so challenging to handle. The associated delivered Power curves and the generated duty ratio values are shown in Figure 4.10. In the initial step, the value $D = 0.4$ produces 470 W while $D = 0.6$ produces a higher level of 481.2 W, causing an entrapment to the MPPT algorithm. Despite the troublesome pattern, the designed HSMA optimizer effectively conveyed the operating point to the global maximum level resulting in a 99.99 % efficiency. The dynamic region clustering enabled the algorithm to avoid entrapment into the closest local zone with rapid and masterful decision-making. As can be observed, the GWO algorithm could manage to achieve identical efficiency with the HSMA optimizer, however, this was at the expense of high fluctuations and sluggish convergence. In effect, the HSMA was again the fastest algorithm, with 0.8 seconds, followed by the GWO algorithm, which took 1.8 seconds to converge. In the meanwhile, the PSO and the SMA optimizers failed to recognize the global region and got entrapped into a local MPP zone.

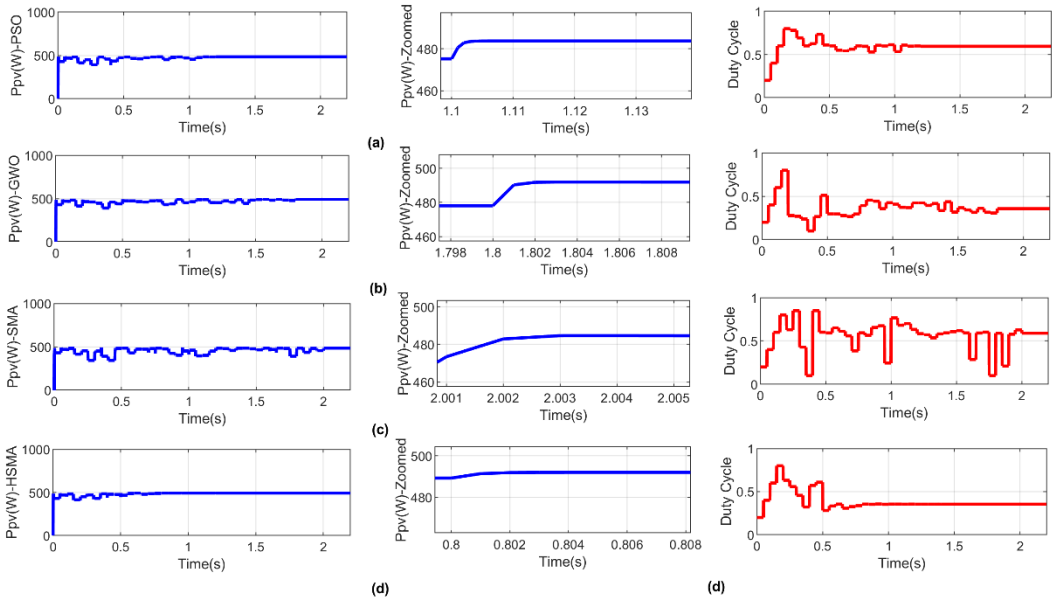

Figure 4.10 Power and Duty cycle Curves during PSC4 for (a) PSO (b) GWO (c) SMA (d) HSMA

In the fifth case, the PV array is exposed to irradiance levels of 1000/300/800/800/500/400/200/100 W/m^2. The resulting 7 peak PV curve exhibits a global maximum located near the extreme left with a power level of 532.2W, while the first local peak was made close at a level of 493 W. The corresponding Power curves and duty ratio adaptation are provided in Figure 4.11. Similar to PSC2 and PSC3, the global region cannot be revealed after transmitting the initial set of duty cycles. In turn, the GWO and PSO algorithms failed to recognize the optimum zone and rapidly got stuck at the 493 W level. The SMA has also got stuck in that zone in the first 4 iterations, yet, due to the re-initialization mechanism of that algorithm, it could manage to escape into the global region afterward. However, the exploitation phase could only achieve a power level of 523 W, which is still far off the GMPP location resulting in poor efficiency and slow convergence. In the meantime, due to the masterful exploration mechanism of the HSMA optimizer, the global region was spotted in the first iteration and took 0.8 seconds to converge.

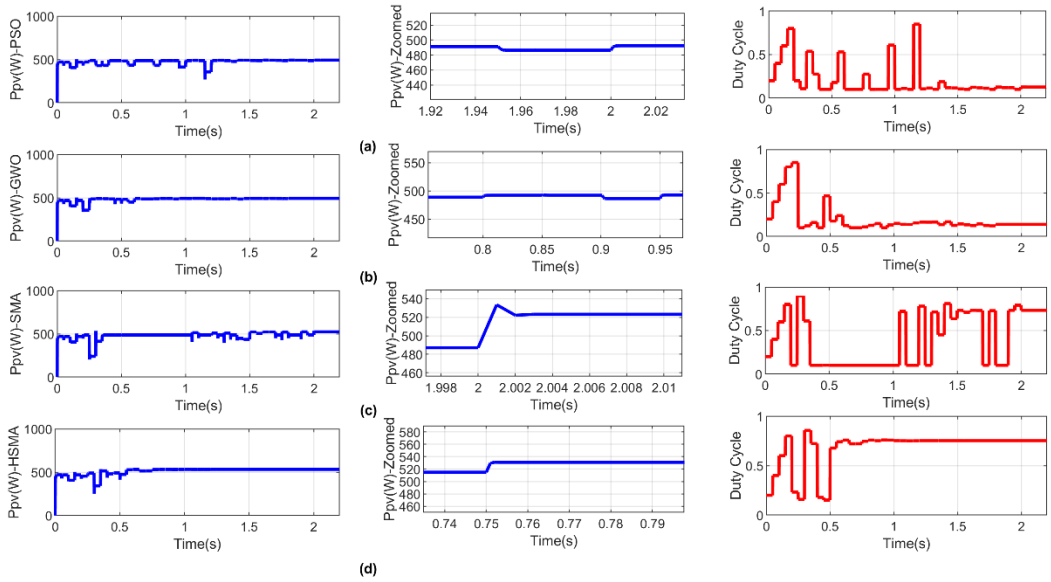

Figure 4.11 Power and Duty cycle Curves during PSC5 for (a) PSO (b) GWO (c) SMA (d) HSMA

In the sixth experiment, the PV curve consists of 8 peaks, with the global max located at the extreme left at a power level of 171.7 W. The resulting Power curves and duty ratio adaptation are provided in Figure 4.12. All algorithms could manage to successfully land at the global peak level with identical efficiency of 99.99 %. However, as with the other cases, the HSMA optimizer provides the best convergence trend with 0.8 seconds tracking time and the slightest amount of fluctuations.

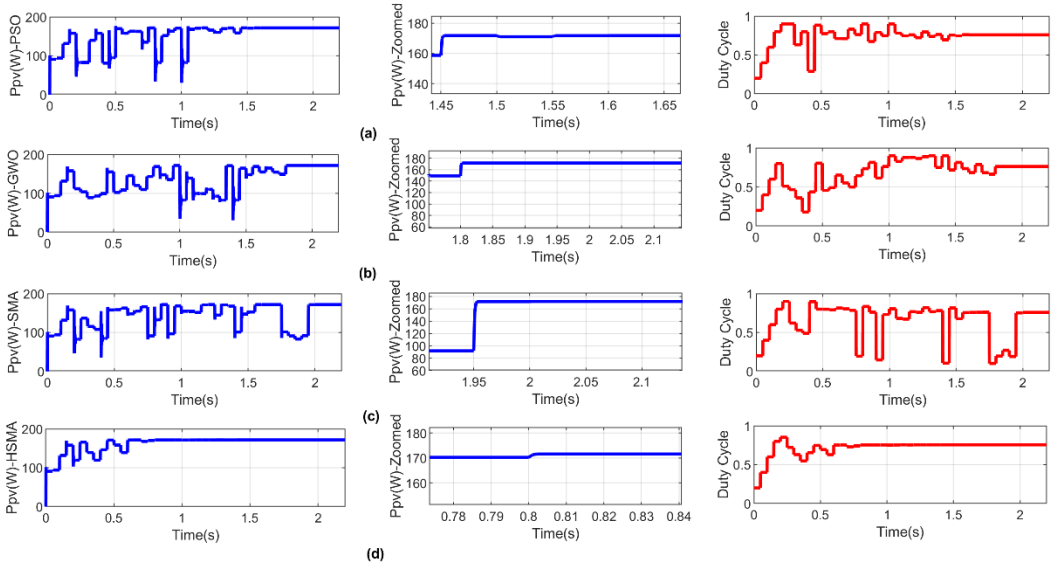

Figure 4.12 Power and Duty cycle Curves during PSC6 for (a) PSO (b) GWO (c) SMA (d) HSMA

The last trial involved an 8 peak PV curve by exposing the system to irradiance levels of 1000/900/800/600/500/400/350/300 W/m^2. The global peak is located at the extreme right with a power level of 655.7 W, while the nearest local maximum is located at a power level of 486 W. The resulting Power curves and the traced duty ratio progression are provided in Figure 4.13. It happened that the HSMA, GWO, and PSO algorithms were able to recognize the global optimum region while the standard SMA optimizer failed in this task. The HSMA and PSO algorithms attained identical power levels of 655.6 W and a corresponding efficiency of 99.98%, however, the GWO achieved 654.6 W resulting in a lower efficiency of 99.83 %. Despite their similar accuracy scores, the tracking process of the developed HSMA optimizer is way better than those of its competitors. This is perceivable from its respective power curves from which one can observe smaller convergence time, faster decision making and fewer perturbations to the operating point. Moreover, the GWO and PSO algorithms' search process generates previously produced and evaluated solutions causing sluggish convergence and poor accuracy.

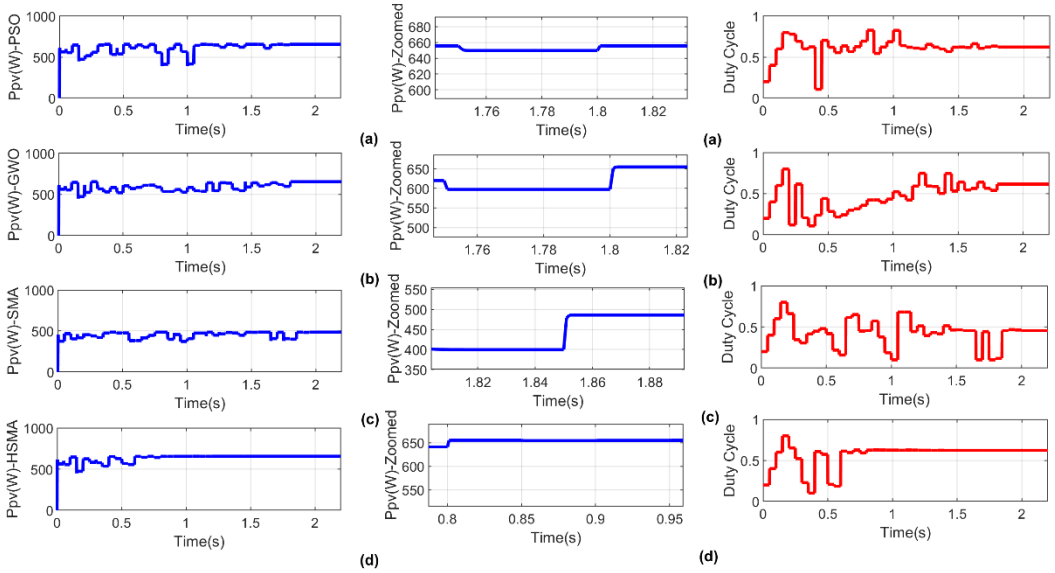

Figure 4.13 Power and Duty cycle Curves during PSC7 for (a) PSO (b) GWO (c) SMA (d) HSMA

To assess the HSMA optimizer in achieving identical efficiency levels at the same irradiance, it was tested under varying load conditions. The system was exposed to the last PS conditions with a load change from 50 Ω to 25 Ω after 1.25 seconds. It can be seen from the resulting curves in Figure 4.14, that the algorithm was able to recognize the change in the power level and reinitialized the search starting from the next sampling cycle. Once again the algorithm maintained its behavior during the search process with 99.98% efficiency in both load conditions and 0.8 seconds tracking time.

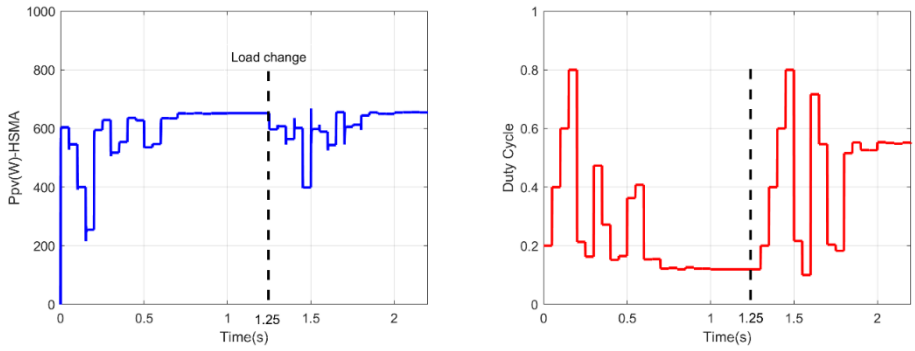

Figure 4.14 Power and Duty cycle Curves during PSC7 of the HSMA optimizer under Dynamic Load Conditions

4.4 EXPERIMENTAL VALIDATION

To support the results obtained through the simulation trials, the HSMA optimizer was examined on an experimental setup shown in Figure 4.15 for real time performance investigation. The system is made up of a PV array emulator employed to generate the intended Partial shading conditions, a Buck-Boost converter and DSpace (D1104) as the controller that transmits the generated PWM signals to the gate driver. The Chroma 62150H PV Emulator was used to setup a PV generator consisting of 6 modules connected in series. The selected solar module is the SunPower SPR-305-WHT having the following characteristics: $V_{mpp} = 10.9V$, $I_{mpp} = 5.59\ A, V_{oc} = 13.1\ V, I_{sc} = 5.92\ A$. The generated Voltage V_{PV} and Current I_{PV} from the PV simulator were measured by a voltage (LEM LV-25-P) sensor and a current (LEM LA-25-NP) sensor which provide readings to the ADC pins of the DSpace microcontroller. The employed boost converter consists of an input capacitor $C1$ = 1200 μF, an output capacitor $C2$ = 550 μF, an inductor L = 470 μH and a variable load resistor fixed at R = 20 Ω with the switching frequency set to 20 Khz. Based on the buck boost converter settling trend, the sampling time was selected to be 50ms to provide accurate readings of voltage and current to the microcontroller. This section is devoted to the analysis of the algorithm records on the used experimental setup.

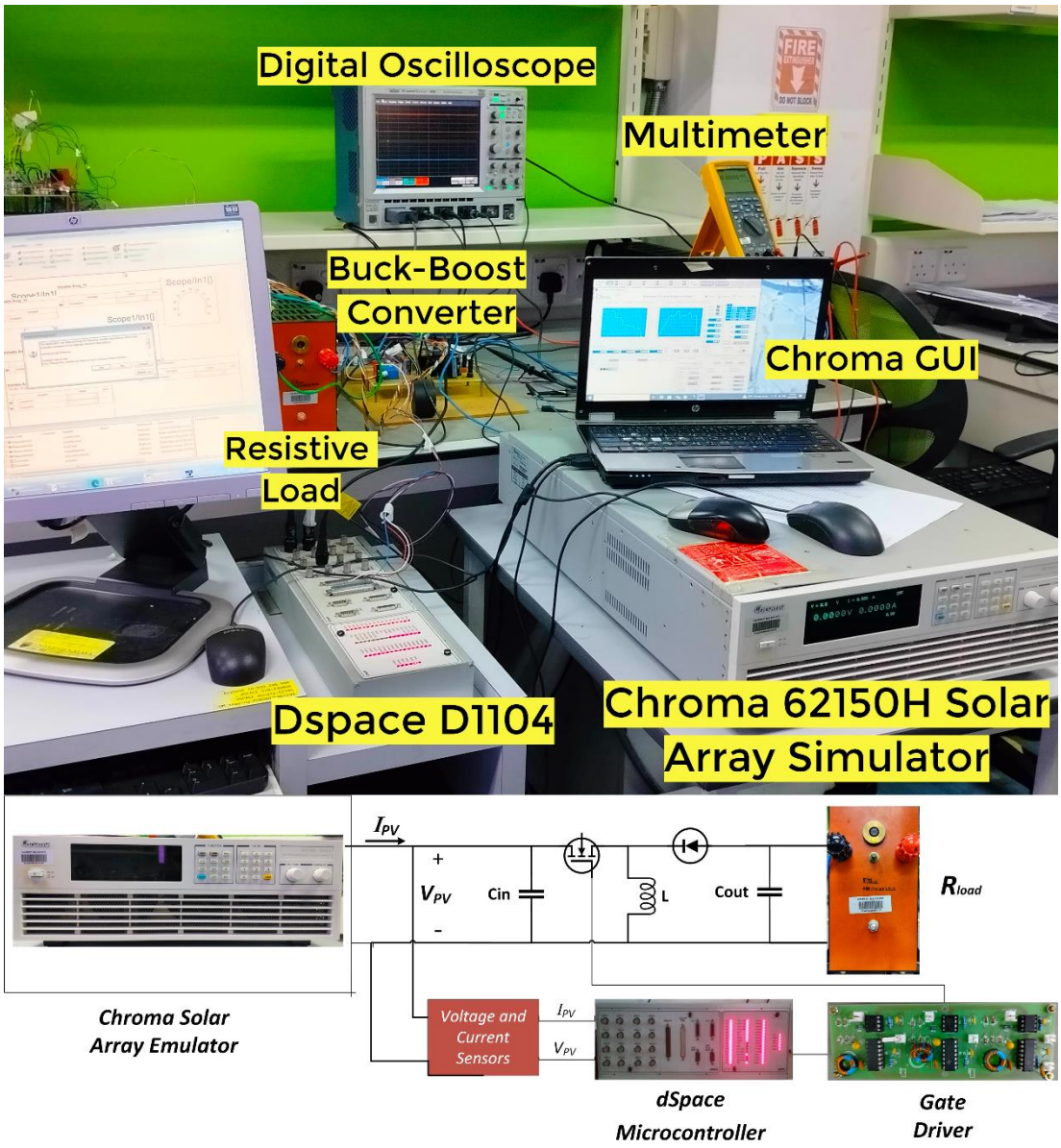

Figure 4.15 Employed Experimental Setup

In the first scenario, the system receives solar irradiance levels of $1000, 1000, 900, 800, 700\ and\ 600\ W/m^2$ resulting in a PV curve of 5 peaks. The global peak is located at the extreme right with a power level of $261.51\ W$ as indicated in the screen of the PV emulator. The resulting Power curves and duty cycle progression are provided in Figure 4.16. The red point on the PV and IV curves corresponds to the steady state reached after the optimization process. The algorithm was able to stand at a power level of $261.3\ W$ with 99.92 % efficiency within 0.8 seconds, matching the simulation records. Disregarding the first fluctuations which correspond to the initial set of duty cycles, it is apparent that the algorithm induced

tiny perturbations during the optimization process before steady state. This feature is attributed to the smooth exploration phase that allows digging around the best two solutions before deciding which of which the optimum region is.

In the second test case, the system is exposed to irradiance levels of $1000, 1000, 900, 800, 500\ and\ 400\ W/m^2$. The associated 5 peaks PV curve is shown in Figure 4.17, with an MPP level of $217.5\ W$. As recorded in the figure, the algorithm successfully located the GMPP region with 99.8 % efficiency. Although the tracking time was 0.95 s which is a bit longer than that of the other cases, the duty cycle perturbation in the last iterations are very tiny with unnoticeable power fluctuations during these moments.

The PV and IV curves corresponding to the third trial are provided in Figure 4.18. The global MPP is located in the middle with power level of 146.9.9 W. Again, the HSMA optimizer was able to convey the operating point into the GMPP with 99.95 % efficiency within 0.6 seconds. It is perceivable from the duty cycle progression that the algorithm was able to quickly decide which region is the optimum one, resulting in a few and tiny perturbations and hence small power losses.

In the fourth case, the Global MPP is located in the extreme left of the PV curve as depicted in Figure 4.19. The system is exposed to irradiance levels of $1000, 1000, 350, 300, 150, and\ 100\ \mathrm{W}/m^2$. The algorithm was able to attain a power level of 124 W out of $124.3\ W$ resulting in 99.75 % efficiency. The tracking time was 0.8 seconds, which is again, in accordance with the one of the simulation part.

The fifth experiment involves 6 peaks resulting from exposing the PV generator to irradiance levels of 1000/500/400/250/150 and 100 W/m^2. The global peak is located in the middle at a power level of $86.86\ W$ as shown in Figure 4.20. The HSMA optimizer was able to deliver $86.74\ W$ resulting in $99.87\ W$. The algorithm this time took a bit longer to settle down and consumed 1.2 seconds to converge. Despite this slower convergence, the perturbations during the tracking stage are small and the corresponding power fluctuations are small.

In the last experimental trial, the system was exposed to a dynamic irradiance of two partial shading patterns. The first pattern is the same as PSC2 and the second pattern is set as PSC4. This experiment is important to testify the algorithm performance in detecting irradiance changes which usually occur in practice. As can

be perceived from the outcomes of Figure 4.21, the HSMA optimizer was able to reinitialize the tracking process immediately once the change occurred. Along the first pattern, the algorithm took around 1.1 seconds to converge while in the second case, it consumed only 0.6 seconds to settle down at the global optimum operating point.

To support the rival and superior performance of the HSMA optimizer, the previously considered algorithms were implemented on the same experimental setup and conditions. The produced power, current, voltage and duty cycle graphs of each algorithm are provided in Figures 4.22-4.36. The detailed outcomes of all algorithms along the investigated experimental cases are reported in Table 2. In overall, the results are much the same as the ones obtained during the simulation trials. Clearly, a high number of fluctuations and jumps characterizes the power curves produced by the PSO, GWO and the SMA optimizers before arriving at steady state conditions. This highly random and unguided search process caused lots of power perturbations and eventually sluggish tracking speed. The HSMA optimizer in the other hand could achieve a very small tracking time of 0.6 seconds, while the largest recorded time was 1.2 seconds. With the investigated cases, the HSMA optimizer settles down on average within 0.87 seconds, which is nearly 4.3 iterations. In terms of tracking accuracy, the designed algorithm was able to achieve experimentally an efficiency level as high as 99.95 % and 99.87 % on average, which is very promising, bearing in mind its rapid convergence trend and its low fluctuations. In general, the reported results of Table 4.3 indicate that the HSMA optimizer comes at the first rank in both average tracking time and average efficiency with the least amount of perturbations.

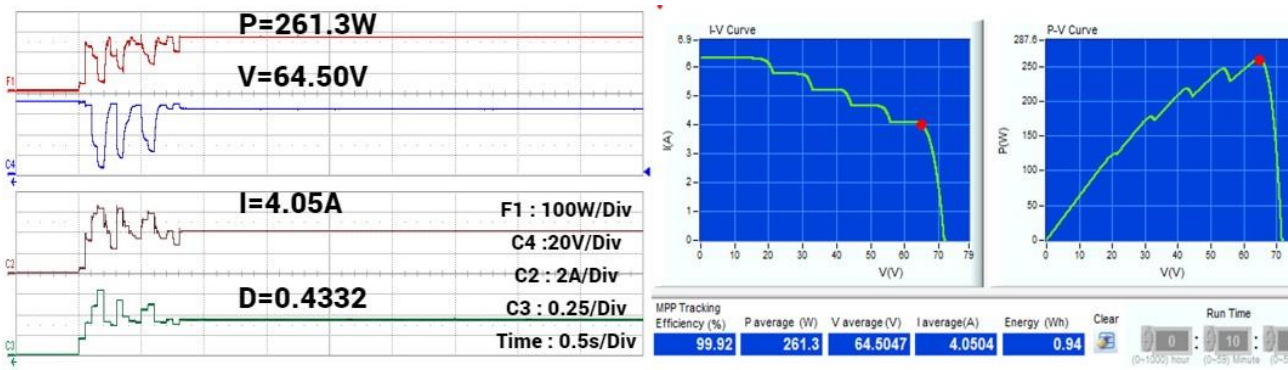

Figure 4.16 HSMA resulting curves along Experimental Trial PSC1

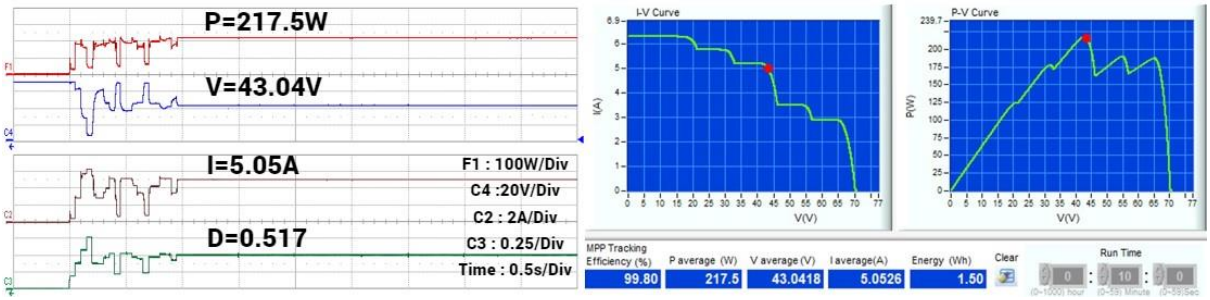

Figure 4.17 HSMA resulting curves along Experimental Trial PSC2

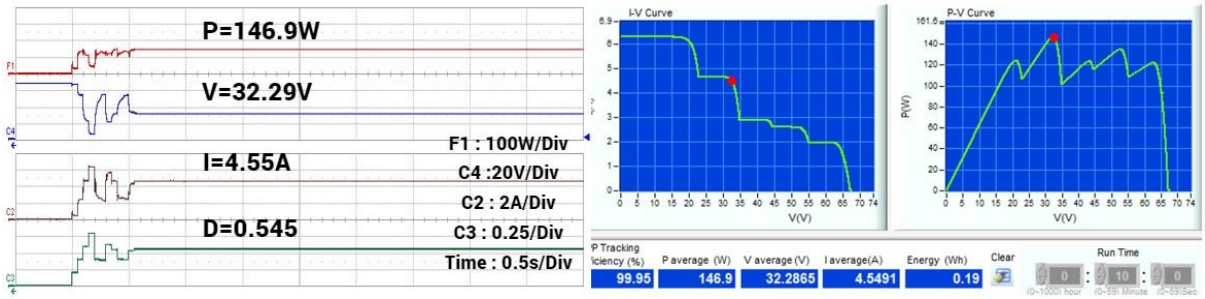

Figure 4.18 HSMA resulting curves along Experimental Trial PSC3

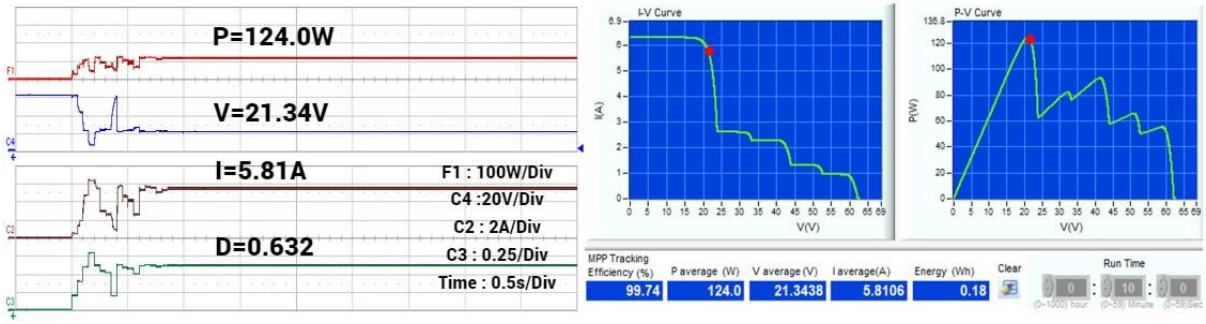

Figure 4.19 HSMA resulting curves along Experimental Trial PSC4

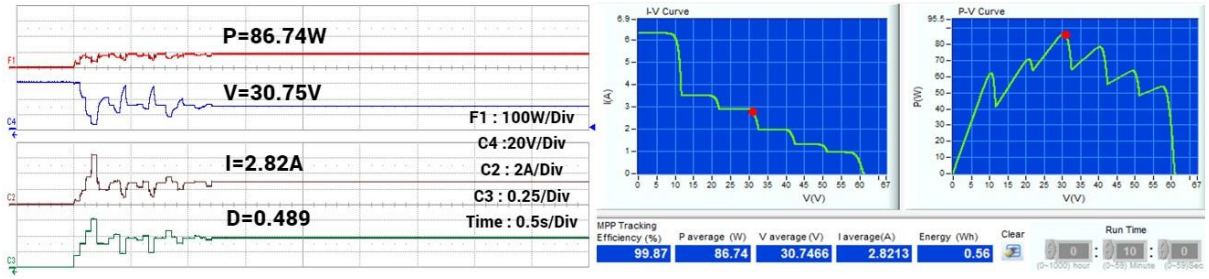

Figure 4.20 HSMA resulting curves along Experimental Trial PSC5

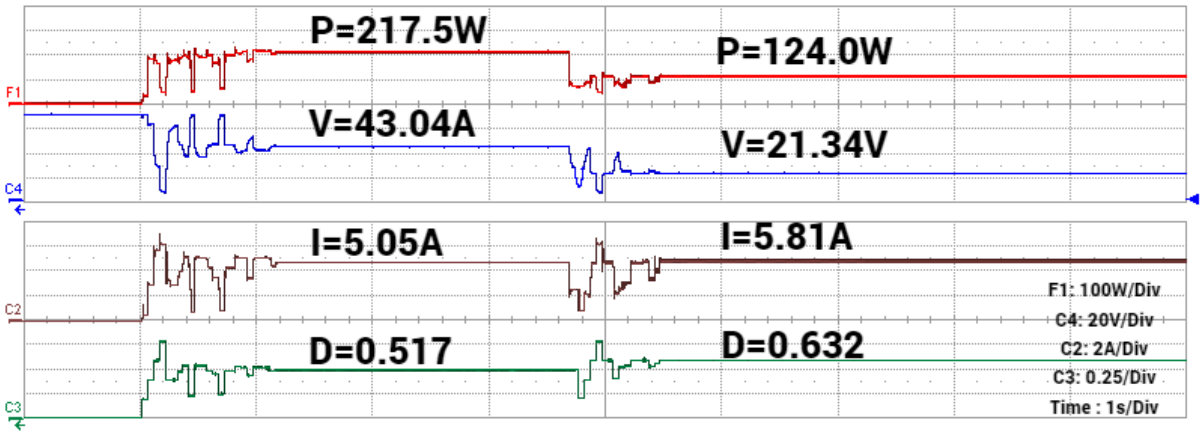

Figure 4.21 HSMA resulting curves along Experimental Trial PSC2-PSC4

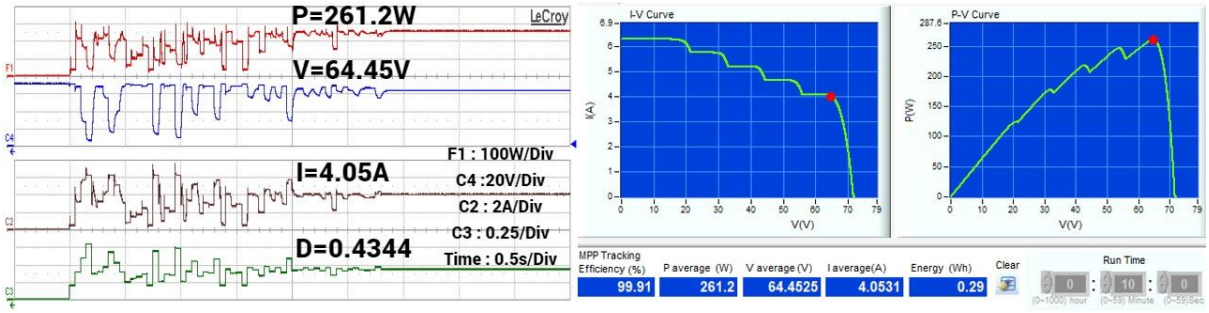

Figure 4.22 PSO resulting curves along Experimental Trial PSC1

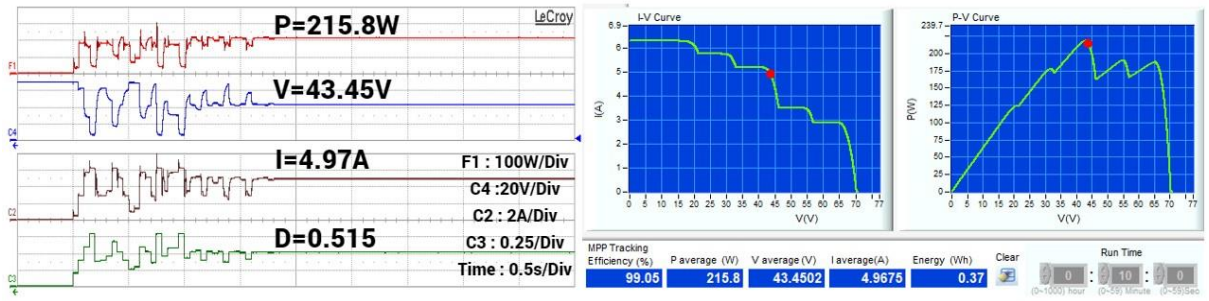

Figure 4.23 PSO resulting curves along Experimental Trial PSC2

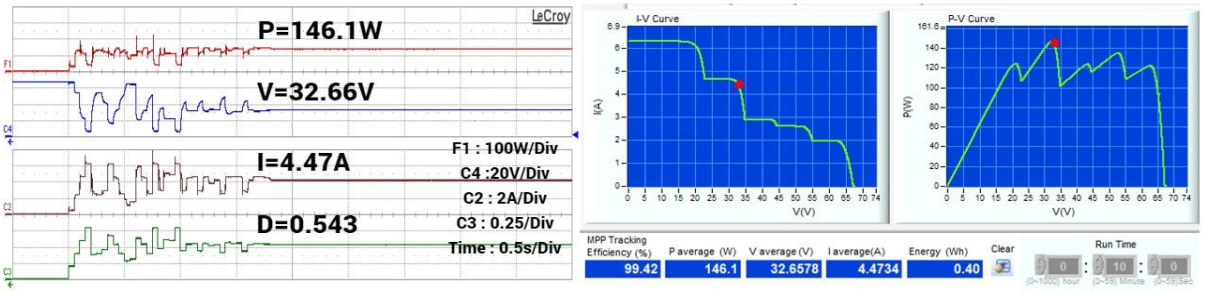

Figure 4.24 PSO resulting curves along Experimental Trial PSC3

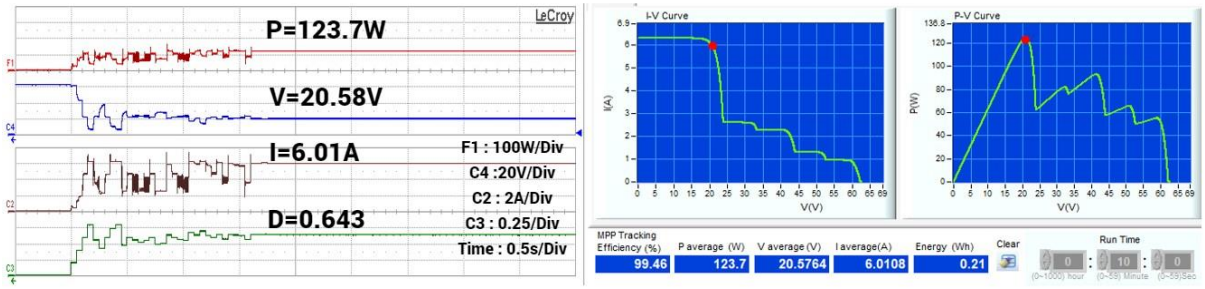

Figure 4.25 PSO resulting curves along Experimental Trial PSC4

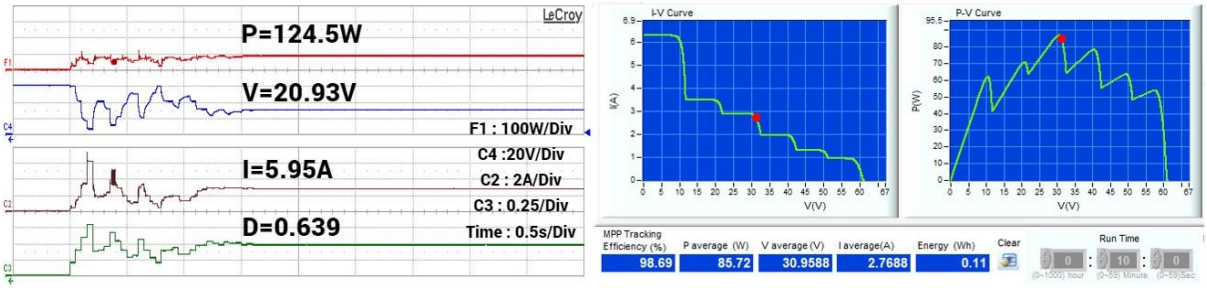

Figure 4.26 PSO resulting curves along Experimental Trial PSC5

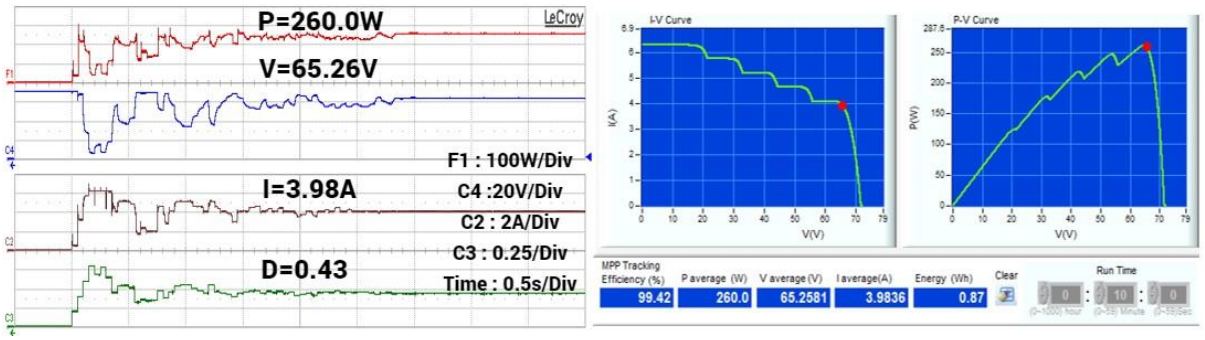

Figure 4.27 GWO resulting curves along Experimental Trial PSC1

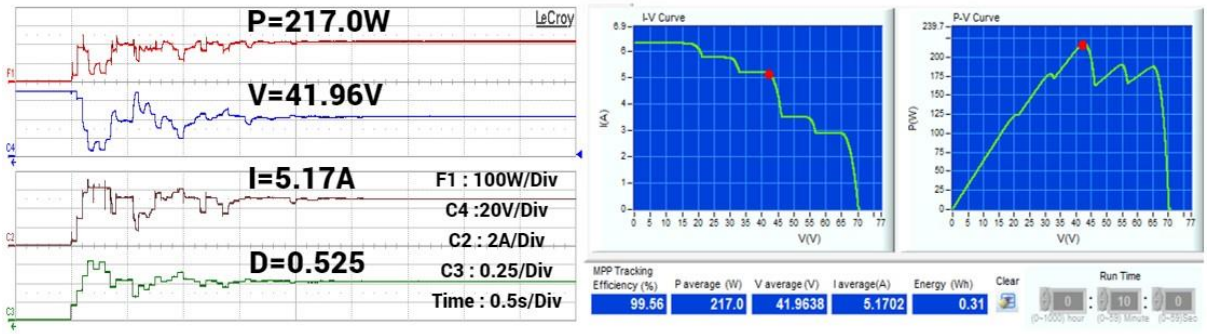

Figure 4.28 GWO resulting curves along Experimental Trial PSC2

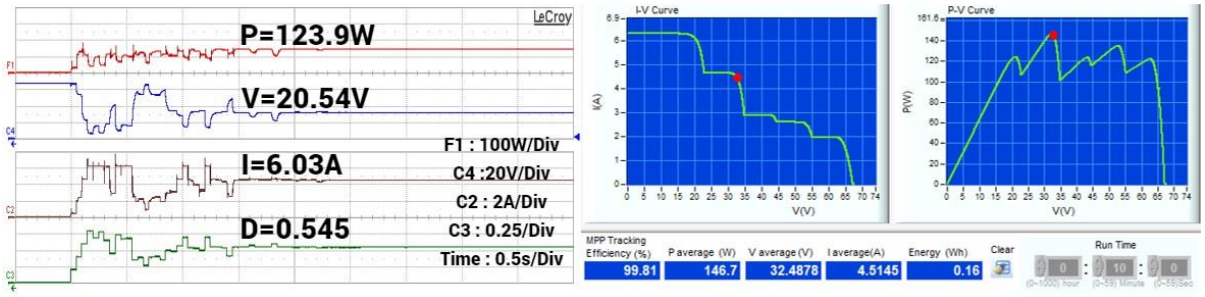

Figure 4.29 GWO resulting curves along Experimental Trial PSC3

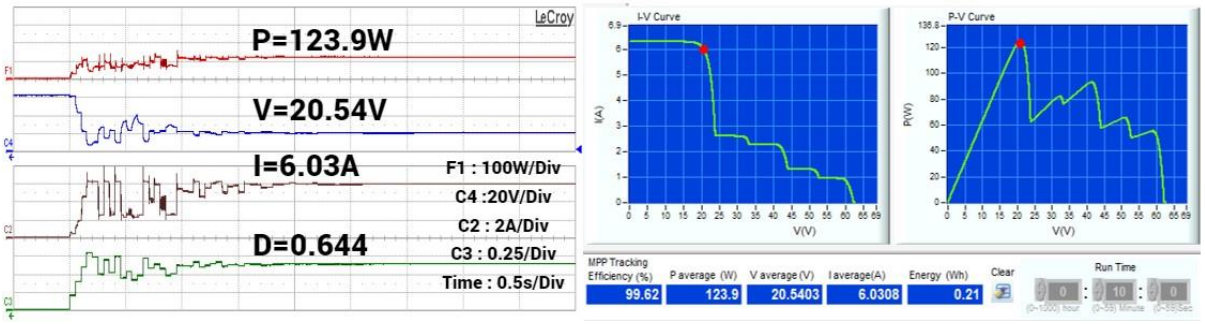

Figure 4.30 GWO resulting curves along Experimental Trial PSC4

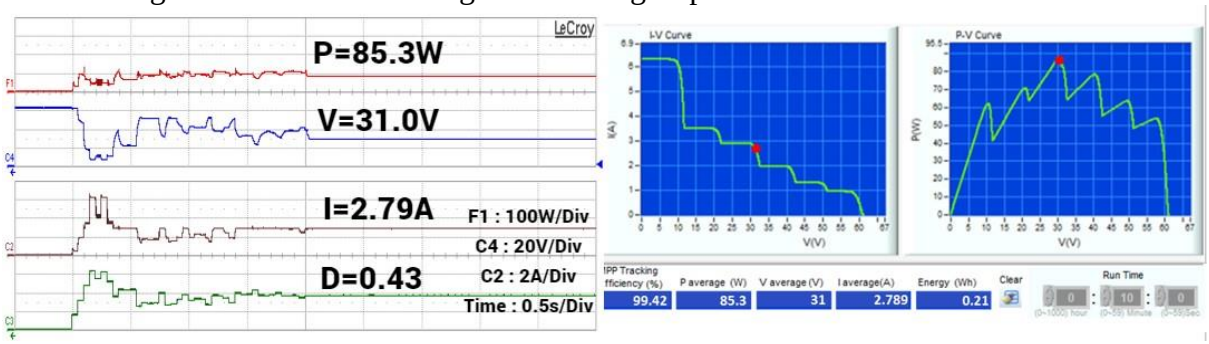

Figure 4.31 GWO resulting curves along Experimental Trial PSC5

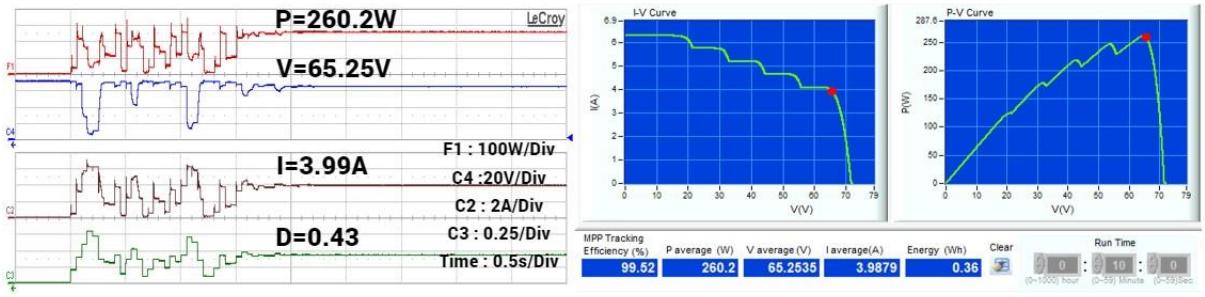

Figure 4.32 SMA resulting curves along Experimental Trial PSC1

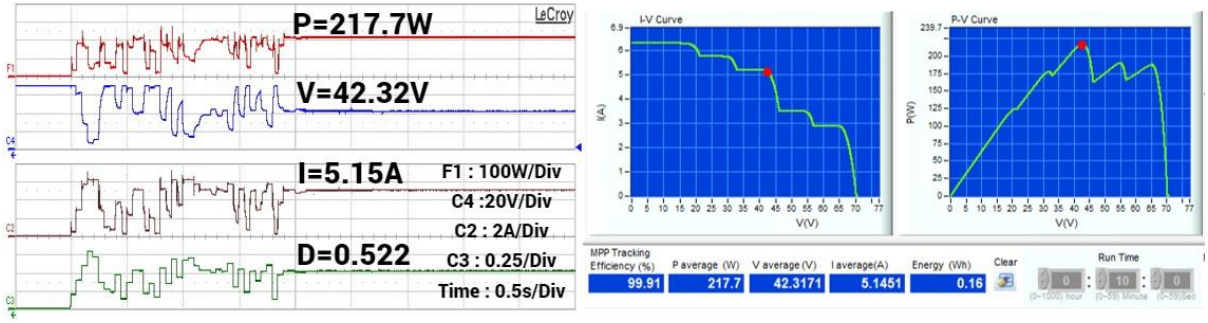

Figure 4.33 SMA resulting curves along Experimental Trial PSC2

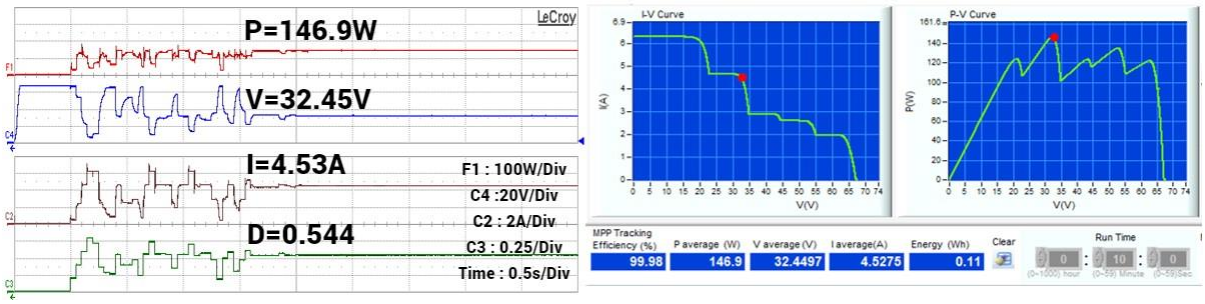

Figure 4.34 SMA resulting curves along Experimental Trial PSC3

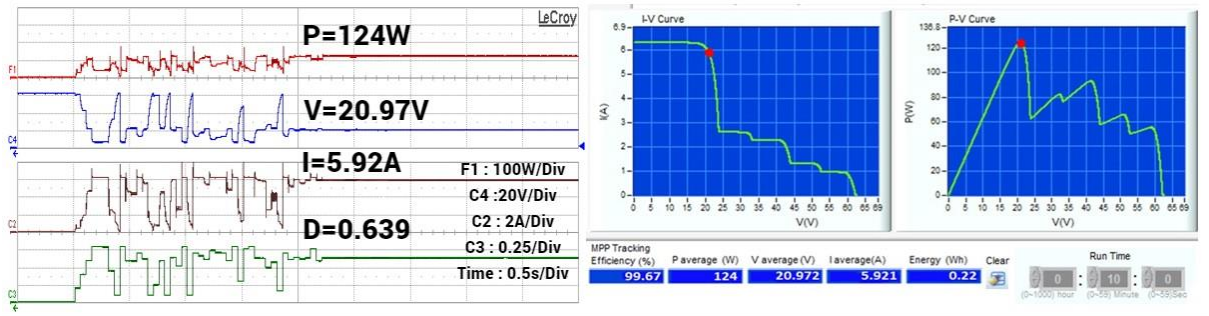

Figure 4.35 SMA resulting curves along Experimental Trial PSC4

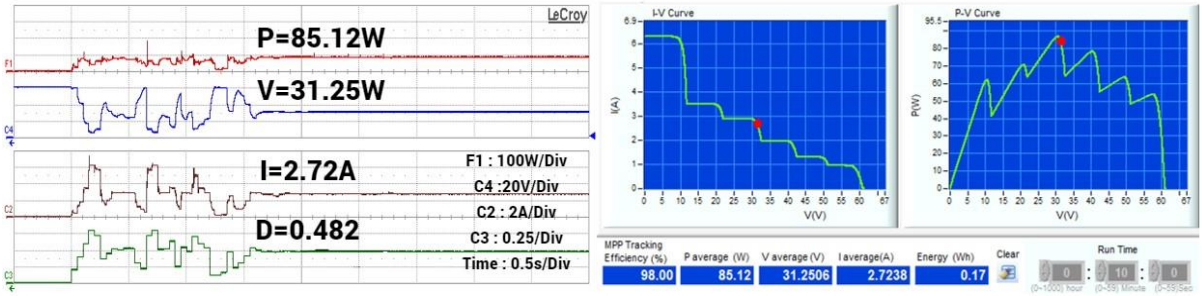

Figure 4.36 SMA resulting curves along Experimental Trial PSC5

Table 4.3 Reported Results of the Considered Algorithms along the Experimental Trials

		HSMA	GWO	PSO	SMA
PSC 1	Efficiency (%)	99.92	99.42	99.91	99.52
	Convergence Time (s)	0.8	2.7	2.7	2.1
PSC 2	Efficiency (%)	99.80	99.56	99.05	99.91
	Convergence Time (s)	0.95	2.0	1.75	2.1
PSC 3	Efficiency (%)	99.74	99.81	99.42	99.98
	Convergence Time (s)	0.6	2.2	1.75	2.0
PSC 4	Efficiency (%)	99.95	99.62	99.46	99.67
	Convergence Time (s)	0.8	2.0	1.6	2.2
PSC 5	Efficiency (%)	99.97	99.42	98.69	98.0
	Convergence Time (s)	1.2	2.0	1.6	2.2
Average Efficiency (%)		99.876	99.566	99.306	99.416
Average Convergence Time (s)		0.87	2.18	1.88	2.08

4.5 OVERALL COMPARISON

The various phases of the HSMA optimizer can be summarized into five distinct sections: Power evaluations, sorting, weight calculation, duty cycle update and Memory saving. The computational complexity can then be derived as follows:

$$O(HSMA) = O(T \times Power\ Evaluation) + O(T \times Sorting) + O(T \times Weight\ Computation) + O(T \times duty\ cycle\ update)$$

Where T denotes the number of iterations. Since the previous processes depend on the number of generated solutions N, the computational complexity can be further computed as follows:

$$O(HSMA) = O(T \times N) + O(T \times N) + O(T \times NlogN) + O(T \times N) = O(\mathrm{T} \times \mathrm{N} \times (3 + logN))$$

It has to be highlighted that the main operations of the HSMA optimizer are similar to those in most Metaheuristic algorithms. The process starts by generating an initial set of candidate solutions, and then in each iteration, the solutions are updated by the framework equations of the algorithm and evaluated by the defined fitness function. After completing the evaluation process, the best solution or a portion of the best solutions is saved for use in the next iterations.

In order to present a comprehensive assessment of the algorithm overall performance compared to other MPPT techniques, a comparative table that covers the major indices is constructed. The Perturb and Observe algorithm (P&O) has been added so that it helps as a reference in the comparison given its minimal computational complexity and rapid tracking speed capabilities.

Table 4.4 Overall Comparison between the HSMA optimizer and other MPPT techniques

MPPT Algorithm	Tracking Speed	Efficiency	Probability of LMPP stagnation under PSC	Fluctuations around the operating point	Fluctuations during the tracking phase	Computational Complexity	Number of tuneable parameters
HSMA	Moderate	High	Low	Low	Low	Moderate	**1** (Convergence Factor c)
SMA	Slow	High	Moderate	Low	High	Moderate	2 (Convergence Factors a, b)
PSO	Slow	High	Moderate	Low	High	Moderate	3 (C_1, C_2, ω)
GWO	Slow	High	Moderate	Low	High	Moderate	**1** (Convergence Factor a)
P&O	Fast	Low	High	High	Very Low	Low	**1** (Duty Cycle perturbation)

Conclusion

In this dissertation, we embarked on a comprehensive exploration of the modelling, identification, and control aspects of photovoltaic (PV) systems, with a focus on enhancing accuracy, stability, and efficiency. The culmination of this research has yielded several significant contributions to the field, affirming the potential for advancements in sustainable energy technologies.

Our efforts in developing an efficient algorithm for extracting PV model parameters have demonstrated a superior level of accuracy and stability compared to existing methodologies. This achievement not only refines the understanding of PV system behaviour but also lays a robust foundation for accurate model-based control strategies.

In the aspect of Maximum Power Point Tracking (MPPT), our novel algorithm designed for standalone PV systems has proven its mettle under challenging conditions, showcasing exceptional speed, efficiency, and reliability. The algorithm's ability to swiftly locate the global Maximum Power Point (MPP) region and adapt to minute perturbations in the operating point positions it as a valuable tool for optimizing energy extraction, particularly in scenarios involving partial shading.

Furthermore, our investigation into Metaheuristic algorithms for identification and control has provided insights into the potential of these advanced optimization techniques. By leveraging the power of Metaheuristics, we have expanded the horizons of control strategies for PV systems, opening avenues for further research and development in this evolving field.

As we conclude this thesis, it is evident that the presented algorithms and methodologies contribute to the ongoing efforts in making PV systems more efficient, reliable, and adaptable to dynamic environmental conditions. The outcomes of this research not only advance the academic understanding of PV systems but also hold practical implications for the deployment of sustainable energy solutions.

Looking ahead, the methodologies and findings presented herein pave the way for future research directions. The integration of advanced algorithms, coupled with

the exploration of emerging technologies, promises to further enhance the performance of PV systems and accelerate the transition to clean energy sources.

In closing, this work stands as a testament to the potential for innovation in the domain of PV systems. The journey from modeling and identification to control strategies has been both challenging and rewarding, and it is our hope that the insights shared here will inspire and guide future endeavors in the pursuit of sustainable energy solutions.

Bibliography

[1] International Renewable Energy Agency. (2019). Future of solar photovoltaic: deployment, investment, technology, grid integration and socio-economic aspects. A Global Energy Transformation.

[2] Patel, N., Kumar, A., Gupta, N., & Chitti Babu, B. (2020). Experimental investigations on voltage sourced inverter interfaced photovoltaic based distributed generation system. *Energy Sources, Part A: Recovery, Utilization, and Environmental Effects*, 1-23.

[3] Chin, V. J., Salam, Z., & Ishaque, K. (2015). Cell modelling and model parameters estimation techniques for photovoltaic simulator application: A review. Applied Energy, 154, 500-519. https://doi.org/10.1016/j.apenergy.2015.05.035

[4] Humada, A. M., Darweesh, S. Y., Mohammed, K. G., Kamil, M., Mohammed, S. F., Kasim, N. K., ... & Mekhilef, S. (2020). Modeling of PV system and parameter extraction based on experimental data: Review and investigation. Solar Energy, 199, 742-760. https://doi.org/10.1016/j.solener.2020.02.068

[5] Gao, X., Cui, Y., Hu, J., Xu, G., & Yu, Y. (2016). Lambert W-function based exact representation for double diode model of solar cells: Comparison on fitness and parameter extraction. Energy conversion and management, 127, 443-460. https://doi.org/10.1016/j.enconman.2016.09.005

[6] Rasool, F., Drieberg, M., Badruddin, N., & Singh, B. S. M. (2017). PV panel modeling with improved parameter extraction technique. Solar Energy, 153, 519-530. https://doi.org/10.1016/j.solener.2017.05.078

[7] Bradai, R., Boukenoui, R., Kheldoun, A., Salhi, H., Ghanes, M., Barbot, J. P., & Mellit, A. (2017). Experimental assessment of new fast MPPT algorithm for PV systems under non-uniform irradiance conditions. *Applied energy*, *199*, 416-429.

[8] Kheldoun, A., Djeriou, S., Kouadri, A., & Refoufi, L. (2015). A Simple and Accurate Maximum Power Point Tracking Algorithm for Photovoltaic Systems. *Progress in Clean Energy, Volume 2: Novel Systems and Applications*, 721-733.

[9] Elgendy, M. A., Zahawi, B., & Atkinson, D. J. (2011). Assessment of perturb and observe MPPT algorithm implementation techniques for PV pumping applications. *IEEE transactions on sustainable energy*, *3*(1), 21-33.

[10] Sera, D., Mathe, L., Kerekes, T., Spataru, S. V., & Teodorescu, R. (2013). On the perturb-and-observe and incremental conductance MPPT methods for PV systems. *IEEE journal of photovoltaics*, *3*(3), 1070-1078.

[11] Kjær, S. B. (2012). Evaluation of the "hill climbing" and the "incremental conductance" maximum power point trackers for photovoltaic power systems. *IEEE Transactions on Energy Conversion*, *27*(4), 922-929.

[12] Motahhir, S., El Hammoumi, A., & El Ghzizal, A. (2020). The most used MPPT algorithms: Review and the suitable low-cost embedded board for each algorithm. *Journal of cleaner production*, *246*, 118983.

[13] Mirza, A. F., Mansoor, M., & Ling, Q. (2020). A novel MPPT technique based on Henry gas solubility optimization. *Energy Conversion and Management*, *225*, 113409.

[14] Cárdenas, A. A., Carrasco, M., Mancilla-David, F., Street, A., & Cárdenas, R. (2016). Experimental parameter extraction in the single-diode photovoltaic model via a reduced-space search. IEEE Transactions on Industrial Electronics, 64(2), 1468-1476. https://doi.org/10.1109/TIE.2016.2615590
[15] Lun, S. X., Du, C. J., Yang, G. H., Wang, S., Guo, T. T., Sang, J. S., & Li, J. P. (2013). An explicit approximate I–V characteristic model of a solar cell based on padé approximants. Solar energy, 92, 147-159. https://doi.org/10.1016/j.solener.2013.02.021
[16] Ćalasan, M., Aleem, S. H. A., & Zobaa, A. F. (2020). On the root mean square error (RMSE) calculation for parameter estimation of photovoltaic models: A novel exact analytical solution based on Lambert W function. Energy conversion and management, 210, 112716.
[17] Gao, X., Cui, Y., Hu, J., Xu, G., & Yu, Y. (2016). Lambert W-function based exact representation for double diode model of solar cells: Comparison on fitness and parameter extraction. Energy conversion and management, 127, 443-460. https://doi.org/10.1016/j.enconman.2016.09.005
[18] Lun, S. X., Du, C. J., Guo, T. T., Wang, S., Sang, J. S., & Li, J. P. (2013). A new explicit I–V model of a solar cell based on Taylor's series expansion. Solar Energy, 94, 221-232. https://doi.org/10.1016/j.solener.2013.04.01
[19] Sarkar, D., Kumar, A., & Sadhu, P. K. (2021). Different diode models comparison using Lambert W function for extracting maximum power from BIPV modules. International Journal of Energy Research, 45(1), 691-702.
[20] Malik, P., & Chandel, S. S. (2021). A new integrated single-diode solar cell model for photovoltaic power prediction with experimental validation under real outdoor conditions. International Journal of Energy Research, 45(1), 759-771.
[21] Ishaque, K., Salam, Z., Mekhilef, S., & Shamsudin, A. (2012). Parameter extraction of solar photovoltaic modules using penalty-based differential evolution. Applied Energy, 99, 297-308. https://doi.org/10.1016/j.apenergy.2012.05.017
[22] Easwarakhanthan, T., Bottin, J., Bouhouch, I., & Boutrit, C. (1986). Nonlinear minimization algorithm for determining the solar cell parameters with microcomputers. International journal of solar energy, 4(1), 1-12. https://doi.org/10.1080/01425918608909835
[23] Chegaar, M., Ouennoughi, Z., & Hoffmann, A. (2001). A new method for evaluating illuminated solar cell parameters. Solid-state electronics, 45(2), 293-296. https://doi.org/10.1016/S0038-1101(00)00277-X
[24] Elbaset, A. A., Ali, H., & Abd El Sattar, M. (2016). New seven parameters model for amorphous silicon and thin film PV modules based on solar irradiance. Solar energy, 138, 26-35. https://doi.org/10.1016/j.solener.2016.08.056
[25] Abbassi, R., Abbassi, A., Jemli, M., & Chebbi, S. (2018). Identification of unknown parameters of solar cell models: A comprehensive overview of available approaches. Renewable and Sustainable Energy Reviews, 90, 453-474. https://doi.org/10.1016/j.rser.2018.03.011
[26] Storn, R., & Price, K. (1997). Differential evolution–a simple and efficient heuristic for global optimization over continuous spaces. Journal of global optimization, 11(4), 341-359. http://doi.org/10.1023/A:1008202821328
[27] Eberhart, Russell, and James Kennedy. "A new optimizer using particle swarm theory." MHS'95. Proceedings of the Sixth International Symposium on Micro Machine and Human Science. Ieee, 1995. http://doi.org/10.1109/MHS.1995.494215
[28] Rao, R. (2016). Jaya: A simple and new optimization algorithm for solving constrained and unconstrained optimization problems. International Journal of

Industrial Engineering Computations, 7(1), 19-34. https://doi.org/10.1080/0305215X.2016.1164855
[29] Mirjalili, S., & Lewis, A. (2016). The whale optimization algorithm. Advances in engineering software, 95, 51-67.
[30] Karaboga, D., & Basturk, B. (2007). A powerful and efficient algorithm for numerical function optimization: artificial bee colony (ABC) algorithm. Journal of global optimization, 39(3), 459-471. http://doi.org/10.1007/S10898-007-9149-X
[31] Rao, R. V., Savsani, V. J., & Vakharia, D. P. (2012). Teaching–learning-based optimization: an optimization method for continuous non-linear large scale problems. Information sciences, 183(1), 1-15. https://doi.org/10.1016/j.ins.2011.08.006
[32] Li, S., Gu, Q., Gong, W., & Ning, B. (2020). An enhanced adaptive differential evolution algorithm for parameter extraction of photovoltaic models. Energy Conversion and Management, 205, 112443.
[33] Yang, X., Gong, W., & Wang, L. (2019). Comparative study on parameter extraction of photovoltaic models via differential evolution. Energy Conversion and Management, 201, 112113.
[34] Li, S., Gong, W., & Gu, Q. (2021). A comprehensive survey on meta-heuristic algorithms for parameter extraction of photovoltaic models. Renewable and Sustainable Energy Reviews, 141, 110828. https://doi.org/10.1016/j.rser.2021.110828
[35] Jordehi, A. R. (2016). Time varying acceleration coefficients particle swarm optimisation (TVACPSO): A new optimisation algorithm for estimating parameters of PV cells and modules. Energy Conversion and Management, 129, 262-274. https://doi.org/10.1016/j.enconman.2016.09.085
[36] Jordehi, A. R. (2018). Enhanced leader particle swarm optimisation (ELPSO): An efficient algorithm for parameter estimation of photovoltaic (PV) cells and modules. Solar Energy, 159, 78-87. https://doi.org/10.1016/j.solener.2017.10.063
[37] Liang, J., Ge, S., Qu, B., Yu, K., Liu, F., Yang, H., ... & Li, Z. (2020). Classified perturbation mutation based particle swarm optimization algorithm for parameters extraction of photovoltaic models. Energy Conversion and Management, 203, 112138. https://doi.org/10.1016/j.enconman.2019.112138
[38] Yu, K., Liang, J. J., Qu, B. Y., Chen, X., & Wang, H. (2017). Parameters identification of photovoltaic models using an improved JAYA optimization algorithm. Energy Conversion and Management, 150, 742-753. https://doi.org/10.1016/j.enconman.2017.08.063
[39] Yu, K., Qu, B., Yue, C., Ge, S., Chen, X., & Liang, J. (2019). A performance-guided JAYA algorithm for parameters identification of photovoltaic cell and module. Applied Energy, 237, 241-257. https://doi.org/10.1016/j.apenergy.2019.01.008
[40] Li, S., Gong, W., Yan, X., Hu, C., Bai, D., Wang, L., & Gao, L. (2019). Parameter extraction of photovoltaic models using an improved teaching-learning-based optimization. Energy Conversion and Management, 186, 293-305. https://doi.org/10.1016/j.egyr.2021.06.097
[41] Chen, X., Yu, K., Du, W., Zhao, W., & Liu, G. (2016). Parameters identification of solar cell models using generalized oppositional teaching learning based optimization. Energy, 99, 170-180. https://doi.org/10.1016/j.energy.2016.01.052
[42] Yu, K., Chen, X., Wang, X., & Wang, Z. (2017). Parameters identification of photovoltaic models using self-adaptive teaching-learning-based optimization. Energy Conversion and Management, 145, 233-246. https://doi.org/10.1016/j.egyr.2021.06.097
[43] Chen, X., Xu, B., Mei, C., Ding, Y., & Li, K. (2018). Teaching–learning–based

artificial bee colony for solar photovoltaic parameter estimation. Applied energy, 212, 1578-1588.
[44] Zou, F., Wang, L., Hei, X., & Chen, D. (2015). Teaching–learning-based optimization with learning experience of other learners and its application. Applied Soft Computing, 37, 725-736. https://doi.org/10.1016/j.asoc.2015.08.047
[45] Jiao, S., Chong, G., Huang, C., Hu, H., Wang, M., Heidari, A. A., ... & Zhao, X. (2020). Orthogonally adapted Harris hawks optimization for parameter estimation of photovoltaic models. Energy, 203, 117804.
[46] Heidari, A. A., Mirjalili, S., Faris, H., Aljarah, I., Mafarja, M., & Chen, H. (2019). Harris hawks optimization: Algorithm and applications. Future generation computer systems, 97, 849-872.
[47] Agwa, A. M., El-Fergany, A. A., & Maksoud, H. A. (2020). Electrical characterization of photovoltaic modules using farmland fertility optimizer. Energy Conversion and Management, 217, 112990.
[48] Shayanfar, H., & Gharehchopogh, F. S. (2018). Farmland fertility: A new metaheuristic algorithm for solving continuous optimization problems. Applied Soft Computing, 71, 728-746.
[49] Gomes, G. F., da Cunha, S. S., & Ancelotti, A. C. (2019). A sunflower optimization (SFO) algorithm applied to damage identification on laminated composite plates. Engineering with Computers, 35(2), 619-626. http://doi.org/10.1007/s00366-018-0620-8
[50] Qais, M. H., Hasanien, H. M., & Alghuwainem, S. (2019). Identification of electrical parameters for three-diode photovoltaic model using analytical and sunflower optimization algorithm. Applied Energy, 250, 109-117. https://doi.org/10.1016/j.apenergy.2019.05.013
[51] Chin, V. J., & Salam, Z. (2019). Coyote optimization algorithm for the parameter extraction of photovoltaic cells. Solar Energy, 194, 656-670.
[52] Pierezan, J., & Coelho, L. D. S. (2018, July). Coyote optimization algorithm: a new metaheuristic for global optimization problems. In 2018 IEEE congress on evolutionary computation (CEC) (pp. 1-8). IEEE. http://doi.org/10.1109/CEC.2018.8477769
[53] Rizk-Allah, R. M., & El-Fergany, A. A. (2020). Conscious neighborhood scheme-based Laplacian barnacles mating algorithm for parameters optimization of photovoltaic single-and double-diode models. Energy Conversion and Management, 226, 113522.
[54] Sulaiman, M. H., Mustaffa, Z., Saari, M. M., & Daniyal, H. (2020). Barnacles mating optimizer: A new bio-inspired algorithm for solving engineering optimization problems. Engineering Applications of Artificial Intelligence, 87, 103330. https://doi.org/10.1016/j.engappai.2019.103330
[55] Vandrasi, R. K., Sravana Kumar, B., & Devarapalli, R. (2022). Solar photo voltaic module parameter extraction using a novel Hybrid Chimp-Sine Cosine Algorithm. *Energy Sources, Part A: Recovery, Utilization, and Environmental Effects*, 1-20.
[56] Khishe, M., & Mosavi, M. R. (2020). Chimp optimization algorithm. *Expert systems with applications*, *149*, 113338.
[57] Mirjalili, S. (2016). SCA: a sine cosine algorithm for solving optimization problems. *Knowledge-based systems*, *96*, 120-133.
[58] Ishaque, K., Salam, Z., Amjad, M., & Mekhilef, S. (2012). An improved particle swarm optimization (PSO)–based MPPT for PV with reduced steady-state oscillation. *IEEE transactions on Power Electronics*, *27*(8), 3627-3638.

[59] Liu, Y. H., Huang, S. C., Huang, J. W., & Liang, W. C. (2012). A particle swarm optimization-based maximum power point tracking algorithm for PV systems operating under partially shaded conditions. *IEEE transactions on energy conversion*, *27*(4), 1027-1035.
[60] Ishaque, K., Salam, Z., Amjad, M., & Mekhilef, S. (2012). An improved particle swarm optimization (PSO)–based MPPT for PV with reduced steady-state oscillation. *IEEE transactions on Power Electronics*, *27*(8), 3627-3638.
[61] Liu, Y. H., Huang, S. C., Huang, J. W., & Liang, W. C. (2012). A particle swarm optimization-based maximum power point tracking algorithm for PV systems operating under partially shaded conditions. *IEEE transactions on energy conversion*, *27*(4), 1027-1035.
[62] Gopalakrishnan, S. K., Kinattingal, S., Simon, S. P., & Ark Kumar, K. (2020). Enhanced energy harvesting from shaded PV systems using an improved particle swarm optimisation. *IET Renewable Power Generation*, *14*(9), 1471-1480.
[63] Mohanty, S., Subudhi, B., & Ray, P. K. (2015). A new MPPT design using grey wolf optimization technique for photovoltaic system under partial shading conditions. *IEEE Transactions on Sustainable Energy*, *7*(1), 181-188.
[64] Eltamaly, A. M., & Farh, H. M. (2019). Dynamic global maximum power point tracking of the PV systems under variant partial shading using hybrid GWO-FLC. *Solar Energy*, *177*, 306-316.
[65] Mirza, A. F., Mansoor, M., Ling, Q., Yin, B., & Javed, M. Y. (2020). A Salp-Swarm Optimization based MPPT technique for harvesting maximum energy from PV systems under partial shading conditions. *Energy Conversion and Management*, *209*, 112625.
[66] Jamaludin, M. N. I., Tajuddin, M. F. N., Ahmed, J., Azmi, A., Azmi, S. A., Ghazali, N. H., ... & Alhelou, H. H. (2021). An effective salp swarm based MPPT for photovoltaic systems under dynamic and partial shading conditions. *Ieee Access*, *9*, 34570-34589.
[67] Sundareswaran, K., Sankar, P., Nayak, P. S. R., Simon, S. P., & Palani, S. (2014). Enhanced energy output from a PV system under partial shaded conditions through artificial bee colony. *IEEE transactions on sustainable energy*, *6*(1), 198-209.
[68] Sahoo, S. K., Balamurugan, M., Anurag, S., Kumar, R., & Priya, V. (2017, April). Maximum power point tracking for PV panels using ant colony optimization. In *2017 Innovations in Power and Advanced Computing Technologies (i-PACT)* (pp. 1-4). IEEE.
[69] Diab, A. A. Z., & Rezk, H. (2017). Global MPPT based on flower pollination and differential evolution algorithms to mitigate partial shading in building integrated PV system. *Solar Energy*, *157*, 171-186.
[70] Chaieb, H., & Sakly, A. (2018). A novel MPPT method for photovoltaic application under partial shaded conditions. *Solar Energy*, *159*, 291-299.
[71] Dileep, G., & Singh, S. N. (2017). An improved particle swarm optimization based maximum power point tracking algorithm for PV system operating under partial shading conditions. *Solar Energy*, *158*, 1006-1015.
[72] Refaat, A., Khalifa, A. E., Elsakka, M. M., Elhenawy, Y., Kalas, A., & Elfar, M. H. (2023). A novel metaheuristic MPPT technique based on enhanced autonomous group Particle Swarm Optimization Algorithm to track the GMPP under partial shading conditions-Experimental validation. Energy Conversion and Management, 287, 117124.

[73] Li, H., Yang, D., Su, W., Lü, J., & Yu, X. (2018). An overall distribution particle swarm optimization MPPT algorithm for photovoltaic system under partial shading. *IEEE Transactions on Industrial Electronics*, *66*(1), 265-275.
[74] Javed, S., & Ishaque, K. (2022). A comprehensive analyses with new findings of different PSO variants for MPPT problem under partial shading. *Ain Shams Engineering Journal*, *13*(5), 101680.
[75] Gong, L., Hou, G., & Huang, C. (2023). A two-stage MPPT controller for PV system based on the improved artificial bee colony and simultaneous heat transfer search algorithm. *ISA transactions*, *132*, 428-443.
[76] Moghassemi, A., Ebrahimi, S., Padmanaban, S., Mitolo, M., & Holm-Nielsen, J. B. (2022). Two fast metaheuristic-based MPPT techniques for partially shaded photovoltaic system. *International Journal of Electrical Power & Energy Systems*, *137*, 107567.
[77] Swetha, K. T., Reddy, V., & Robinson, A. (2023). An innovative grey wolf optimizer with Nelder–mead search method based MPPT technique for fast convergence under partial shading conditions. Sustainable Energy Technologies and Assessments, 59, 103412.
[78] Mohammed, K. K., & Mekhilef, S. (2023). Improved Snake Optimizer Algorithm-Based GMPPT With a Fast Response to the Load Variations Under Different Weather Conditions for PV Systems. IEEE Transactions on Industrial Electronics.
[79] Chin, V. J., Salam, Z., & Ishaque, K. (2015). Cell modelling and model parameters estimation techniques for photovoltaic simulator application: A review. Applied Energy, 154, 500-519.
[80] Lasnier, F., & Ang, T. G. (2017). Photovoltaic engineering handbook. Routledge.
[81] Jordehi, A. R. (2016). Parameter estimation of solar photovoltaic (PV) cells: A review. Renewable and Sustainable Energy Reviews, 61, 354-371.
[82] Allam, D., Yousri, D. A., & Eteiba, M. B. (2016). Parameters extraction of the three diode model for the multi-crystalline solar cell/module using Moth-Flame Optimization Algorithm. Energy Conversion and Management, 123, 535-548. https://doi.org/10.1016/j.enconman.2016.06.052
[83] Abdollahzadeh, B., Gharehchopogh, F. S., & Mirjalili, S. (2021). African vultures optimization algorithm: A new nature-inspired metaheuristic algorithm for global optimization problems. Computers & Industrial Engineering, 158, 107408. https://doi.org/10.1016/j.cie.2021.107408
[84] Abdollahzadeh, B., Gharehchopogh, F. S., & Mirjalili, S. (2021). African vultures optimization algorithm: A new nature-inspired metaheuristic algorithm for global optimization problems. Computers & Industrial Engineering, 158, 107408. https://doi.org/10.1016/j.cie.2021.107408
[85] Xiong, G., Zhang, J., Shi, D., Zhu, L., & Yuan, X. (2020). Parameter extraction of solar photovoltaic models with an either-or teaching learning based algorithm. Energy Conversion and Management, 224, 113395. https://doi.org/10.1016/j.enconman.2020.113395
[86] Chen, X., Yue, H., & Yu, K. (2019). Perturbed stochastic fractal search for solar PV parameter estimation. Energy, 189, 116247.
[59] Zhang, H., Heidari, A. A., Wang, M., Zhang, L., Chen, H., & Li, C. (2020). Orthogonal Nelder-Mead moth flame method for parameters identification of photovoltaic modules. Energy Conversion and Management, 211, 112764. https://doi.org/10.1016/j.enconman.2020.112764

[60] Ismaeel, A. A., Houssein, E. H., Oliva, D., & Said, M. (2021). Gradient-based optimizer for parameter extraction in photovoltaic models. IEEE Access, 9, 13403-13416.
[61] Chen, X., & Yu, K. (2019). Hybridizing cuckoo search algorithm with biogeography-based optimization for estimating photovoltaic model parameters. Solar Energy, 180, 192-206.
[62] Yousri, D., Rezk, H., & Fathy, A. (2020). Identifying the parameters of different configurations of photovoltaic models based on recent artificial ecosystem-based optimization approach. International Journal of Energy Research, 44(14), 11302-11322.
[63] Wang, S., Yu, Y., & Hu, W. (2021). Static and dynamic solar photovoltaic models' parameters estimation using hybrid Rao optimization algorithm. Journal of Cleaner Production, 315, 128080.
[64] Mostafa, M., Rezk, H., Aly, M., & Ahmed, E. M. (2020). A new strategy based on slime mould algorithm to extract the optimal model parameters of solar PV panel. Sustainable Energy Technologies and Assessments, 42, 100849. https://doi.org/10.1016/j.seta.2020.100849
[65] Zhang, Y., Jin, Z., & Mirjalili, S. (2020). Generalized normal distribution optimization and its applications in parameter extraction of photovoltaic models. Energy Conversion and Management, 224, 113301. https://doi.org/10.1016/j.enconman.2020.113301
[66] Sun, L., Wang, J., & Tang, L. (2021). A Powerful Bio-Inspired Optimization Algorithm Based PV Cells Diode Models Parameter Estimation. Frontiers in Energy Research, 9, 147.
[67] Abdel-Basset, M., Mohamed, R., El-Fergany, A., Abouhawwash, M., & Askar, S. S. (2021). Parameters identification of PV triple-diode model using improved generalized normal distribution algorithm. Mathematics, 9(9), 995. https://doi.org/10.3390/math9090995
[68] Ramadan, A. E., Kamel, S., Khurshaid, T., Oh, S. R., & Rhee, S. B. (2021). Parameter Extraction of Three Diode Solar Photovoltaic Model Using Improved Grey Wolf Optimizer. Sustainability, 13(12), 6963. https://doi.org/10.3390/su13126963
[69] Long, W., Wu, T., Xu, M., Tang, M., & Cai, S. (2021). Parameters identification of photovoltaic models by using an enhanced adaptive butterfly optimization algorithm. Energy, 229, 120750. https://doi.org/10.1016/j.energy.2021.120750
[70] Liang, J., Qiao, K., Yu, K., Ge, S., Qu, B., Xu, R., & Li, K. (2020). Parameters estimation of solar photovoltaic models via a self-adaptive ensemble-based differential evolution. Solar Energy, 207, 336-346. https://doi.org/10.1016/j.solener.2020.06.100
[71] Xiong, G., Zhang, J., Shi, D., & Yuan, X. (2019). Application of supply-demand-based optimization for parameter extraction of solar photovoltaic models. Complexity, 2019. https://doi.org/10.1155/2019/3923691
[72] Abdel-Basset, M., Mohamed, R., Mirjalili, S., Chakrabortty, R. K., & Ryan, M. J. (2020). Solar photovoltaic parameter estimation using an improved equilibrium optimizer. Solar Energy, 209, 694-708. https://doi.org/10.1016/j.solener.2020.09.032
[73] Naeijian, M., Rahimnejad, A., Ebrahimi, S. M., Pourmousa, N., & Gadsden, S. A. (2021). Parameter estimation of PV solar cells and modules using Whippy Harris Hawks Optimization Algorithm. Energy Reports, 7, 4047-4063. https://doi.org/10.1016/j.egyr.2021.06.085
[74] Abdel-Basset, M., El-Shahat, D., Chakrabortty, R. K., & Ryan, M. (2021). Parameter estimation of photovoltaic models using an improved marine predators

algorithm. Energy Conversion and Management, 227, 113491. https://doi.org/10.1016/j.enconman.2020.113491
[75] Long, W., Cai, S., Jiao, J., Xu, M., & Wu, T. (2020). A new hybrid algorithm based on grey wolf optimizer and cuckoo search for parameter extraction of solar photovoltaic models. Energy Conversion and Management, 203, 112243. https://doi.org/10.1016/j.enconman.2019.112243
[76] Liu, Y., Chong, G., Heidari, A. A., Chen, H., Liang, G., Ye, X., ... & Wang, M. (2020). Horizontal and vertical crossover of Harris hawk optimizer with Nelder-Mead simplex for parameter estimation of photovoltaic models. Energy Conversion and Management, 223, 113211.